



ISSN: 3105-1723 (Print)
ISSN: 3105-1731 (Online)


Emerging Trends in Engineering and Sustainability


A quarterly Peer-Reviewed Scientific Journal
Published by Al-Naji University



Volume 2 | Issue 1 | 2026

Deposit number at the National Library in Baghdad 2922 for 2025

 Al-Yarmouk, Mansour District, Baghdad 10035, Iraq

 etes@alnaji-uni.edu.iq

Blank Page

About Journal

Emerging Trends in Engineering and Sustainability (ETES) is a peer-reviewed, open-access scientific journal published by **Al-Naji University** in alignment with the academic standards and publishing regulations of the **Ministry of Higher Education and Scientific Research in Iraq**.

ETES is dedicated to the dissemination of high-impact research and the promotion of innovative practices across all fields of engineering, with a strong emphasis on sustainability. The journal welcomes **original research articles and review papers** that contribute to advancing sustainable solutions, technologies, and methodologies relevant to engineering disciplines.

To ensure academic rigor and scholarly integrity, ETES employs a **double-blind peer review process** involving at least two independent external reviewers for each submission. The journal adheres strictly to the ethical guidelines set forth by the **Committee on Publication Ethics (COPE)**.

As an **open-access** journal, ETES provides immediate and unrestricted access to all published articles. Readers may freely read, download, and distribute full-text content without requiring prior permission from authors or the publisher, supporting global knowledge sharing.

ETES follows a **quarterly publication schedule**, with four issues released annually. The journal is committed to becoming a reputable international platform for scholars and researchers working at the intersection of engineering innovation and sustainable development.

ETES published **quarterly**, with **four** regular issues released each year. The journal's long-term vision is to be widely indexed, cited, and read by a global scholarly community, contributing meaningfully to the advancement of sustainable engineering solutions worldwide.

Blank Page

Aims

Emerging Trends in Engineering and Sustainability (ETES) is an international, open-access, peer-reviewed journal committed to advancing innovation and sustainability across all disciplines of engineering. The journal seeks to serve as a platform for disseminating high-quality, original research and comprehensive reviews that address contemporary challenges and transformative practices in engineering with a focus on sustainable development. ETES aims to foster intellectual exchange among researchers, academics, professionals, and postgraduate students by promoting interdisciplinary collaboration and publishing research that contributes to the evolution of sustainable engineering practices worldwide.

Scope / Categories

ETES welcomes submissions of original research articles and scholarly review papers that explore emerging concepts, methodologies, and technologies in the diverse fields of engineering, particularly those that contribute to sustainability. The journal encourages contributions that reflect rigorous scientific inquiry, innovative thinking, and practical applications.

Core areas of interest include, but are not limited to:

- Mechanical Engineering
- Petroleum Engineering
- Chemical Engineering
- Environmental Engineering
- Sustainability and Green Technologies
- Electrical and Electronic Engineering
- Computer Science, Software Engineering, and Informatics
- Structural and Geotechnical Engineering
- Engineering Management and Decision-Making
- Transportation and Infrastructure Engineering
- Water Resources and Hydraulic Engineering
- Architectural Design and Urban Sustainability
- Energy Systems and Power Engineering
- Advanced Materials and Materials Engineering
- Control Systems, Electronics, and Signal Processing
- Communication and Networking Technologies
- Renewable and Clean Energy Technologies
- Civil Engineering

ETES is committed to publishing research that bridges theory and practice, fosters interdisciplinary solutions, and contributes to sustainable development goals (SDGs) in engineering contexts.

Blank Page

Editorial Board

Prof. Dr. Moneer Hameed Tolephih, Editor-in-Chief

College of Engineering, Al-Naji University, Baghdad, Iraq

Expertise: Mechanical Engineering, Renewable Energy, Sustainability

Email: monerht@alnaji-uni.edu.iq

Asst. Prof. Dr. Omar Al-Fatlawi, Managing Editor

College of Engineering, Al-Naji University, Baghdad, Iraq

Expertise: Geoscience, Gas Engineering, Reservoir Simulation, Petroleum Engineering

Email: omar.al-fatlawi@alnaji-uni.edu.iq

Editorial Board Members

Prof. Dr. Riadh Al-Mahaidi

Department of Civil and Construction Engineering, Swinburne University of Technology, Melbourne, Australia

Expertise: Civil Engineering, Structural Engineering, Concrete, Steel, Fiber Reinforced Polymers

Email: ralmahaidi@swin.edu.au

Assoc. Prof. Dr. Sarmad Al-Anssari

College of Engineering, Al-Naji University, Baghdad, Iraq

Expertise: Nanofluids, Carbon storage, Enhanced oil recovery, Water treatment, Nanoparticles

Email: al-anssari@alnaji-uni.edu.iq

Associate Prof. Dr. Harith Hasoon Al-Moameri

Materials Engineering Department, Mustansiriyah University, Baghdad, Iraq

Expertise: Polyurethane, Polymer, Blowing Agent, Simulation, Catalysts, Surfactant, Materials Engineering, Building Materials

Email: almoamerih@uomustansiriyah.edu.iq

Prof. Dr. Hamed Karami

Department of Signal and Information Processing for Sensing Systems Institute for Bioengineering of Catalonia, Spain

Expertise: Gas Sensors, Signal Processing, Drying Technology, Food Quality and Control

Email: hkarami@ibecbarcelona.eu

Associate Prof Dr. Nizar F.O. Al-Muhsen

Department of Power Mechanics, Technical Instructors Training Institute (TITI), Middle Technical University (MTU), Baghdad, Iraq

Expertise: Bio-Fuel Combustion and Emissions, Internal Combustion Engines, Renewable and Sustainable Energy Systems.

Email: nizar.almuhsen@mtu.edu.iq

Prof. Dr. Maha Salman

Department of Architecture, School of Architecture and Interior Design, Canadian University Dubai, Dubai, UAE

Expertise: Sustainability, Smart cities, AI in architecture, Passive design, Energy-Efficiency in buildings, Indoor Air Quality, Human Wellbeing

Email: maha.salman@tud.ac.ae

Prof. Dr. Mazen J. Al-Kheetan

Civil and Environmental Engineering Department, College of Engineering, Mutah University, Karak, Jordan

Expertise: Sustainability in construction, low-carbon cementitious materials, concrete, asphalt materials, additive manufacturing, pavement

Email: mazen.al-kheetan@mutah.edu.jo

Prof. Dr. Ali Kadkhodaie

Earth Sciences Department, Faculty of Natural Sciences, University of Tabriz, Tabriz, Iran

Expertise: Formation Evaluation, Petrophysics, Petroleum Geology.

Email: kadkhodaie_ali@tabrizu.ac.ir

Prof. Dr. Ali Al-Ataby

Chair and Associate Professor, Electrical and Electronics Engineering, School of Engineering & Computer Science, AURAK, Ras Al Khaimah, UAE

Expertise: Signal/Image Processing, Machine Learning/AI, Robotics, IoT Sensors.

Email: ali.ataby@aurak.ac.ae

Prof. Dr. Hussein Znad

Chemical Engineering, Curtin University, Perth, Australia

Expertise: microalgae, resources recovery, wastewater treatment, CO2 mitigation, biofuel production (biohydrogen and biodiesel), Functionalized nanomaterials.

Email: h.znad@curtin.edu.au

Blank Page

Asst. Prof. Dr. Dhifaf Jaafar Sadeq

Department of Petroleum Engineering, College of Engineering, Al-Naji University, Baghdad, Iraq

Expertise: Gas Engineering, Gas Hydrate, Flow Assurance, Petroleum Production Engineering.

Email: dhifaf.jaafar@alnaji-uni.edu.iq

Prof. Dr. Ahmed Razzaq Hasan Al-Manea

Al-Rumaitha Technical Institute, Al-Furat Al-Awsat Technical University, Najaf, Iraq

Expertise: Solar energy and sustainability, Finite Element Analysis, CFD, Numerical Simulation and Modeling, FLUENT, Computational Simulation and Analysis, Laser Applications, and Condensation.

Email: Dr.ahmed.almanea@atu.edu.iq

Prof. Dr. Hussein A Kazem

Faculty of Engineering, Sohar University, Sohar, Oman

Expertise: Solar Thermal, Photovoltaic, Renewable Energy, Dust, Photovoltaic / Thermal, Nano-PCM

Email: H.Kazem@su.edu.om

Prof. Dr. Satiye Korkmaz

Department of Photonics and Optoelectronics, Electrical and Electronics Engineering, Faculty of Engineering, Karabuk University, Karabuk, Turkey

Expertise: Nanotechnology, Energy storage, Photonics, Optoelectronics.

Email: satiyekorkmaz@karabuk.edu.tr

Prof Dr. Makram A. Fakhri

Department of Laser Engineering and Electronic Optics, University of Technology-Iraq, Baghdad, Iraq

Expertise: Nano materials, Nanostructures, Optoelectronics devices, Photonics devices, Photonics crystals, sensors, lasers, photodetectors.

Email: Makram.a.fakhri@uotechnology.edu.iq

Asst. Prof. Dr. Samar Sabie

Faculty of Information, University of Toronto, Toronto, Canada

Expertise: Climate Change, Building Automation Systems, Social Sustainability.

Email: samar.sabie@utoronto.ca

Prof. Dr. Ahmed Falh Hasan

Department of Materials Engineering, University of Diyala, Diyala, Iraq

Expertise: Materials design and Engineering

Email: ahmed_hasan_eng@uodiyala.edu.iq

Dr. Fahd Saeed Alakbari

Interdisciplinary Research Center for Hydrogen Technologies and Carbon Management, King Fahd University of Petroleum and Minerals, Dhahran 31261, Saudi Arabia

Expertise: Machine learning applications in engineering, Drilling fluid engineering, Carbon dioxide capture, utilization, and storage

Email: fahd.akbari@kfupm.edu.sa

Assoc. Prof. Dr. Mohammed N. Abdulrazaq Alshekhly

Chair of University Research Council, Gulf University, Kingdom of Bahrain

Expertise: Robotics, IoT, Smart Cities, Metaverse, Sustainability, Metal processing

Email: dr.mohammed.alshekhly@gulfuniversity.edu.bh

Prof. Dr. Mofazzal Hossain

Western Australian School of Mines (WASM), Energy Engineering, Curtin University, Perth, Australia

Expertise: Computational modelling; fluid flow stimulation, design and optimization of hydraulic fracturing;; well design and geomechanical analysis.

Email: md.hossain@curtin.edu.au

Asst. Prof. Ghamgeen Izat Rashed

School of Electrical Engineering and Automation, Wuhan University-China

Expertise: FACTS devices, Reliability of power System, Renewable energy, Smart Grid

Email: ghamgeen@whu.edu.cn

Proofreading

Prof. Dr. Dima F. Ameen

Department of English, College of Education, Al-Naji University, Baghdad, Iraq

Production

Rawan Nihad Al-Sammarraie

Al-Naji University, Baghdad, Iraq

Blank Page

Publication Ethics

Emerging Trends in Engineering and Sustainability (ETES) is dedicated to maintaining the highest standards of research integrity and academic publishing. As an adherent to the principles established by the Committee on Publication Ethics (COPE), ETES strictly follows COPE's guidelines in addressing ethical concerns and potential misconduct.

Authors submitting to ETES are expected to uphold the principles of ethical research and responsible authorship. Misrepresentation of data, results, or authorship undermines the credibility of the journal, damages the scholarly record, and erodes public trust in science. To preserve the integrity of academic publishing, authors must comply with the following ethical standards:

Originality and Exclusivity: Manuscripts must be original and should not be under review by another journal simultaneously. Submissions must not have been previously published, either in part or in full, in any language or format, unless the new manuscript represents a significant extension of prior work. In such cases, authors must clearly disclose previous publications to avoid self-plagiarism and text recycling.

Justified Secondary Publication: In rare and justified cases, secondary or concurrent publication (e.g., translated work or work adapted for a distinct audience) may be permitted, provided that all conditions for ethical secondary publication are met and transparent disclosure is made.

Avoidance of Redundant Publication: Fragmentation of a single research project into multiple submissions ("salami publishing") solely to increase publication count is discouraged and considered unethical.

Proper Attribution and Avoidance of Plagiarism: All sources, data, theories, and text derived from other authors must be appropriately cited. Verbatim quotations must be placed within quotation marks and accompanied by citations. Any reuse of copyrighted material must be supported by proper permission and acknowledgment.

Accuracy and Transparency: Authors must present their findings clearly, accurately, and honestly, without data fabrication, falsification, or inappropriate manipulation (including of images). Field-specific standards for data collection and analysis should be rigorously followed.

By submitting a manuscript to ETES, authors affirm their commitment to ethical conduct in research and publication. Non-compliance may result in manuscript rejection, retraction of published articles, or notification of institutional misconduct boards, as deemed appropriate by the editorial team.

Plagiarism and AI Policy

Emerging Trends in Engineering and Sustainability (ETES) is committed to upholding the highest standards of academic integrity, originality, and responsible authorship. All submitted manuscripts are rigorously screened for plagiarism using Turnitin (<https://www.turnitin.com/>). Plagiarism—including textual duplication, data fabrication or falsification, duplicate submissions, and improper attribution of authorship—constitutes a serious breach of ethical publishing practices and will not be tolerated. Concurrent submission of the same manuscript to multiple journals is also strictly prohibited.

To maintain scholarly integrity, manuscripts must have an overall similarity index below 20%, with no more than 5% similarity from any single source. It is the responsibility of the author(s) to ensure these thresholds are met and sustained throughout the review and publication process. While similarity reports provide a quantitative measure of textual overlap, legitimate citations and common academic language may contribute to the score. Therefore, editorial judgment is essential in interpreting these reports to determine if ethical concerns are warranted.

ETES maintains strict guidelines regarding the use of artificial intelligence in scholarly writing. The use of generative AI tools for drafting, composing, or editing the intellectual content of a manuscript is not permitted. Manuscripts must reflect the original work and critical thinking of human authors. Authors are required to confirm, upon submission, that the content has not been produced or substantively modified by AI tools. Minor AI-assisted improvements for grammar or language clarity are acceptable, but their use

Blank Page

should not compromise the authenticity or originality of the research. AI-generated images are generally prohibited unless explicitly disclosed, clearly labeled, and appropriately cited.

Open Access

In alignment with the principles of transparency, accessibility, and knowledge dissemination upheld by Emerging Trends in Engineering and Sustainability (ETES), all published articles are made freely available to the public without any subscription or access fees. The journal operates under the Creative Commons Attribution 4.0 International License (CC BY 4.0) [<https://creativecommons.org/licenses/by/4.0/legalcode>], which permits users to freely access, download, reproduce, distribute, and share the full content of the articles in any format or medium. Furthermore, readers may link to, index, or utilize the articles for scholarly purposes, provided that appropriate credit is given to the original author(s) through proper citation.

Authors retain full copyright of their published work, while ETES ensures that their intellectual contributions receive due recognition in accordance with the licensing terms. This licensing framework fosters open scientific communication and encourages the broad dissemination and reuse of research in engineering and sustainability, supporting global efforts towards sustainable development and innovation.

Blank Page

Guidelines for Authors

Manuscript Preparation

Emerging Trends in Engineering and Sustainability (ETES) is a multidisciplinary, double-blind, peer-reviewed journal committed to publishing high-quality research that spans all areas of engineering, with a particular emphasis on innovations that promote sustainability. The journal strictly adheres to the ethical guidelines set forth by the Committee on Publication Ethics (COPE) to maintain the integrity of the scholarly record. To ensure originality, all submissions undergo thorough screening using advanced plagiarism detection software. Authors are expected to disclose any potential conflicts of interest in their cover letter. Manuscripts that do not comply with the journal's *Instructions for Authors* will not be considered for further processing.

Submission Declaration and Verification

By submitting a manuscript to *Emerging Trends in Engineering and Sustainability (ETES)*, authors affirm that the work is original and has not been previously published, except in limited forms such as abstracts, academic theses, or invited lectures. The submission must not be under review or consideration by any other journal or publication outlet. Furthermore, all listed authors must have approved the submission, and, where applicable, authorization must be granted by the relevant institutional or organizational authorities where the research was conducted. Authors also agree that, if accepted, the manuscript will not be published elsewhere in the same or substantially similar form, in English or any other language, including electronic platforms. To ensure adherence to these standards, all submissions may be subjected to plagiarism and duplication checks using Crossref Similarity Check and other recognized originality verification tools.

Language and Manuscript Submission

Manuscripts submitted to *Emerging Trends in Engineering and Sustainability (ETES)* must be written in clear, high-quality English. Either American or British English is acceptable, but consistency in spelling and usage must be maintained throughout the manuscript. Authors may use AI-assisted tools strictly to enhance grammar and readability; however, the intellectual content, structure, and originality of the manuscript must remain the authors' own.

Peer Review Policy

Emerging Trends in Engineering and Sustainability (ETES) adheres to a double-blind peer review process to ensure objectivity, fairness, and academic integrity. In this model, the identities of both authors and reviewers are concealed throughout the review process. All submitted manuscripts are typically evaluated by a minimum of two independent experts with relevant subject-matter expertise, who assess the originality, scientific merit, methodological soundness, and relevance of the work.

The final decision regarding the acceptance, revision, or rejection of a manuscript lies solely with the Editor, who considers reviewers' feedback alongside the manuscript's alignment with the journal's scope and quality standards. All editorial decisions are final.

To maintain transparency and avoid conflicts of interest, Editors are excluded from the review and decision-making process for manuscripts in which they have a personal, professional, or financial interest—including submissions authored by themselves, their colleagues, or family members. In such cases, an independent editor will be assigned to oversee the peer review process to uphold the journal's ethical standards.

Template Compliance

All authors are required to prepare and submit their manuscripts in strict adherence to the *Emerging Trends in Engineering and Sustainability (ETES)* manuscript template. The template has been designed to ensure consistency, clarity, and a professional appearance across all submissions. Authors must carefully follow all formatting guidelines, including the prescribed font styles, section headings, and layout specifications.

Under no circumstances should the template's header, footer, page size, or margin settings be altered. These elements are essential for maintaining uniformity in the publication process.

Blank Page

Additionally, all figures, tables, and equations are should be embedded appropriately within the template and labeled according to the ETES style guide.

In addition to the manuscript, author(s) are required to submit the followings:

- Cover letter
- Title Page
- Copyright Form.

Authors must ensure that their full names and institutional affiliations are presented accurately and consistently in the manuscript, as specified in the ETES template. Affiliations should include the department (if applicable), institution or university, city, and country. This information must appear directly below each author's name as formatted in the template.

Generative AI Policy for Authors

Emerging Trends in Engineering and Sustainability (ETES) upholds the highest standards of research integrity, originality, and authorship. In alignment with these principles, the use of generative AI or AI-assisted technologies for drafting, writing, or substantively editing the content of a manuscript is strictly prohibited. Authorship entails full intellectual responsibility for the work submitted, including its conception, methodology, analysis, interpretation, and written expression—responsibilities that cannot be delegated to non-human tools.

Manuscripts must be the product of human scholarly effort and critical thinking. Text generated by AI, even when used for language refinement or content development, poses significant risks of inaccuracy, bias, lack of originality, and potential plagiarism. Furthermore, reliance on such tools may obscure issues related to authorship attribution and accountability.

Authors are required to affirm, upon submission, that the manuscript has been written entirely by the listed authors without the use of generative AI tools. Failure to comply with this policy may result in the rejection of the submission or retraction of the published article, in accordance with the journal's ethical guidelines and the standards of the Committee on Publication Ethics (COPE).

The use of **AI-generated images** is generally not allowed unless explicitly disclosed in the captions and subject to thorough review. Authors must ensure that any such images are clearly identified and accompanied by appropriate citations and permissions, as necessary.

Authors should only use the AI-assisted technologies for enhancing readability and language of their manuscript.

AI Declaration Statement

The authors are responsible for completing the **AI Declaration Statement** in ETES word Template. The **statement is:** “The authors confirm that the manuscript has been written without the assistance of generative AI or AI-based writing tools.”

Blank Page

ETES Copyright and License Agreement (Open Access – CC BY 4.0)

Title of Paper/Article:

Contributing Author(s):

i. License of Publishing Rights

I (we), the undersigned author(s), hereby grant to the Emerging Trends in Engineering and Sustainability (ETES) an exclusive license to publish the above-titled article in all formats (print, electronic, and future technologies), in all languages and media, worldwide, for the full duration of copyright. This includes the right to reproduce, archive, disseminate, and distribute the Article, and to authorize others to do so for scholarly purposes.

The author(s) retain full copyright in the Article.

ii. Open Access and Licensing

The Article will be published under the terms of the Creative Commons Attribution 4.0 International License (CC BY 4.0).

This license permits others to:

- Share — copy and redistribute the material in any medium or format
- Adapt — remix, transform, and build upon the material for any purpose, including commercial use

As long as appropriate credit is given to the original author(s), a link to the license is provided, and it is clearly indicated if changes were made.

License link: <https://creativecommons.org/licenses/by/4.0/>

iii. Author Reuse Rights

The author(s) retain the right to:

- Reuse the Article in their own future works (books, compilations, theses, etc.)
- Deposit the Article in institutional or subject repositories
- Share the Article via personal websites or academic networks
- Use the Article for teaching, presentations, and other academic purposes

All reuse must credit the original publication in ETES and include a link to the published version and CC BY license.

iv. Supplemental Materials

If any Supplemental Materials (e.g., data sets, videos, software, enhanced graphics) are submitted along with the Article, ETES has the non-exclusive right to publish and link to these materials in any media or format.

The author(s) confirm they have secured all necessary permissions for such materials.

v. Reversion of Rights

If the Article is not accepted for publication or is withdrawn prior to acceptance, this license agreement becomes null and void. However, ETES may retain a non-public archival copy for record purposes.

vi. Revisions and Addenda

No changes to this License Agreement shall be valid unless confirmed in writing by ETES. This agreement supersedes any prior agreements regarding the Article.

vii. Warranties and Author Declarations

The author(s) declare that:

- The work is original and has not been published elsewhere,
- All co-authors have reviewed and approved the manuscript,
- The Article does not infringe any copyright, patent, or other rights,
- Necessary permissions for third-party materials have been obtained,
- There are no undisclosed conflicts of interest.

viii. Indemnification

The author(s) agree to indemnify and hold harmless ETES from any claims, damages, or expenses arising from a breach of the above warranties.

ix. Joint Authorship

For jointly authored works, all authors must sign this agreement, or one author must sign with authority on behalf of all listed authors.

Author's Name	Signature	Date

Blank Page

Contents

Volume 02, No. 01 (2026)

Paper Title	Pages
Comparative Analysis of Fatigue Performance in Asphalt Concrete Modified with Nano-Alumina and Nano-Silica	1-12
Amjad H. Al Bayati, Ali M. Al Hamdou	
Multi-Functional Enhancement of Water-Based Drilling Fluid Using Copper Nanoparticles: A Study on Lubricity, Rheology, and Filtration Properties	13-20
Massara S. Hameed, Nada S. Al-Zubaidi, Asawer A. Alwasiti	
A Quantitative Analysis of Factors Affecting the Adoption of Micro-management in Engineering Projects	21-29
Tamara A. Obaid, Hatem K. Breesam	
Optimization of ESP Performance Using Pump Frequency and Wellhead Pressure Sensitivity Analysis in the Rmelan Oil Field (PIPESIM-Based Study)	30-42
Ahmed M. Hussein, Abu Zied Ahmed, Tarek M. Aboul-Fotouh, Sayed Gomaa	
Effect of Solar Module Operating Temperature on Electric Parameters of Photovoltaic Monocrystalline Module	43-50
Nadeem F. Kadhum, Emad T. Hashim	
Simulation Approaches for Polyurethane Materials: A Multiscale Review	51-64
Ahmed K. Al-Kamal	

Blank Page



IRAQI
Academic Scientific Journals



Comparative Analysis of Fatigue Performance in Asphalt Concrete Modified with Nano-Alumina and Nano-Silica

Amjad H. Al Bayati¹  , Ali M. Al Hamdou¹  , Yu Wang²  

¹ Department of Civil Engineering, College of Engineering, University of Baghdad, Baghdad, Iraq.

² School of Science, Engineering & Environment, University of Salford, Manchester M5 4WT, UK

Article Info	ABSTRACT
<p>Received: 04 Dec. 2025 Revised: 24 Dec 2025 Accepted: 12 March 2026 Available online: 31 March 2026</p> <p>Keywords: Nano-Aluminum Oxide; Nano-Silica Oxide; Asphalt binders; Fatigue Performance; Rheology; IDEAL-CT; LAS.</p>	<p>This comparative study systematically evaluated the fatigue and cracking performance of asphalt binder and asphalt concrete mixtures, modified with different dosages (2%, 4%, and 6% by binder weight) of Nano-Alumina (NA) and Nano-Silica (NS). The experimental methodology involved binder testing, including the evaluation of physical properties, rheological behaviour, and fatigue characteristics using the Superpave parameter ($G^* \sin \delta$) and Linear Amplitude Sweep (LAS) test. Additionally, compatibility was assessed through storage stability testing and Scanning Electron Microscopy (SEM). Mixture performance was evaluated using Indirect Tensile Cracking Test (IDEAL-CT) to determine the Cracking Tolerance Index (CT-Index), Flexibility Index (FI), and Crack Resistance Index (CRI). The results showed that nanomaterials substantially improved binder stiffness and thermal stability, with (NA) consistently causing the strongest stiffening effect, indicating that NA provided a stable and gradual improvement in fatigue life from 2% to 6%. (NS) showed a strong effect on increasing viscosity, achieving better initial cracking tolerance and fatigue life at low concentrations (2% to 4%). Notably, the study identified a narrow optimal range for NS; at 6%. NA provided a balanced improvement, maximizing CT-Index at 6% and CRI at 4%, while NS achieved very high CT-Index at 2% but decreased at higher dosages. Collectively, an optimal practical dosage of 2–4% for NS and 4–6% for NA are recommended, highlighting the importance of material-specific optimization to achieve better durability and fatigue life under repeated loading.</p>

1. Introduction

Fatigue cracking, one of the principal distresses affecting flexible pavements, where, repeated traffic loading is identified as the primary cause of fatigue damage and subsequent loss of serviceability [1]. Fatigue distress in asphalt cement (AC) generally occurs through two mechanisms, cohesive failure within the mastic phase and adhesive failure at the AC–aggregate interface [2]. The mechanical response of asphalt binder is governed by loading duration,

temperature, and the level of applied stress or strain. At short loading times, the binder exhibits largely elastic behavior, comparable to its response at low temperatures, due to limited time for molecular rearrangement. In contrast, elevated temperatures or prolonged loading periods (or low loading rates) promote a more viscous response [3,4].

Fatigue life varies according to mixture properties, asphalt layer thickness, loading mode and frequency, rest periods between loads, and the environmental conditions [5]. Laboratory methods



used to quantify fatigue performance may include four-point bending beam fatigue test and the indirect tensile fatigue test, conducted under either stress- or strain-controlled mode [6,7]. Numerous studies have confirmed a strong correlation between binder-level and mixture-level performance [8–10]. Additionally, extensive research demonstrated that nanomaterial modification of asphalt binders significantly enhanced pavement performance [11].

Saltan et al. [12] reported that 0.3% NS dosage produced the most favorable fatigue performance in Dynamic Shear Rheometer (DSR) testing, whereas lower or higher dosages resulted in diminished benefits. Similarly, Leiva-Villacorta et al. [13] concluded that adding (3–6% NS) improved fatigue resistance, while 0.5% produced adverse effects, highlighting the sensitivity of binder behavior to NS content. Nazari et al. [14] confirmed that (2–4% NS) extended fatigue life at all shear strain levels due to the formation of a reinforcing nano-network within the binder. Complementary results were reported by Shafabakhsh et al. [15], who found that (4–6% NS) enhanced fatigue life in both LAS and four-point bending tests, with performance declined at 8% under aging conditions. The findings designate that fatigue performance of NS-modified asphalt is highly dosage-dependent, with optimal contents varying according to binder characteristics, nano-silica properties, and the applied testing methodology.

As for NA, Eghlim et al. [16] demonstrated substantial improvements in fatigue life across a wide temperature and stress range (2–8% NA), with 8% providing the best performance due to enhanced cohesion and adhesion at the binder–aggregate interface. Karahancer et al. [17] also observed consistent gains in fatigue performance for mixtures modified with 3–7% NA, with an optimum at 5%. Bhat et al. [18] showed that low NA dosages (0.5–2%) improved fatigue response at 25°C using Time Sweep Test, while Mamuye et al. [19] reported increased CT Index values in IDEAL-CT testing for binders modified with 1–3% NA, with the highest enhancement at 3%.

The present study aims to systematically evaluate and compare the fatigue performance of asphalt binders and mixtures modified with nano-silica (NS) and nano-alumina (NA). By investigating the influence of these nanomaterials

on binder rheology and mixture cracking resistance, the research seeks to identify the optimal additive type and dosage for enhancing durability and fatigue life under static loading. Experimental procedure employed in this study is summarized in the workflow presented in Figure 1.

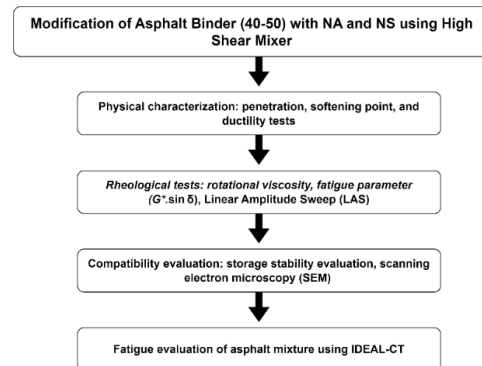


Figure 1. Workflow for Experimental Evaluation of Nano-Modified Asphalt Binders and Mixtures.

2. Materials

2.1. Asphalt Binder

Asphalt binder with penetration grade 40–50 is implemented within the course of experimental course for this study, its obtained from the Dora refinery, south-west of Baghdad. The physical and rheological properties as per the standard tests and the Superpave PG system (AASHTO M320 [20]) are summarized in Table 1.

Table 1. Physical and Rheological Behavior of 40–50 Asphalt Binder.

Property	Standard	Measured value	Limit
Penetration (0.1 mm)	AASHTO T 49	44	(40–50)
Ductility (cm)	AASHTO T 51	+100	>100
Softening point (°C)	AASHTO T 53	48.7	-
Rotational Viscosity (mPa·s)	AASHTO M 320	745	3000 (max)
$G^* \sin \delta$ (kPa) (70 °C and 76 °C)	AASHTO M 320	1.45 and 0.70	1.00 kPa (min)
Mass loss (%)	AASHTO M 320	0.254	1% (max)
$G^* \sin \delta$ (kPa) (22°C and 25 °C)	AASHTO M 320	6796 and 5019	5000 kPa (max)

2.2. Nanomaterials

Two inorganic nanomaterials are implanted in this study, these are NS and NA. They were added to asphalt binders to improve performance. NS increases viscosity, stiffness, and fatigue resistance due its fine, porous structure as well as high surface area [24], in the other hand, NA enhances stiffness, thermal stability, and crack resistance via mechanical interlocking [25]. The physical properties of NS and NA employed in this study are summarized in Table 2. Scanning Electron Microscopy (SEM) analysis (Figure 2) revealed the distinct microstructural features of NS and NA, providing a microstructural basis for the observed improvements in rheological and mechanical behavior of the modified asphalt binders. In this study, both NS and NA were incorporated at dosages ranging from 2% to 6% by binder weight, which were selected to optimize the balance between enhanced stiffness and fatigue performance while maintaining acceptable workability and minimizing the risk of particle agglomeration.

Table 2. Physical Characteristics of Nano-Silica and Nano-Alumina.

Properties	Nano-Alumina	Nano-Silica
Chemical formula	Al ₂ O ₃	SiO ₂
Appearance	White Powder	White Powder
Average particle size (nm)	10–20	25–35
Purity (%)	99.9	99.8
Specific surface area (m ² /gm)	120–160	190–250
Bulk Density (g/mL)	0.2	0.08
Nanomaterials Prices (USD/kg)	28.5	26.8

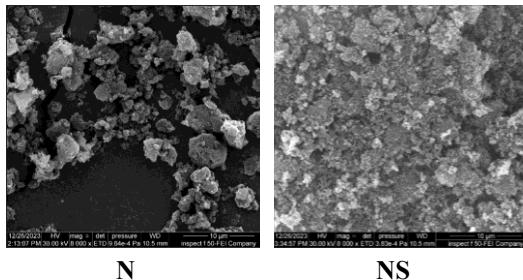


Figure 2. SEM images of nanomaterials used in asphalt modification at 8,000× magnification.

2.3 Aggregate Materials

The study used Type D5 aggregate gradation per ASTM D3515 [26], ensuring dense-graded mixtures with adequate durability, stability, and resistance to traffic deformation. The gradation and limits are shown in Figure 3

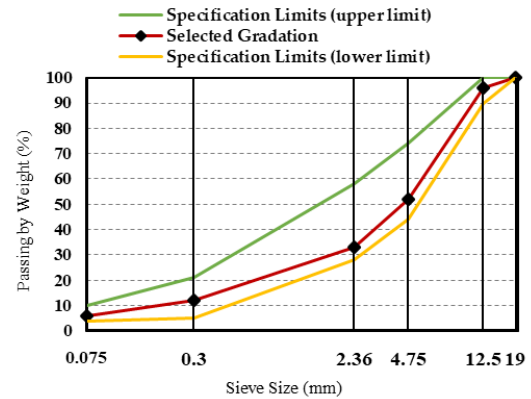


Figure 3. Gradation and Specification Limits of Surface Coarse Aggregates.

3. Preparation of Test Specimens

The selection of mixing and blending procedures for nano-modified asphalt binders therefore often depends on expert judgment. Following this approach, Al-Bayati et al. [27] incorporated nano-silica, titanium, and alumina at dosages of 2%–8% by binder weight, employing a dry mixing process at (140 °C, 4000 rpm, 20 minutes), with nanomaterials added at a rate of 4 g/min. In the present study, NS and NA were added at 2%–6% by binder weight to 500 g of asphalt. Initial blending was conducted using a high-shear mixer at 400 rpm, with 10 g of nanomaterials introduced gradually over 4 minutes (2.5 g/min) at 140 °C, then subjected to high-shear mixing (3000 rpm) at 140–150 °C for 20 minutes to ensure uniform dispersion.

4. Experimental Methodology for Materials Testing

4.1 Evaluation of Physical Properties

In the scope of this research, a series of standardized tests were performed on asphalt binders to determine their performance characteristics. To evaluate the consistency of the binder, the Penetration Test was conducted in accordance with ASTM D5-06. The binder's thermal susceptibility, an indicator of its

performance at high in-service temperatures, was assessed using the Softening Point Test as specified by ASTM D36-06. The binder tensile deformation capacity for was evaluated using ductility tests at 25 °C as per the ASTM D113. Collectively, these tests provide a comprehensive characterization of modified binder fundamental behavior.

4.2 Evaluation of Rheological Properties

4.2.1 Rotational viscosity (RV)

This parameter was measured to evaluate flow behavior at elevated temperatures, which is critical for mixing and compaction processes. Testing was conducted according to AASHTO T316, using a rotational viscometer at 135 °C.

4.2.2 Fatigue parameter assessment of asphalt binders

For the Pressure Aging Vessel (PAV) aged which simulated asphalt binder field condition (after placement), fatigue parameter $G^* \sin \delta$ was assessed using the Anton Paar – Smart Pave 102e Dynamic Shear Rheometer (DSR) system (figure 4), following the procedures outlined in AASHTO T315. [28]. The assessment aimed to characterize the viscoelastic response under repeated loading and resistance to fatigue cracking. The fatigue parameter ($G^* \sin \delta$) was measured at 25 °C, specification limit of 5000 kPa was applied to control fatigue susceptibility.

4.2.3 LAS test

Linear Amplitude Sweep (LAS) test on a DSR with 8 mm parallel plates and a 2 mm gap (figure 5) was conducted following AASHTO T391 and T315. Binder samples were aged via RTFOT (AASHTO T240) and PAV (AASHTO R28) prior to testing. The test included a frequency sweep at 0.1% strain 0.2–30 Hz (linear viscoelastic behavior), followed by an amplitude sweep at 10 Hz with strain increasing from 0% to 30% over 3100 cycles. Shear strain, shear stress, phase angle (δ), and complex modulus (G^*) were recorded, and fatigue life (Nf) was predicted using the VECD framework (Equation 1).

$$Nf = A(Y_{max})^{-B} \quad \text{Eq. (1)}$$

Where: Y_{max} = estimated maximum strain anticipated within the pavement structure, A = describes the binder's damage evolution behavior

and B = intrinsic property of the binder in its undamaged state.



Figure 4. Smart Pave

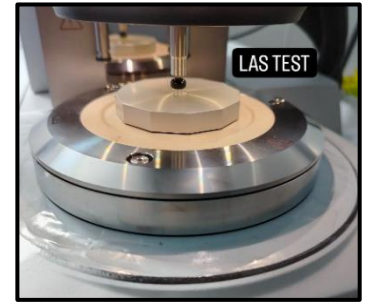


Figure 5. LAS test.

4.3 Compatibility Assessment

The asphalt binders' storage stability was assessed by placing the materials in aluminum tubes (14 cm × 3.5 cm), sealing them, and storing them vertically by conditioning at 163°C for 48 hours. After cooling, each tube was sectioned into three equal parts, and the softening points of the top and bottom segments were determined. A temperature stability difference of 2.5 °C or less was regarded as acceptable, whereas larger differences signaled phase separation [32,64].

Microstructural characterization was performed using a VEGA- II apparatus (up to 2000×) to examine particle distribution and dispersion within the binder.

4.4 Marshall Mix Design

The test was performed according to ASTM D6926 [33]. Specimens were compacted with 75 blows per face. Stability, flow, air voids, and VMA were determined following ASTM D6927, D2726, and D2041 [34–36]. The control mixture's optimum asphalt content was established at 5.0% and consistently applied to all nano-modified mixtures, ensuring that performance differences were exclusively due to the type and concentration of nanomaterials.

4.5 Evaluation of Asphalt Mixture Fatigue Performance

The Indirect Tensile Cracking Test (IDEAL-CT) was conducted to evaluate the fatigue resistance of asphalt concrete specimens with dimensions of 101.6 mm (4 in.) in height and 63 mm (2.5 in.). This test, known for its simplicity

and efficiency, involved subjecting the cylindrical specimens to a consistent vertical load, recording load and displacement data. The specimens were compacted to an air void level of around ($4 \pm 0.5\%$) using a Marshall compactor. The test was conducted following ASTM D8225 [37], During the test, specimens were loaded diametrically at 50 mm/min and tested at 25 °C using a 12.7 mm loading strip. Each set of samples was tested in triplicate, and the average results were reported. CT Index was calculated using Equation (2).

$$CT_{Index} = \frac{t}{62} \times \frac{i_{75}}{D} \times \frac{G_f}{m_{75}} \times 10^6 \quad \text{Eq. (2)}$$

Where: G_f = fracture energy, m_{75} = post-peak slope at 75% of the peak load, i_{75} = displacement at 75% of peak load during IDEAL-CT test.

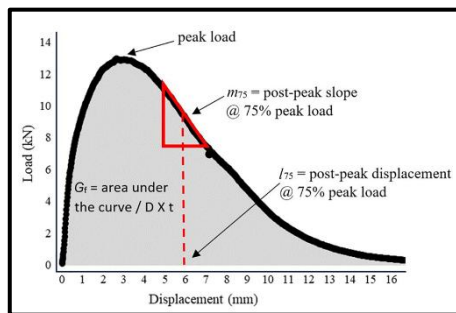


Figure 6. IDEAL-CT load–displacement curve.

The Flexibility Index (FI) and Crack Resistance Index (CRI) were calculated to provide a more comprehensive analysis of the fatigue behavior of the asphalt mixtures [38]. The FI was determined using Equation (3), while the CRI was evaluated using Equation (4):

$$FI = \frac{G_f}{|m|} \times 0.01 \quad \text{Eq. (3)}$$

Where: FI = flexibility index, G_f = fracture energy (J/m²), m = post-peak slope (kN/mm),

$$CRI = \frac{G_f}{P_{max}} \quad \text{Eq. (4)}$$

Where: CRI = Crack Resistance Index, G_f = fracture energy and p_{max} = peak load.

5. Results and Discussion

5.1 physical test Results

The physical properties (figure 7-9) demonstrate that incorporating NA and NS

noticeably enhanced binder consistency and thermal stability relative to the neat asphalt. Penetration decreased substantially with nano-aluminum, falling from 44 to 22 (0.1 mm), representing a 50% reduction, while nano-silica produced decreases of 4.5%, 2.3%, and 13.6% at 2%, 4%, and 6%, respectively confirming increased hardness for both modifiers. Softening point improved consistently, with nano-aluminum increasing it by 11.3%, 11.0%, and 14.6%, and nano-silica producing increases of 10.1%, 8.0%, and 17.5%, reflecting enhanced high-temperature stiffness. Ductility remained unchanged at 100 cm for all nano-aluminum dosages and for nano-silica up to 4%, while a slight decline to 95 cm (5% decrease) at 6% nano-silica suggests a minor reduction in elongation only at higher loading. The improvement in softening point with nano-aluminum is attributed to the formation of a nanoparticle network that enhances thermal stability [39], consistent with previous findings [40,41]. For nano-silica, the increases in hardness and softening point are related to its adsorption of light volatiles, rise in asphaltene content, and strong molecular interactions resulting from its high surface area and reactive surface chemistry, which enhance interaction with the asphalt matrix [42,43], consistent with findings from previous studies that reported similar improvements in binder stiffness upon nanomaterial incorporation [44,12,45].

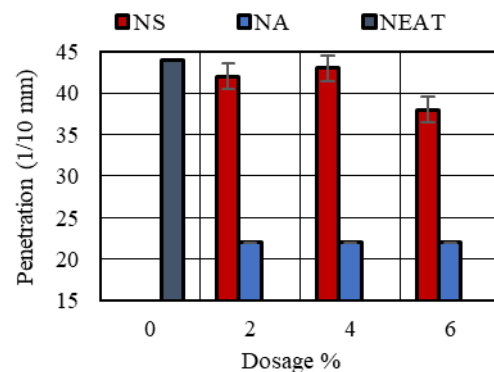


Figure 7. Penetration of nano-modified asphalt.

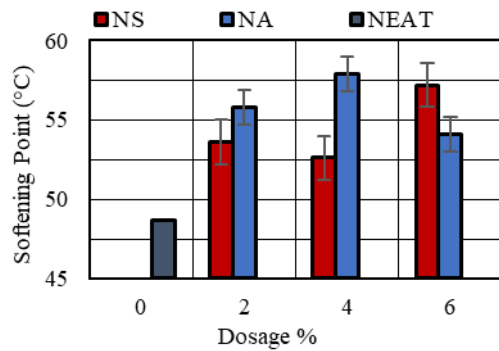


Figure 8. Softening of nano-modified asphalt.

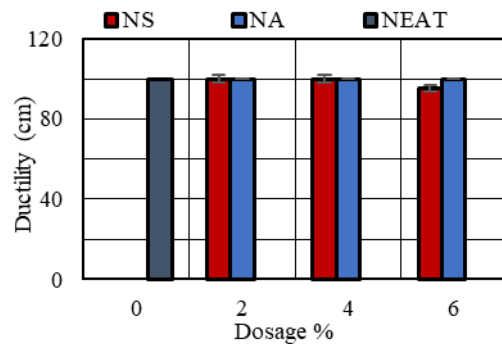


Figure 9. Ductility of nano-modified asphalt.

5.2 Evaluation of Rheological Properties

5.2.1 Rotational Viscosity Assessment

The results of RV exhibited in Figure 10 show a clear stiffening effect resulted from the use of both nanomaterials, i.e. nano-aluminum oxide (Al_2O_3) and nano-silica (SiO_2), as all modified binders showed higher viscosity than the neat asphalt (745 mPa·s). For nano-aluminum, RV increased to 1112, 1214, and 1245 mPa·s at 2%, 4%, and 6%, corresponding to 49.2%, 62.9%, and 67.2% increases. NS displayed a similar pattern, with RV rising to 1129, 1183, and 1368 mPa·s, representing increases of 51.5%, 58.8%, and 83.6% of each dosage respectively. Strong viscosity-building effect of nano-silica is attributed to high surface area and reactivity [46], absorption of maltene components which increases asphaltene content [47], and the diffusion of silica particles into the binder that reduces oily fractions and introduces stiffer solid phases [48]. Additionally, the hardening effect is reinforced by improved dispersion of NS layers, which could result in an improved bonding strength via restricting binder flow [49]. For NA, the viscosity increase arises from its stiffening effect and high surface area that increases particle

interactions and promotes stronger attraction with surrounding asphalt molecules [19], further supported by better dispersion that limits binder mobility and strengthens the matrix [50].

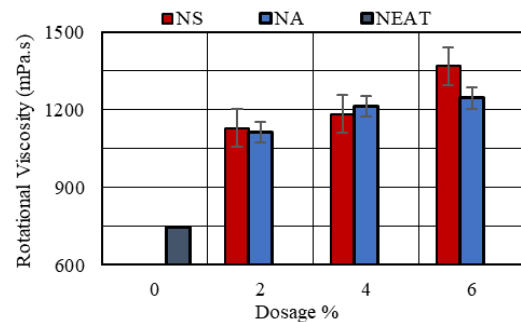


Figure 10. Viscosity Behavior of Modified Asphalt Binder

5.2.2 Results of the Rheological Fatigue Indicator ($G^* \cdot \sin \delta$)

The $G^* \cdot \sin \delta$ fatigue parameter in Figure 11 reflects the influence of nano-aluminum oxide (Al_2O_3) and nano-silica (SiO_2) on the binder's susceptibility to fatigue cracking. For NA, the 2% dosage produced a slight increase (1.0%), indicating no improvement in fatigue performance, whereas the 4% and 6% dosages resulted in substantial reductions of 28.2% and 15.2%, respectively. A notable enhancement in the binder's fatigue resistance at intermediate and higher contents, is likely due to improved viscoelastic balance and greater energy dissipation capacity under repeated loading. NS at 2% and 4% produced identical reductions (15.4%). The 6% NS produced an increase of 11.4, possibly due to particle agglomeration or excessive stiffening that limits the binder's ability to dissipate strain energy. Both nanomaterials enhanced fatigue performance at specific optimal dosages, confirming their ability to improve the resistance to microcrack initiation and propagation, findings are consistent with the previous studies reporting fatigue resistance improvements in nano-modified asphalt binders [50, 51, 52].

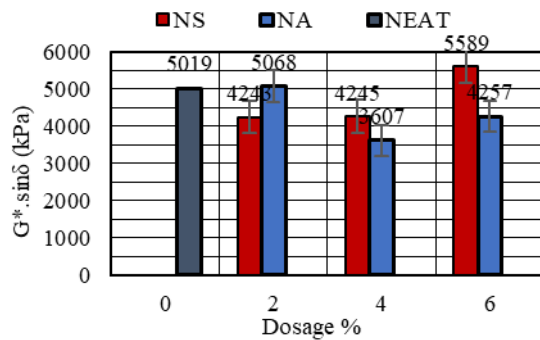


Figure 11. $G^* \cdot \sin \delta$ for Neat and Nano-Modified Asphalt Binders (25 °C).

5.2.3 LAS Test Results

The incorporation of nanoparticles altered the mechanical behavior and fatigue performance of asphalt binders, with distinct effects observed for NS and NA. When comparing the NEAT binder which exhibited the highest ultimate shear stress, modified binder with 2%, 4%, and 6% NS showed slightly reduced peak stresses, with corresponding strains at maximum stress of 19.1%, 20.1%, and 18.1%, respectively. The reduction in ductility at higher NS dosages, particularly at 6%, suggests that excessive nanoparticle addition slightly stiffen the binder matrix, restricting large deformations prior to failure. Despite this modest reduction in peak stress, fatigue life was substantially enhanced across both 2.5% and 5% strain levels, with the greatest improvement observed at 2% NS (16.6×10^6 and 6.42×10^5 cycles), followed by minor decreases at 4% (16.17×10^6 and 6.31×10^5 cycles) and 6% (16.08×10^6 and 5.46×10^5 cycles). This pattern emphasized the existence of an optimal NS dosage, beyond which benefits plateau or slightly diminishes. The improvements are mostly attributed to high specific surface area, which promotes uniform dispersion, strengthens the internal microstructure, and delays microcrack initiation [53, 54, 55].

For NA, the strain at ultimate stress decreased with increased dosage, from 20.11% for the NEAT binder to 19.10%, 18.09%, and 17.13% for 2%, 4%, and 6% NA, respectively. Unlike NS, the fatigue performance of NA-modified binders exhibited a consistent, dose-dependent improvement across both strain levels, with fatigue life increasing from 9.64×10^6 and 3.84×10^5 cycles for the NEAT binder to 1.59×10^7 , 1.81×10^7 , and 2.08×10^7 cycles at 2.5% strain, and 5.80×10^5 , 7.04×10^5 , and 8.35×10^5 cycles at 5% strain for 2%,

4%, and 6% NA, respectively. NA ability to reinforce the binder matrix, improve microstructural integrity, enhance energy dissipation, and delay crack nucleation and propagation under repeated loading led to its superior performance [56, 57]. While both NS and NA improved fatigue resistance, NS showed better performance at lower dosages due to potential agglomeration at higher contents, whereas NA provided consistent, dose-dependent reinforcement, this emphasized the importance of nanoparticle type and dosage optimization. Figure 12 depicts the stress–strain behavior of asphalt binders modified with different nanoparticles, whereas Figure 13 shows the corresponding fatigue life curves.

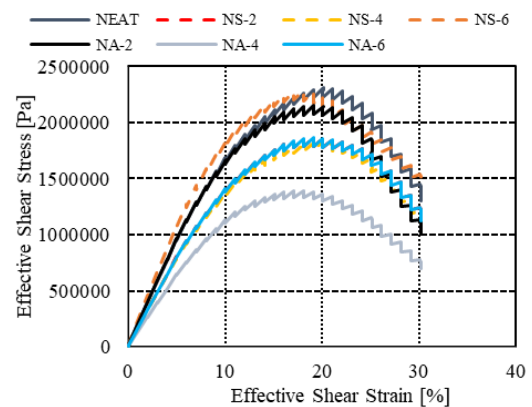


Figure 12. Characterization of Shear Stress–Strain Performance in Nanomodified Asphalt Binders

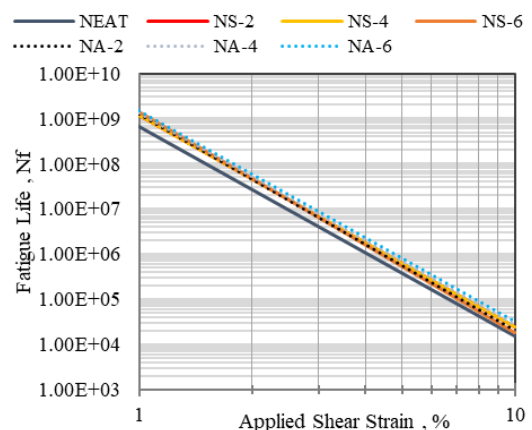


Figure 13 Fatigue Life Response of Asphalt Binders Modified with Nanomaterials

5.3 Results of the Compatibility Assessment

5.3.1 Findings of the Storage Stability Test

The storage-stability results (figure 14) show that adding (NA) and (NS) increased softening-point separation (ΔSP), indicating reduced thermal stability compared with the neat binder (0.5°C). For NA, ΔSP rose from about 0.8°C at 2% to 1.1°C at 4% and 1.6°C at 6%, reflecting a clear decline in stability with dosage. NS showed lower separation, increasing from roughly 0.3°C at 2% to 0.8°C at both 4% and 6%, suggesting better stability than NA at higher contents. Although both nanomaterials exhibit some segregation, all ΔSP values remain within an acceptable range.

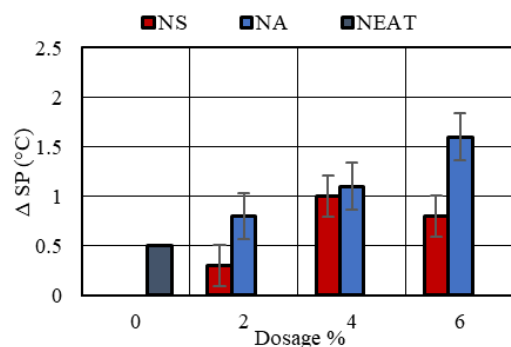


Figure 14. Variation in Asphalt Binder Softening Point (ΔSP) with Different Nanomaterial Dosages.

5.3.2 Microstructure Analysis of Nano-Modified Asphalt Binder

The Scanning Electron Microscopy (SEM) evaluation (Figure 15) demonstrated clear variations in surface morphology between the neat asphalt and the binders modified with nano-silica (NS) and nano-alumina (NA) at concentrations of 2%, 4%, and 6%. The neat asphalt displayed a typically smooth, amorphous, and mildly undulating surface. Incorporation of NS produced a gradual increase in surface roughness and heterogeneity with rising dosage, with the 6% NS sample exhibiting pronounced textural irregularities, reflecting reduced uniformity in particle distribution. In contrast, the NA-modified binders showed more uniform dispersion at lower dosages (2% and 4%). At 6% NA, the surface appeared relatively smooth but characterized by distinct, deeper wrinkle-like features, which may indicate the development of an internal nanoscale reinforcement network, suggesting enhanced compatibility and potentially more favorable

implications for the structural integrity and rheological behavior of the asphalt binder.

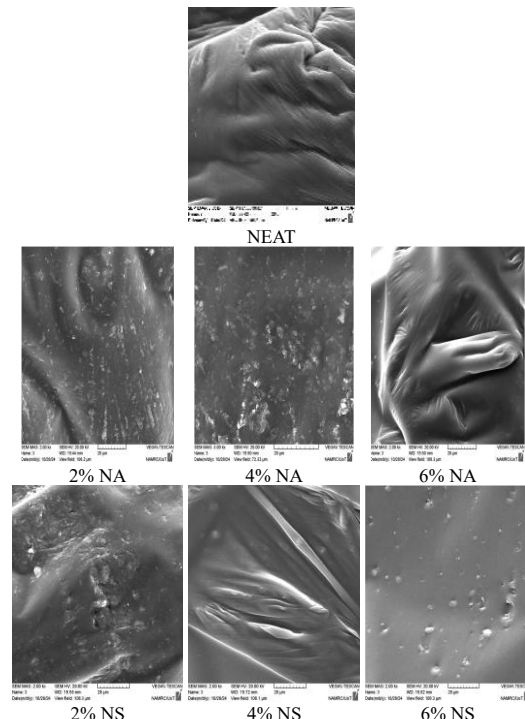


Figure 15. SEM of NEAT and nano-modified asphalt binder.

5.4.1 IDEAL CT Test Results

As presented in figure 16-18, incorporation of (NA) and (NS) induced notable variations in fatigue performance of asphalt binder, which was quantitatively assessed using the CT-Index, Flexibility Index (FI), and Crack Resistance Index (CRI). For NA modified binder, CT-Index increased markedly from 35 in the NEAT binder to 65, 78, and 84 for 2%, 4%, and 6%, respectively, indicating improved resistance to fatigue initiation. FI values exhibited a peak (21.77) at 2%, followed by a slight decline at higher concentrations. This result may imply that moderate NA dosages enhance binder flexibility, whereas excessive addition may compromise ductility. Similarly, CRI reached its maximum at 4% (604.81). Reducing the sensitivity of asphalt mixtures to temperature and stress is an effective approach to prolong their fatigue life, and the application of NA achieves this purpose [58, 59]. In contrast, NS modified binders displayed a distinct trend. The CT-Index attained its highest value at 2% (105), substantially exceeding those of NA modified and NEAT binders, superior initial fatigue resistance at low NS content was observed. However, further increases in NS concentration to

4% and 6% resulted in reduced CT-Index values (59 and 53, respectively), this shows the potential detrimental effects of excessive NS on fatigue performance. When viewing figure 17, FI parameter was decreased progressively with increasing NS content, from 21.85 at 2% to 13.64 at 6%. CRI followed a similar pattern, peaking at 4% (615.53) before declining slightly at NS-6%, suggesting the existence of an optimal NS concentration for crack resistance enhancement.

After the viewing the results, it verified that the incorporation of nanomaterials into asphalt significantly enhances its mechanical performance and durability [60]. Nanoparticles improve the viscoelastic properties of bitumen, increase tensile strain capacity, and delay micro-crack formation, thereby extending fatigue life compared to conventional binder [61,62]. Specifically, NS reduces micro-crack growth and resists creep-induced damage, resulting in higher fatigue life. Similar to NS, the addition of NA also improves fatigue performance and may enhance cohesion and adhesion between the modified bitumen and aggregates, minimizes relative aggregate displacement, and slows down crack initiation and propagation [16]. NA also reduces tensile strain and significantly prolongs the fatigue life of asphalt mixtures. Experimental results show that fatigue life and cumulative dissipated energy (CDE) increase with NS content across different strain levels, reflecting improved energy absorption and cracking resistance [63].

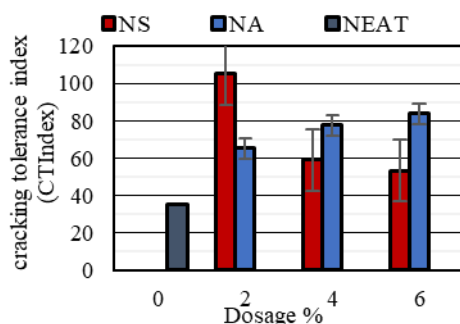


Figure 16. Cracking tolerance of modified asphalt mixture.

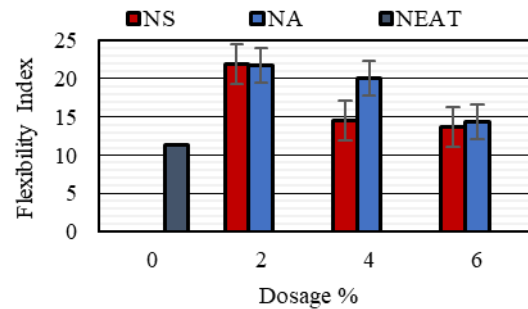


Figure 17. Flexibility Index of modified asphalt mixture.

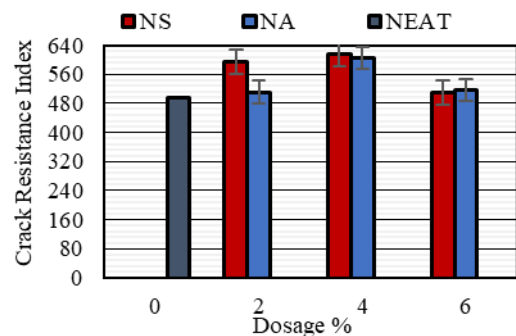


Figure 18. Crack Resistance Index (modified asphalt mixtures).

6. Conclusions

Within the limitations of materials and testing program used in this work, the following principal conclusions are made based on the findings of the investigations:

1. Both of the implemented nanomaterials, NS as well as NA. the physical, rheological and the resistance to fatigue cracking for the asphalt binder and hence asphalt mixtures are substantially improved. The improvement magnitude is mainly dependent on nanomaterials dosage.
2. Based on the physical tests, NA showed the most significant stiffening effect, reflected in a 50% reduction in penetration at 6%, while NS exhibited a pronounced increase in softening point at the same dosage. Rotational viscosity increased consistently for both modifiers, with NS particularly at 6% exhibiting the highest viscosity rise due to its superior surface area and stronger interaction with the binder matrix.

3. The surface roughness of the modified binder as evaluated based on the SEM microstructural analysis showed that NS, specifically at higher dosages is more heterogeneous than those muddled with NA. the latter promoted relatively uniform dispersion and the formation of a nanoscale reinforcement network at higher contents
4. At 4 and 6% dosages, NA improved fatigue resistance. In the other hand, NS performed optimally at 2% and 4%, with performance deterioration observed at 6%. The LAS results support these trends
5. Based on the asphalt concrete mixture performance against fatigue mode of distress, NA showed progressive improvements in CT-Index, FI, and CRI, with CT-Index maximizing at 6%, FI at 2%, and CRI at 4%. NS, conversely, exhibited exceptional fatigue tolerance at low dosage (CT-Index = 105 at 2%), while higher contents (4–6%) reduced flexibility and post-peak ductility, though CRI peaked at 4%, which indicates a narrow optimum window for effective performance.
6. The main findings which can be abstracted from the obtained results revealed that the optimal practical dosage for NS is approximately (2–4%), with 2% being the most effective for balanced fatigue and mechanical performance. Whereas for NA, the optimal dosage range lies between (4–6%), with 6% offering the most comprehensive improvement across binder- and mixture-level.

During this study, the performance was evaluated based on fatigue cracking. Other types of distresses which associated with the high environmental temperature, permanent deformation (rutting) as well as poor water drainage (moisture damage) should be further investigated to prove the overall performance of modified binder using the NS and NA. Also, the synergic use of these two nanomaterials could be further implemented. Also, assessing the economic feasibility, workability implications, and compatibility of these nanomaterials with different binder grades and aggregate types will

support broader implementation in pavement engineering practice.

Conflict of interest

The authors declare no conflicts of interest concerning this research.

Funding

No funding was received for conducting this study.

Author Contribution

A.H. Al Bayati: Supervision, Validation, Methodology, Selection of discussion sections, Writing – review & editing.

A.M. Al Hamdou and Yu Wang: Writing – original draft, Literature collection, Data organization, Writing – review & editing.

AI Declaration Statement

The authors confirm that the manuscript has been written without the assistance of generative AI or AI-based writing tools.

References

- [1] B. Sengoz and A. Topal, “Use of asphalt roofing shingle waste in HMA,” *Constr. Build. Mater.*, vol. 19, no. 5, pp. 337–346, 2005.
<https://doi.org/10.1016/j.conbuildmat.2004.08.005>
- [2] D. Cheng, D. Little, R. Lytton, and J. Holste, “Surface energy measurement of asphalt and its application to predicting fatigue and healing in asphalt mixtures,” *Transp. Res. Rec.*, vol. 1810, pp. 44–53, 2002.
<https://doi.org/10.3141/1810-06>
- [3] R. S. Lakes, *Viscoelastic Materials*. Cambridge, U.K.: Cambridge Univ. Press, 2009.
- [4] C. Hintz, “Understanding mechanisms leading to asphalt binder fatigue,” Ph.D. dissertation, Univ. Wisconsin–Madison, Madison, WI, USA, 2012.
- [5] H. Wen, “Fatigue performance evaluation of WesTrack asphalt mixtures based on viscoelastic analysis of indirect tensile test,” Ph.D. dissertation, North Carolina State Univ., Raleigh, NC, USA, 2001.

- [6] A. F. Mirhosseini et al., "Evaluating fatigue behavior of asphalt binders and mixes containing date seed ash," *J. Civ. Eng. Manag.*, vol. 23, no. 8, pp. 1164–1175, 2017. <https://doi.org/10.3846/13923730.2017.1396560>
- [7] F. Xiao, S. Amirkhanian, and C. H. Juang, "Prediction of fatigue life of rubberized asphalt concrete mixtures containing reclaimed asphalt pavement using artificial neural networks," *J. Mater. Civ. Eng.*, vol. 21, no. 6, pp. 253–261, 2009. [https://doi.org/10.1061/\(ASCE\)0899-1561\(2009\)21:6\(253\)](https://doi.org/10.1061/(ASCE)0899-1561(2009)21:6(253))
- [8] E. Santagata et al., "Correlating creep properties of bituminous binders with anti-rutting performance of corresponding mixtures," *Int. J. Pavement Res. Technol.*, vol. 10, no. 1, pp. 38–44, 2017. <https://doi.org/10.1016/j.ijprt.2016.11.008>
- [9] N. Saboo and P. Kumar, "Performance characterization of polymer modified asphalt binders and mixes," *Adv. Civ. Eng.*, vol. 2016, Art. no. 5938270, 2016. <https://doi.org/10.1155/2016/5938270>
- [10] F. Safaei, C. Castorena, and Y. R. Kim, "Linking asphalt binder fatigue to asphalt mixture fatigue performance using viscoelastic continuum damage modeling," *Mech. Time-Depend. Mater.*, vol. 20, pp. 299–323, 2016. <https://doi.org/10.1007/s11043-016-9304-1>
- [11] C. Fang et al., "Nanomaterials applied in asphalt modification: A review," *J. Mater. Sci. Technol.*, vol. 29, no. 7, pp. 589–594, 2013. <https://doi.org/10.1016/j.jmst.2013.04.008>
- [12] M. Saltan, S. Terzi, and S. Karahancer, "Examination of hot mix asphalt and binder performance modified with nano silica," *Constr. Build. Mater.*, vol. 156, pp. 976–984, 2017. <https://doi.org/10.1016/j.conbuildmat.2017.09.069>
- [13] F. Leiva-Villacorta and A. Vargas-Nordbeck, "Optimum content of nano-silica to ensure proper performance of an asphalt binder," *Road Mater. Pavement Des.*, vol. 20, no. 2, pp. 414–425, 2017. <https://doi.org/10.1080/14680629.2017.1385510>
- [14] H. Nazari, K. Naderi, and F. M. Nejad, "Improving aging resistance and fatigue performance of asphalt binders using inorganic nanoparticles," *Constr. Build. Mater.*, vol. 170, pp. 591–602, 2018. <https://doi.org/10.1016/j.conbuildmat.2018.03.107>
- [15] G. Shafabakhsh, M. Rajabi, and A. Sahaf, "The fatigue behavior of SBS/nanosilica composite modified asphalt binder and mixture," *Constr. Build. Mater.*, vol. 229, Art. no. 116796, 2019. <https://doi.org/10.1016/j.conbuildmat.2019.116796>
- [16] A. Lotfi-Eghlim and M. S. Karimi, "Fatigue behavior of hot mix asphalt modified with nano Al₂O₃—An experimental study," *Adv. Sci. Technol. Res. J.*, vol. 10, no. 31, pp. 58–63, 2016. <https://doi.org/10.12913/22998624/64011>
- [17] S. Karahancer, "Effect of aluminum oxide nanoparticle on modified bitumen and hot mix asphalt," *Pet. Sci. Technol.*, vol. 38, no. 13, pp. 773–784, 2020. <https://doi.org/10.1080/10916466.2020.1783292>
- [18] F. S. Bhat and M. S. Mir, "Investigating the effects of nano Al₂O₃ on high and intermediate temperature performance properties of asphalt binder," *Road Mater. Pavement Des.*, vol. 22, no. 11, pp. 2604–2625, 2020. <https://doi.org/10.1080/14680629.2020.1778509>
- [19] Y. Mamuye, N.-D. Do, and M.-C. Liao, "Nano-Al₂O₃ composite on intermediate and high temperature properties of neat and modified asphalt binders," *SSRN*, 2022. <https://doi.org/10.2139/ssrn.4017442>
- [20] AASHTO M 320, Standard Specification for Performance-Graded Asphalt Binder. Washington, DC, USA: AASHTO, 2013.
- [21] AASHTO T 49, Standard Test Method for Penetration of Bituminous Materials. Washington, DC, USA: AASHTO, 2020.







- [22] AASHTO T 51, Standard Test Method for Ductility of Asphalt Materials. Washington, DC, USA: AASHTO, 2020.
- [23] AASHTO T 53, Standard Test Method for Softening Point of Bitumen (Ring-and-Ball Apparatus). Washington, DC, USA: AASHTO, 2020.
- [24] M. Enieb and A. Diab, "Characteristics of asphalt binder and mixture containing nanosilica," *Int. J. Pavement Res. Technol.*, vol. 10, no. 2, pp. 148–157, 2016. <https://doi.org/10.1016/j.ijprt.2016.11.009>
- [25] G. H. Hamed and N. Esmaeili, "Investigating the effects of nano-materials on moisture susceptibility of asphalt mixtures containing glass cullets," *AUT J. Civ. Eng.*, vol. 3, no. 1, pp. 107–118, 2018. <https://doi.org/10.22060/ajce.2018.14665.5492>
- [26] ASTM D3515-01, Standard Specification for Hot-Mixed, Hot-Laid Bituminous Paving Mixtures. West Conshohocken, PA, USA: ASTM Int., 2001.
- [27] A. H. Albayati et al., "Experimental study to investigate performance-related properties of modified asphalt concrete using nanomaterials Al_2O_3 , SiO_2 , and TiO_2 ," *Materials*, vol. 17, no. 17, Art. no. 4279, 2024. <https://doi.org/10.3390/ma17174279>
- [28] AASHTO T 315-12, Standard Method for Determining Rheological Properties of Asphalt Binder Using Dynamic Shear Rheometer (DSR). Washington, DC, USA: American Association of State Highway and Transportation Officials (AASHTO), 2012.
- [29] AASHTO T 391-20, Standard Method for Determining Asphalt Binder Fatigue Properties Using Linear Amplitude Sweep (LAS) Test. Washington, DC, USA: AASHTO, 2020.
- [30] AASHTO T 240-13, Standard Method for Effect of Heat and Air on Asphalt Binder Using Rolling Thin-Film Oven Test (RTFOT). Washington, DC, USA: AASHTO, 2013.
- [31] AASHTO R 28-12, Standard Practice for Accelerated Aging of Asphalt Binder Using a Pressurized Aging Vessel (PAV). Washington, DC, USA: AASHTO, 2012.
- [32] F. Zhang, J. Yu, and J. Han, "Effects of thermal oxidative ageing on modified asphalts," *Constr. Build. Mater.*, vol. 25, no. 1, pp. 129–137, 2011. <https://doi.org/10.1016/j.conbuildmat.2010.06.048>



IRAQI
Academic Scientific Journals



Multi-Functional Enhancement of Water-Based Drilling Fluid Using Copper Nanoparticles: A Study on Lubricity, Rheology, and Filtration Properties

Massara S. Hameed^{1*}  , Nada S. Al-Zubaidi²  , Asawer A. Alwasiti³  

¹ Oil Exploration Company, Ministry of Oil, Baghdad, Iraq; Department of Petroleum Engineering, College of Engineering, Al-Naji University, Baghdad, Iraq.

² Department of Petroleum Engineering, College of Engineering, Al-Naji University, Baghdad, Iraq.

³ Department of Chemical Engineering, University of Technology, Baghdad, Iraq

Article Info	ABSTRACT
<p>Received: 24 Nov 2025 Revised: 19 Jan 2026 Accepted: 08 Mar 2026 Available online: 31 March 2026</p>	<p>Nanoparticle additives emerge as a modern solution to eliminate the performance gap between conventional water-based drilling fluids (WBDFs), and more superior but environmentally challenging oil-based drilling fluids (OBDFs). This study focuses on the enhancement of KCl polymer mud using nano-additives. While nano-additives like copper oxide (CuO NPs) were studied and showed promising results, another form of copper (elemental copper nanoparticles, Cu NPs) with a potential as a multifunction mud additive remains largely unexplored. This research systematically investigates the impact of Cu NPs (0.04–0.8 wt%) on the lubricity, rheology, and filtration properties of KCl polymer mud. All the measurements were done in the lab at room temperature, using lubricity tester, viscometer, and low-pressure filter press. Most additives tend to enhance one property of the mud, but the Cu NPs acted as a more superior properties enhancer, as it didn't enhance only one aspect of KCL polymer mud, but acted as multifunctional additive. For the lubricity, the effect of Cu NPs was significant on the coefficient of friction (CoF), with maximum reduction of 41.68% observed at 0.8% concentration, however at the 0.2% concentration, a relatively similar result of CoF reduction was observed with 39.78% making it the optimal concentration for the lubricity aspect. For the rheological properties, the addition of Cu NPs to the KCL polymer mud enhanced the overall rheological properties, increasing the plastic viscosity (PV), yield point (YP), apparent viscosity (AV), and gel strength, the highest values [PV (44.5 cP), YP (69.4 lb/100ft²), AV (77.35 cP)] were observed at 0.2% concentration. Unlike its beneficial effects on lubricity and rheology, the addition of Cu NPs to KCl polymer mud resulted in increased fluid loss and thicker filter cakes. The study concludes that a concentration of 0.2 %wt of Cu NPs is optimal for the simultaneous enhancement of lubricating and rheological properties in KCl polymer mud. This study highlights the potential of Cu NPs as a multifunctional additive that can be used in advanced water-based drilling fluids systems.</p>
<p>Keywords:</p> <p>KCl Polymer Mud Copper Nanoparticles Lubricity Rheology Filtration</p>	

1. Introduction

The drilling fluid has become an important component in drilling operations, with several

functions that are to be optimized, such as controlling the formation pressures, the removal of drill cuttings from the wellbore, maintaining stability of the wellbore, transmitting hydraulic energy to downhole tools and bits, cooling and



lubrication, and sealing permeable formations. Failure in these functions leads to a major economic impact, affecting resources and time, compromising success, and causing major drilling problems [1, 2].

While oil-based drilling fluids (OBDFs) give superior performance, their high cost and environmental challenges have pushed the industry towards advanced water-based systems (WBDFs). KCl polymer mud is key here for inhibiting shale, but it still falls short of OBDFs in lubricity, rheology and filtration control. This gap is the reason for researching novel additives [3].

Nano-additives have emerged as a modern solution here. Their high surface area and unique properties can alter fluid behavior. Specifically, copper oxide nanoparticles (CuO NPs) have been widely studied. Previous works show they enhance rheology [4-10], improve high-pressure high-temperature (HPHT) filtration [6, 8, 11, 12], work as shale inhibitors [11, 13], and boost thermal stability [4, 8].

On the other hand, its elemental or metallic counterpart, namely copper nanoparticles (Cu NPs), is far less understood; the oxide usually covers most of the literature landscape. Only one previous study has been conducted on Cu NPs up until now, to the best of our knowledge [14], and that too concerning extreme-pressure lubricity in simple WBM.

This study directly targets that gap. Where the prior work [14] focused on lubricity at extreme-pressure conditions in simple WBM, we provide a full, multi-functional evaluation of Cu NPs in KCl polymer mud. We systematically test their impact on lubricity, rheology, and filtration together. This approach shows the broader potential and the trade-offs. The novelty is in this first integrated assessment of Cu NPs as a multifunctional additive, establishing a foundation for their optimized use in WBDFs.

2. Materials and Methods

2.1. Materials

Raw Materials. The additives used in the preparation process of KCl polymer mud were the following: Commercial Bentonite, Potassium Chloride (KCl), Caustic Potash (KOH), Low Viscous Poly Anionic Cellulose (PAC-LV),

Xanthan Gum (XC-Polymer), and Barite. All of the above additives were provided by Oren Hydrocarbons Middle East Incorporation.

Nanomaterials. The Nanomaterials that had been used in this research was Cu NPs (10 – 30 nm size, 99.99% purity, supplied by Nanjing Nano Technology Co., Ltd.).

2.2. Drilling Fluid Preparation

The effect of Cu NPs with different concentrations was explored in a water-based drilling fluid system, namely KCl polymer mud. And to understand the behavioral changes of the additive on the drilling fluid system, a blank sample of KCl polymer mud was prepared using the procedure described in **Table 1**, All mixing was performed using a Hamilton Beach Mixer, with rotational speeds of (13,000 RPM).

Table 1. The preparation of KCl polymer mud blank sample.

Additives	Concentration	Mixing Procedure
Bentonite	8 gm/350ml of distilled water	20 minutes of mixing, then the suspension was aged in a sealed container for 16 hrs.
KCl	10 gm/350ml	2 minutes of mixing
KOH	0.5 gm/350 ml	2 minutes of mixing
PAC polymer	2 gm/ 350ml	2 minutes of mixing
XC polymer	1 gm/350ml	2 minutes of mixing
Barite	100 gm/350ml	2 minutes of mixing, then after the last additive, the whole mixture was mixed for 10 minutes.

The Cu NPs with concentrations of 0.04, 0.1, 0.2, 0.4, 0.8 %wt were added to blank sample of KCl polymer mud, then each slurry was mixed for 10 minutes, to guarantee the homogenous dispersion of the nano-additive within the sample, an Ultrasonic Bath was used for another 10 minutes (the desparation was carried out at frequency of 40 kHz and a power of 100 W, the water bath temperature was monitored and maintained below 35°C to prevent thermal

degradation of drilling fluid components). Before any testing, KCl polymer mud samples were remixed for an extra period of time (5 - 15 min.).

2.3. Lubricity Measurements

The lubricating properties of the KCl Polymer mud samples were measured using OFITE EP and Lubricity Tester in the lab and as following:

- To ensure the reliability of the measurements, OFITE EP and lubricity tester was calibrated with distilled water before each test, in accordance with the equipment's standard calibration protocol, then the correction factor (CF) was calculated using Equation 1.

$$CF = \frac{34}{\text{meter reading}} \quad (1)$$

where the constant 34 is defined by the equipment manufacturer as the reference meter reading for distilled water under standard calibration conditions [15].

- Then the coefficient of friction (CoF) for each sample was calculated manually using the obtained values for apparatus, using Equation 2.

$$CoF = \frac{CF * \text{meter reading}}{100} \quad (2)$$

2.4. Rheology Measurements

Rheological properties of KCl Polymer mud samples were measured using OFITE Model 900 viscometer, and the procedure of the test is as follows:

- To ensure accurate results, the apparatus was calibrated before each test with a special calibration fluid (provided by the device manufacturer), to get offset values that were ranging from 0 to ± 0.1 .
- Plastic viscosity (PV), yield point (YP), and gel strength values were measured using OFITE Model 900 viscometer. But for the apparent viscosity (AV), it was calculated

manually for each sample using Equation 3.

$$AV = \frac{\phi 600}{2} \quad (3)$$

To ensure the repeatability and the accuracy of the results, each test was repeated three times, and the average values were taken into account to ensure the reliability of the results.

2.5. Filtration Measurements

OFITE low-pressure filter press with dead weight hydraulic assembly was used for the filtration loss measurements. The filtrate loss volume was measured at 7.5min (V7.5), and 30 min (V30).

All measurements (lubricity, rheology, and filtration properties) were conducted at room temperature (approximately 35°C).

The overall experimental procedure for evaluating the effect of Cu NPs on KCl Polymer mud is summarized in Error! Reference source not found..

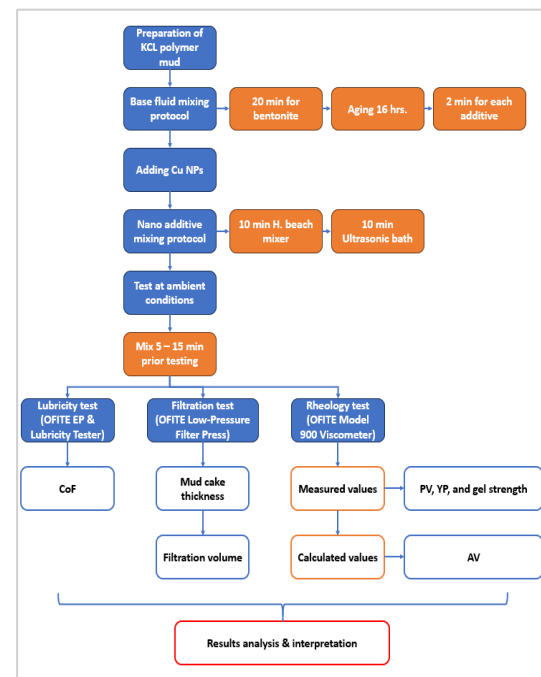


Figure 1. Experimental workflow for evaluating the effect of Cu NPs on KCl polymer mud.

3. Results and Discussion

All the measurements in this study (lubricity, rheology, and filtration) were conducted in ambient temperature (approximately 35 C). This

approach was used to understand the fundamentals of how Cu NPs can affect KCl polymer mud behavior without adding complex variables like high temperature. Although this approach is helpful to understand the base behavior of the additive, it acts as a limitation for this study, where the drilling fluid is subjected to a higher temperature during drilling operations. The observed behavior for (lubricity, rheology, and filtration) are specific to the tested conditions of this study, and future work should validate the results in high temperature conditions.

3.1. Lubrication Behavior

The effect of Cu NPs addition to KCl polymer mud across the selected concentrations range on the CoF can be found in **Table 2** and to have a better view of the additive behaviors across different concentrations, the results are illustrated in **Error! Reference source not found.**

Table 2. Lubricity performance of KCl polymer mud with varying concentrations of Cu NPs.

Cu NPs Concentration, wt%	CoF	CoF Reduction, %
0	0.367	----
0.04	0.235	35.96
0.1	0.221	39.78
0.2	0.221	39.78
0.4	0.25	31.88
0.8	0.214	41.68

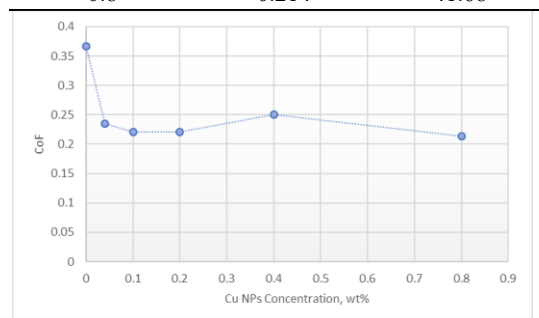


Figure 1. Effect of Cu NPs concentration on CoF of KCl polymer mud.

The addition of Cu NP caused a reduction in the CoF value across all of the concentrations. A reduction in CoF up to 35.96% was observed at the lowest concentration of 0.04 wt%. The CoF decreased further with increasing nanoparticle concentration, reaching a minimum value of 0.221 (a 39.78% reduction) at concentrations between 0.1 and 0.2 wt%.

However, a non-regular behavior was observed at a higher concentration (0.4 wt%) where the CoF increased to a value of 0.25, making it higher than the lower concentrations, but still an enhanced value compared to the blank sample. This behavior may be due to a process known as nanoparticle agglomeration, where individual nanoparticles, in some concentrations, start to group together and form a large cluster of particles that can change how the additive behaves. At the highest concentration (0.8 wt%) the CoF improved again, reaching the maximum enhancement across all the concentrations, and gave a CoF value of 0.214.

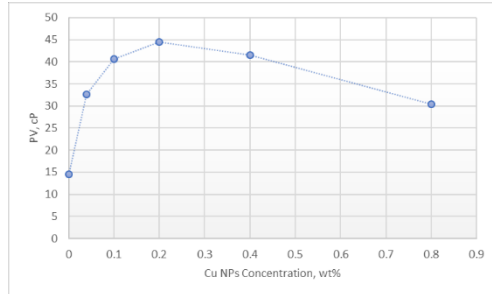
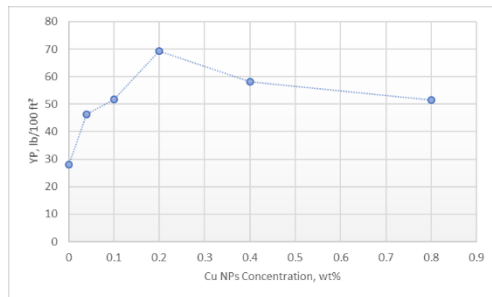
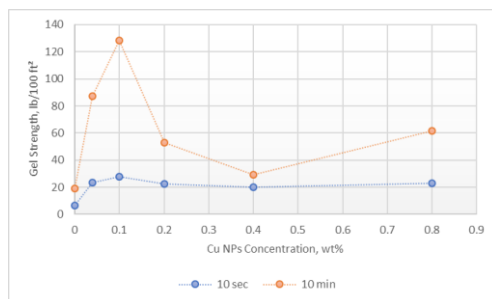
The mechanism behind the lubricity improvement is attributed to the formation of soft and low shear strength film on the metal surfaces. This soft and low shear film separates the contacting surfaces, thus reducing the frictional forces between them [16-19].

3.2. Rheological Properties

Cu NPs additive had a significant effect on the rheological properties of KCL polymer mud. The results, including PV, YP, AV and gel strength are presented in **Table 3** and for better understanding of how significant the change in these properties across different concentrations, the results are illustrated in **Figure 2****Figure 3****Figure 4**.

Table 3. Rheological properties of KCl polymer mud with varying concentrations of Cu NPs.

Cu NPs Concentration, wt%	PV, cP	YP, lb/100 ft ²	AV, cP	YP/PV, lb/100 ft ² /cP	Gel Strength, lb/100 ft ²	
					10 sec	10 min
0	14.6	27.9	29.65	1.91	6.4	19.2
0.04	32.7	46.2	56.15	1.412	23.2	87.2
0.1	40.6	51.7	66.55	1.273	27.9	128.2
0.2	44.5	69.4	77.35	1.559	22.5	52.9
0.4	41.6	58.2	70.45	1.399	20	29.2
0.8	30.4	51.5	57.6	1.694	22.7	61.7

**Figure 2.** Effect of Cu NPs concentration on PV of KCl polymer mud.**Figure 3.** Effect of Cu NPs concentration on YP of KCl polymer mud.**Figure 4.** Effect of Cu NPs Concentration on Gel Strength of KCl Polymer Mud.

The addition of Cu NPs to KCl polymer mud results in enhanced rheological properties (PV, YP, AV and gel strength) across all of the tested concentrations compared to the blank sample. For the tested range, the 0.2% concentration delivered the optimal enhancement combination for the rheological properties [PV (44.5 cP), YP (69.4 lb/100 ft²), and AV (77.35 cP)].

PV is an important property of drilling mud, and can be defined as the resistance to flow in a fluid, caused by the internal friction between particles (solids and liquids) of drilling fluid, and the increase of solids in the mud, will therefore increase the PV. The addition of nanoparticles, that are characterized with large surface area to volume ratio (Cu NPs in our case), and this special characterization of nanomaterials will cause an increase in the interaction between the nanoparticles and the drilling fluid particles, that can cause increase in internal friction, leading to an increase in PV [20-22].

YP is a measurement of the electrochemical attraction forces between particles of the drilling fluid at low shear rates. The addition of nanoparticles (Cu NPs in our case) showed an increase of yield point values, and this can be due to fact that the nano-additives characterized by a large surface area to volume ratio, which allow the particles to carry more surface charges, making the electrochemical attraction forces between nanoparticles and other drilling fluid particles stronger, which directly increases the YP of the fluid.

Gel strength is the ability of the drilling fluid to form a network between particles when the mud sits in static conditions, and this property is caused because of the electrostatic forces between drilling fluid particles. The nano-additives can form a stronger network structure, increase surface charges due to its large area to volume ratio, and it may form a crosslink with the KCl polymer chains, to thicken the structure of the mud at static conditions. The 10-second gel strength of the blank sample was 6.4 lb/100 ft². The addition of Cu NPs enhanced this property, with the highest value of (27.9 lb/100 ft²) observed at 0.1% concentration. The 10-minute gel strength showed a more dramatic increase, surging from 19.2

lb/100 ft² for the blank to 128.2 lb/100 ft² at the 0.1% wt. concentration. The subsequent decrease in 10-minute gel strength at higher concentrations may be due to a repulsive force occurring between the nanomaterials, water molecules, and bentonite particles, or due to agglomeration which can disrupt the fluid's microstructure [20, 23].

In conclusion, the addition of Cu NPs enhanced the rheological properties of the KCl polymer mud. The concentration of 0.2% by weight can be considered an effective concentration, providing high values of YP and AV, which are essential for good hole cleaning.

3.3. Filtration Properties

Filtration measurements for KCl polymer mud across the selected range of Cu NPs concentrations are presented in **Table 4** and **Figure 5** **Figure 6**.

Table 4. Filtration properties of KCl polymer mud with varying concentrations of Cu NPs.

Cu NPs Concentration, wt%	V7.5, ml	V30, ml	Mud Cake Thickness, mm
0	4	8	0.622
0.04	4.4	8.8	0.71
0.1	5.4	10.8	0.712
0.2	6.6	13.2	0.814
0.4	6.2	12.4	0.8
0.8	5.8	11.6	0.872

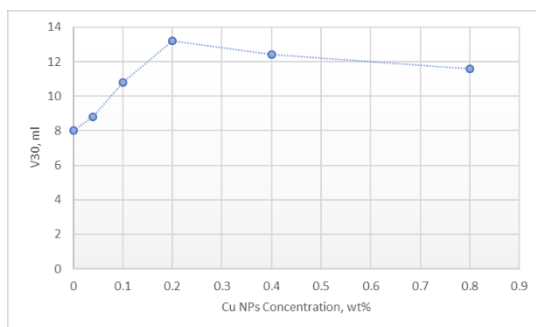


Figure 5. Effect of Cu NPs concentration on V30 of KCl polymer mud.

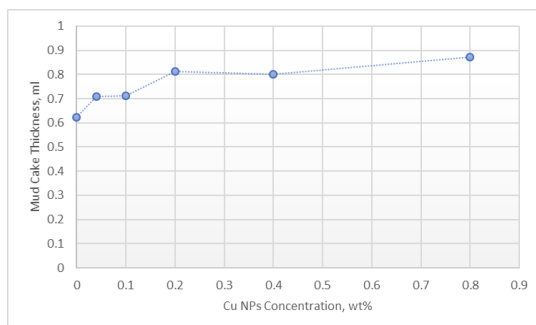


Figure 6. Effect of Cu NPs concentration on mud cake thickness of KCl polymer mud.

The addition of Cu NPs caused an increase in both V30 and mud cake thickness compared to the blank sample.

The blank sample had a V30 of 8 ml and a mud cake thickness of 0.622 mm. With the addition of 0.2 wt% Cu NP, the V30 increased to 13.2 ml and the mud cake thickness increased to 0.814 mm. This represents a 65% increase in V30 and a 30.9% increase in mud cake thickness.

Nano-additives in general, can increase the filtrate loss volume of drilling fluid; this may be explained due to solid accumulation which makes the mud cake less stable, making it harder for the mud with nano-additives to form an impermeable, low porosity mud cake layer, that prevents more filtrate to pass through [24, 25]. The increase in mud cake thickness with the addition of Cu NPs supports this explanation, indicating the formation of a more permeable and less compact filter cake.

The non-regular response of the V30 to Cu NPs concentration may be due to nanoparticle agglomeration at higher concentrations, which can disrupt the mud cake structure.

4. Conclusions

This study provides a comprehensive evaluation of metallic Cu NPs on KCl polymer mud. The key findings reveal Cu NPs as a multifunctional additive for lubricity and rheology enhancement, though with a negative impact on filtration control.

The Cu NPs significantly enhanced lubricity, reducing the CoF by up to 40%. The rheological properties (PV, YP, AV, and gel strength) were also enhanced, giving the mud superior lubricity and improved hole cleaning capacity. However, these enhancements came with increased filtration volume and thicker filter cakes.

Within the tested concentration range (0.04–0.8 wt%), the 0.2 wt% concentration is recommended. This value delivered optimal lubricity improvement and the peak rheological properties increase, albeit alongside elevated fluid loss. Therefore, using Cu NPs is highly recommended in a careful and controlled way, specifically for scenarios where lubricity and cuttings lifting capacity are critical and where the filtration increase can be managed.

This work distinguishes the role of metallic Cu NPs from the widely studied oxide form and establishes a foundation for their application. Future research must focus on validating these findings under high-temperature conditions and developing strategies to mitigate the filtration drawback.

Abbreviations

AV	Apparent viscosity
CF	Correction factor
CoF	Coefficient of friction
Cu	Copper
CuO	Copper oxide
KCl	Potassium chloride
KOH	Caustic potash
NPs	Nanoparticles
OBDFs	Oil-based drilling fluids
PAC	Poly anionic cellulose
PV	Plastic viscosity
V30	Filtrate loss volume at 30 min
V7.5	Filtrate loss volume at 7.5 min
WBDFs	Water-based drilling fluids
XC	Xanthan Gum
YP	Yield point

Conflict of interest

The authors declare no conflicts of interest concerning this research.

Funding

No funding was received for conducting this study

Author Contribution

The manuscript was written by **M.S. Hameed**, who also performed the experiments and analyzed the results. **N.S. Al-Zubaidi** contributed to data analysis and supervision. **A.A. Alwasiti** provided supervision. All authors discussed the results and contributed to the final manuscript.

AI Declaration Statement

The authors confirm that the manuscript has been written without the assistance of generative AI or AI-based writing tools.

References

- [1] H. Rabia, *Well Engineering and Construction*. London, U.K.: Entrac Petroleum, 2001.
- [2] IADC, *IADC Drilling Manual*. Houston, TX, USA: International Association of Drilling Contractors, 2014.
- [3] M. Abduo et al., "Comparative study of using water-based mud containing multiwall carbon nanotubes versus oil-based mud in HPHT fields," *Egypt. J. Pet.*, vol. 25, no. 4, pp. 459–464, 2016. <https://doi.org/10.1016/j.ejpe.2015.10.008>
- [4] J. K. M. William et al., "Effect of CuO and ZnO nanofluids in xanthan gum on thermal, electrical and high-pressure rheology of water-based drilling fluids," *J. Pet. Sci. Eng.*, vol. 117, pp. 15–27, 2014. <https://doi.org/10.1016/j.petrol.2014.03.005>
- [5] M. E. Naderi et al., "Application of copper oxide nanoparticles in improving filtration and rheological properties of water-based drilling fluid," *Iran. J. Oil Gas Sci. Technol.*, vol. 11, no. 3, pp. 52–66, 2022. <https://doi.org/10.22050/ijogst.2022.346128.1645>
- [6] P. Dejtardon et al., "Impact of ZnO and CuO nanoparticles on the rheological and filtration properties of water-based drilling fluid," *Colloids Surf. A*, vol. 570, pp. 354–367, 2019. <https://doi.org/10.1016/j.colsurfa.2019.03.050>
- [7] Y. Lin et al., "Effect of nanoparticles on rheological properties of water-based drilling fluid," *Nanomaterials*, vol. 13, Art. no. 2092, 2023. <https://doi.org/10.3390/nano13142092>
- [8] E. Veisi, M. Hajipour, and E. B. Delijani, "Experimental study on thermal, rheological and filtration control characteristics of drilling fluids: Effect of nanoadditives," *Oil Gas Sci. Technol.*, vol. 75, Art. no. 36, 2020. <https://doi.org/10.2516/ogst/2020033>
- [9] M. Al-Saba et al., "Application of nanoparticles in improving rheological properties of water-based drilling fluids," in *Proc. SPE Kingdom Saudi Arabia Annu. Tech. Symp. Exhib.*, Dammam, Saudi Arabia, 2018. <https://doi.org/10.2118/192239-MS>
- [10] A. O. P., A. O. I., and K. O. M., "Comparative study of impact of zinc oxide and copper (II) oxide nanoparticles on viscosity of water-

- based drilling fluid,” *Int. J. Eng. Manag. Res.*, vol. 10, no. 4, 2020. <https://doi.org/10.31033/IJEMR.10.4.11>
- [11] A. Retnanto et al., “Evaluation of the viability of nanoparticles in drilling fluids as additive for fluid loss and wellbore stability,” *Petroleum*, vol. 9, pp. 342–351, 2023. <https://doi.org/10.1016/j.petlm.2023.02.005>
- [12] A. E. Bayat et al., “Experimental investigation of rheological and filtration properties of water-based drilling fluids in presence of various nanoparticles,” *Colloids Surf. A*, vol. 555, pp. 256–263, 2018. <https://doi.org/10.1016/j.colsurfa.2018.07.001>
- [13] A. Mady et al., “Influence of nanoparticle-based drilling fluids on Egyptian shale swelling—An experimental investigation,” in *Proc. ADIPEC, Abu Dhabi, UAE*, 2023. <https://doi.org/10.2118/216520-MS>
- [14] N. Sabah, A. A. Alswasiti, and M. Salam, “Improving drilling fluid properties at high pressure conditions using selected nanomaterials,” *IOP Conf. Ser.: Mater. Sci. Eng.*, vol. 579, Art. no. 012004, 2019. <https://doi.org/10.1088/1757-899X/579/1/012004>
- [15] OFITE, EP (Extreme Pressure) and Lubricity Tester Instruction Manual. Houston, TX, USA: OFI Testing Equipment, Inc., 2015.
- [16] D. Guo, G. Xie, and J. Luo, “Mechanical properties of nanoparticles: Basics and applications,” *J. Phys. D: Appl. Phys.*, vol. 47, no. 1, Art. no. 013001, 2014. <https://doi.org/10.1088/0022-3727/47/1/013001>
- [17] A. Bardhan et al., “Biogenic copper oxide nanoparticles for improved lubricity and filtration control in water-based drilling mud,” *Energy Fuels*, vol. 38, no. 10, pp. 8564–8578, 2024. <https://doi.org/10.1021/acs.energyfuels.4c00635>
- [18] K. Hua et al., “In-situ surface modified water-soluble Cu nanoparticles as lubrication additives in water-based cutting fluids,” *Colloids Surf. A*, vol. 698, Art. no. 134605, 2024. <https://doi.org/10.1016/j.colsurfa.2024.134605>
- [19] M. Zhang, X. Wang, W. Liu, and X. Fu, “Performance and anti-wear mechanism of Cu nanoparticles as lubricating oil additives,” *Ind. Lubr. Tribol.*, vol. 61, no. 6, pp. 311–318, 2009. <https://doi.org/10.1016/j.triboint.2009.02.012>
- [20] M-I SWACO, M-I Drilling Fluids Manual. Houston, TX, USA: M-I SWACO, 1998.
- [21] A. R. Ismail et al., “Improve performance of water-based drilling fluids using nanoparticles,” in *Proc. Sriwijaya Int. Semin. Energy Environ. Sci. Technol.*, Palembang, Indonesia, 2014.
- [22] A. H. Salih, T. A. Elshehabi, and H. I. Bilgesu, “Impact of nanomaterials on the rheology and filtration properties of water-based drilling fluids,” in *Proc. SPE Eastern Regional Meeting*, Canton, OH, USA, 2016. <https://doi.org/10.2118/184067-MS>
- [23] A. E. M. and A. M., “Effect of Fe₃O₄ nanoparticles on the rheological properties of water-based mud,” *J. Phys. Sci. Appl.*, vol. 5, no. 6, pp. 415–422, 2015. <https://doi.org/10.17265/2159-5348/2015.06.005>
- [24] A. R. Ismail et al., “Effect of nanomaterial on the rheology of drilling fluids,” *J. Appl. Sci.*, vol. 14, no. 11, pp. 1192–1197, 2014. <https://doi.org/10.3923/jas.2014.1192.1197>
- [25] A. Aftab, A. Ismail, and Z. Ibupoto, “Enhancing the rheological properties and shale inhibition behavior of water-based mud using nanosilica, multi-walled carbon nanotube, and graphene nanoplatelet,” *Egypt. J. Pet.*, vol. 26, no. 2, pp. 291–299, 2017. <https://doi.org/10.1016/j.ejpe.2016.05.004>



IRAQI
Academic Scientific Journals



A Quantitative Analysis of Factors Affecting the Adoption of Micro-management in Engineering Projects

Tamara A. Obaid^{1*} , Hatem K. Breesam²

¹ Ministry of Construction and Housing & Municipalities Public, Baghdad, Iraq.

² Department of Civil Engineering, College of Engineering, University of Baghdad, Baghdad, Iraq.

Article Info	ABSTRACT
<p>Received: 06 March 2026 Revised: 28 March 2026 Accepted: 28 March 2026 Available online: 31 March 2026</p> <p>Keywords: Project; project management; Construction management; Micro-management; Micromanager; Engineering companies.</p>	<p>Micro-management is a type of management in which the manager accurately monitors and intervenes or regulates the work of his subordinates or his employees in detail, and it is the attempt of managers to interfere, influence and control anything in the team, situation or place, Everything in this world carries two different directions, one negative and the other positive, and we aim in this research to exploit the advantages of the method of micromanagement and prove that it can be a successful tool if used correctly and at specific times and within certain limits, in this research the factors affecting Applying this method in construction contracting companies in Iraq to take advantage of this method in identifying the most important problems leading to financial corruption in order to eliminate or reduce them in order to advance the current reality of projects, so the researcher reached the most important factors, including (administrative style, organizational culture) and other factors that have been clarified in a way. In detail in this research, the characteristics of the micromanager were also studied, which represent the cornerstone of the success and failure of this technique, as the effect of each characteristic and the possibility of its availability in the vicinity of engineering companies was addressed.</p>

1. Introduction

In response to the micromanagement negativity, we want to study and prove that micromanagement is not a unilateral bad, as is shown in contemporary literature [1]. Goldsmith concluded that Micromanagement is not a dirty word if you do it right. Micro-management is not always an option, but an industry standard, for example during audits, investigations, problem solving, document editing and policy review. So, the question is not whether or not you are doing micromanagement. It's how to do it right. Moreover, Micro-management can be justified if the task is new, complex, of great value and requires great care and quality control. In the event that there are time constraints in fulfilling

customer requests or legal requirements, micromanagement may become an exit vehicle. As a supervisor, if you are stuck with an underperforming staff, then you have no choice but to micromanage [2]. I believe micromanaging is a skill (if done right) that not everyone can master. Not everyone has the ability to monitor and control every step of the process. Bosses who stick their noses to every detail because they have nothing smarter to do are the representatives of the detail management that made a mistake. But heads who watch closely, providing detailed guidance and corrective feedback when needed, are completely opposite [3].

Micromanagement means carefully managing things and assessing or regulating the procedures [4]. Compulsive, equivalent mental



dysfunction may be micromanagement for addicts and alcoholics. They all appear to lack the ability to understand and have a degree of cynicism and uncertainty about their own actions. Micromanagers are control freaks with an obsession with meaningless data. Without excuse, they may set deadlines, refuse to give loans to subordinates, count the amount of paper used for prints and other actions that indicate a major need for supervision and control [5]. Micromanagement now generally refers to the supervision of an enterprise in every detail, with the effect of obstructing change and neglecting larger, higher-level policy problems. Micromanagement was practiced and understood long before we labeled it as an organizational pathology. Despite all the negative aspects that are said about it, it is not devoid of positives that can be used to eliminate some problems or reduce them, as careful monitoring of all details will help in controlling financial matters greatly through knowing the things in which these funds are exploited, as well as continuous monitoring. It can help in diagnosing weak sites at work and thus solutions will be developed in order to address this, and other matters that can be exploited to get the most out of the features of this method,

An important contributing factor to low employee morale is micromanagement. Employees do not want to be micromanaged and most employers don't want to treat them as micromanagers. Micromanagement leaves disempowered, demotivated and disengaged workers. This causes a rift between management and staff, causing employees to resist any administrative changes they want to make, leading to discontent and stagnation as well. Staff has regularly reported that the three most important reasons for leaving the correctional service are conflicts with co-workers, poor leadership and the feeling that management does not value them, both of which are significantly influenced by micromanagement [6].

1.1. Purpose

The purpose of micromanagement:

- Allows greater organizational power
- Makes reliable metrics and minutia awareness
- Can help workers on board (reach speed)

- Improves the efficiency of complex and tailored operations

To avoid the negative effects of micromanagement, Wright proposes four suggestions: being flexible, setting smarter goals, being outcome-oriented, and behaving like a player/coach. As a boss, the use of these four variables has a direct and beneficial effect on productivity and job satisfaction, resulting in lower turnover and higher benefit [7].

1.2. When is micro-management useful for the work?

1. Hire new individuals
2. The start of new operations or initiatives
3. Confrontation with financial or legal issues
4. Staff have a proven record of problems
5. Engaging in high-risk operations
6. Shift Policy Change Strategy
7. Changing top leadership [8]

1.3. We can identify research objectives as follows:

1. Provide an overview of the characteristics and advantages of the micro-management methodology and identify deficiencies, strengths and weaknesses and compare them with other methodologies in order to find a common bridge and promote a better understanding of best practices and uses of project management and construction companies.
2. Study, analysis and evaluation the factors and criteria affecting the application and success of the micro-management methodology.
3. Study the possibility of adopting the micro-management methodology for the engineering companies in its various operations.

Developing a framework for a micro-management methodology that is easy to use in managing engineering companies or in some management functions in Iraq.

1.4. Some Previous studies

No.	Author	Result
1	Jie Li & Umer Khalid (china,Pakistan,Sweden) (2015) (9)	<p>In this report, the researchers researched micro-management in the engineering context, where a quantitative and statistical survey was carried out to assess the effects of micro-management in the engineering environment. Where a study was applied to a group of professional workers, and the findings were that some executives were opposed to using this administrative approach and some of them were supporters as well as staff, some of them opposed this technique and some of them accepted it.</p> <p>The weakness of managerial skills for engineers is the reason researchers resort to studying the application of this system. The main goal of researchers is to understand the administrative requirements in the engineering world, and the following signs of micro-management have ultimately been established:</p> <ol style="list-style-type: none"> 1-Control over methodology 2-Excessive reporting and updates 3-Control and manipulation of time 4-Failure to subordinate self 5-excessive approval requirement <p>The researchers defined the most important micro-management characteristics:</p> <ol style="list-style-type: none"> (1) Rigorous attention to Detail & physical appearance (2) Meticulous training, implementation & follow-up (3) Tight regulation of finance & logistics (4) Testing & surveillance (5) Rigorous preparation and never-ending learning
2	Petter Bergström, Lars Peter Raknes, 2016 (Oslo, Norway) (1)	<p>Supporting it with (6) social modeling and caregiving, and that these categories are completed ,It will have the best effects and turn the concept of (micro-management) into a positive one, away from the known negativity about it. And the researchers said that (micro-management) should be used as a tool in the manager's hands that he uses at particular times and not as a permanent behavior. Thus the manager maintains a certain balance between (micromanager's) actions and achieving a cohesive working atmosphere characterized by intimacy and affection, such that a family relationship is identical to the relationship between the manager and employees. It will be very successful in doing so and the researchers pointed out that this technique's success in places of study does not mean its success everywhere.</p> <p>The researchers concluded that the excessive use of micromanaging actions on the part of the employees contributed to general aversion and great dissatisfaction. During the talk with them, The workers asked to dispense with micromanagement behaviour because it caused them considerable stress and stress during work and its consequences were also bad in organizational management, and they wanted to be the manager A style that provides them with positive input instead of managing them.</p> <p>The researchers explored the Employers' Viewpoint analysis of micromanagement. For them for their smooth and effective work, leadership is a key element in every organization, And they suggested that micromanagement leads to raising the level of employee skills and capabilities and allows them to perform better, and that micromanagers are very coordinated and ideal leaders in their opinion.</p>

Regarding the previous studies, the researcher has benefited from them in determining what causes the most aversion to the employees regarding the behavior of the micromanager.

Accordingly, the most important characteristics that could lead to the progress of work without alienating the employees were determined. The researcher also concluded that the success of this

method in one aspect does not mean its success in every places.

The large number of financial corruption and the use of traditional management led to the delay of projects. The main problem was that managers are far from the details of the project. Therefore it is assumed that if (micro-management) is used in project management and the manager becomes

close to the details, he will get rid of his problems and obstacles.

2. The Research Methodology:

Figure 1 illustrates the methodology of the current research.

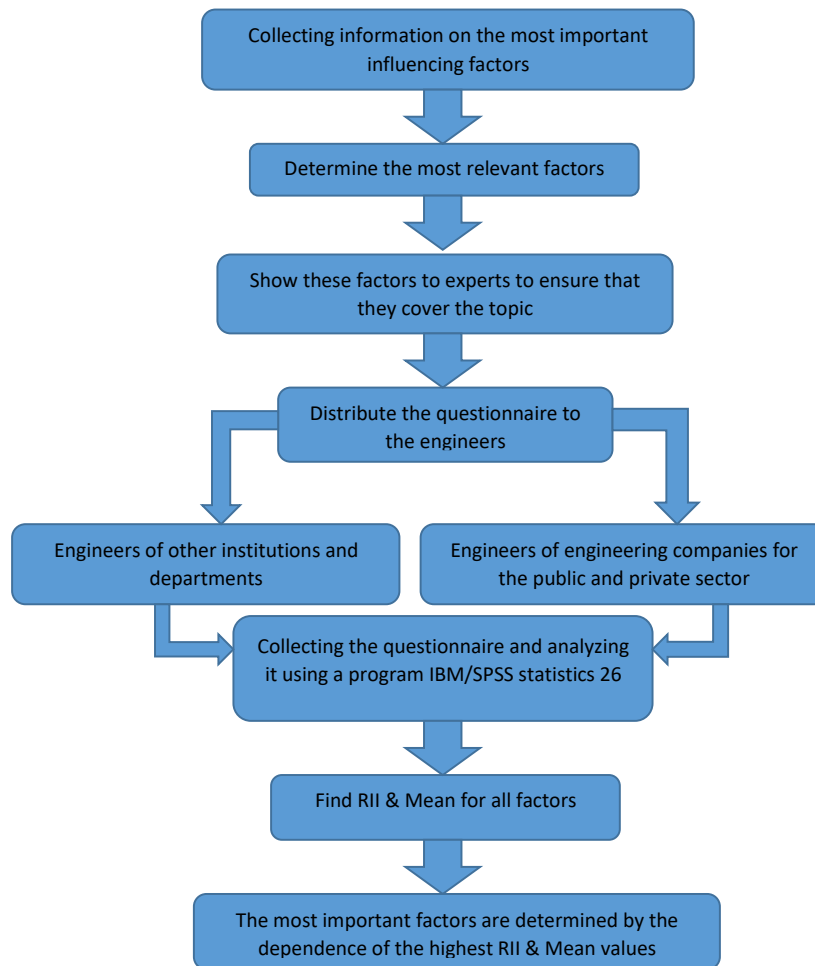


Figure 1. Research methodology.

2.1 Data collection and analysis:

1. The researcher initially collected information from previous studies about the most important factors that could affect the success or failure of applying this administrative method, then these factors and information were presented to specialists in this field with a number of not less than 15 experts in order to discuss the question form and the extent of understanding The question and the

importance and impact of each question, and are these questions sufficient to cover the topic or not. After that, a final version of the questionnaire was reached.

2. After discussing the questionnaire with the experts, and specifying the type of construction projects that will be worked on, which are building projects. the researcher prepared a questionnaire form that includes three axes, the first axis, personal information about the sample to

- know the size of its impact on the results, the second axis includes the evaluation of the explanatory information and the third axis, questionnaire information to determine the factors by the sample
3. The questionnaire was distributed to samples of engineers in the engineering companies of the public sector, engineers in the Baghdad governorate building, school buildings engineers of the Ministry of Education in Baghdad and Kut, as well as engineers in the Ministry of Higher Education in Najaf and Karbala, and engineers in other departments.
 4. Due to the current circumstances, most of the private sector engineering companies stopped working, so it was difficult to reach these companies, so an electronic questionnaire was created and distributed online to public sector engineers in particular.
 5. The questionnaire sample contained bachelors, masters and doctoral degrees, and both male and female genders.
 6. More than 125 questionnaire samples were sent in, and only 98 samples were received.
 7. The central end theory was relied upon by statistics, which indicates that the sample's arrival of more than 30 gives an accuracy of more than 99, so the sample size consisting of 98 questionnaires was considered sufficient to reach the required accuracy
 8. After receiving the samples, they were analyzed using the IBM/ SPSS program, and the results were obtained in the following tables.
 9. The significance of each element was determined based on the (relative importance index (RII)) When two factors are similar with this value, we take the value that is (Mean) higher.

$$RII = \frac{\sum_{k=0}^N (X1 \times S1 + X2 \times S2 + X3 \times S3 + \dots + Xn \times Sn)}{A \times N} \quad (1)$$

Where:

RII= the Relative Importance Index.

S = Weight gives to any factors by responders and will rang (1 to 5) where '1' is less important and '5' is high important. OR range (1 to 3)

X=for each factor or choice, frequency of each rating

N= Total number of responses for that factor or option

A=the highest weights (i.e. in this case 5, or 3)

In case of 5-point Likert scale

RII values	Importance level (RII-Level)	
$0.8 \leq RII \leq 1$	High	H
$0.6 \leq RII \leq 0.8$	High - Medium	H-M
$0.4 \leq RII \leq 0.6$	Medium	M
$0.2 \leq RII \leq 0.4$	Medium-Low	M-L
$0.0 \leq RII \leq 0.2$	Low	L

In case of 3-point Likert scale

RII values	Importance level (RII-Level)	
$0.66 \leq RII \leq 1$	High	H
$0.33 \leq RII \leq 0.66$	Medium	M
$0.0 \leq RII \leq 0.33$	Low	L

10-After the analysis of the sample's experiences, it was found that the sample's experience rate is 16 years, and this means that the sample has good experience and at the same time it has youth energy, and thus an indication of the possibility of community knowledge or acquaintance with this technique as it is a modern technology that has not been applied for a long time.

3. Results and Discussion

Since micromanagement was previously described, it depends heavily on the process, the manager would follow in implementing this technology, so micromanager must be identified by a collection of descriptions to be able to implement this technique. The most important aspect is the micromanager's characteristics, so in this table (1) the sample's opinion on the value of each trait will be studied, while in Table (2) the probability of each feature being met by the current managers is studied.

Table 1. Sample opinion on the importance of micromanager characteristics

No.	Specifications	very important	important	Average importance	Acceptable	not important	Mean	RII	RII Level
1	Proficient in task delegation	47	40	9	1	1	4.34	0.87	H
2	Possesses the ability to plan successfully	68	22	4	2	2	4.55	0.91	H
3	Has the capacity to understand and support the team's progress	64	24	10			4.55	0.91	H
4	Able to provide necessary management training to employees	30	45	18	5		4.02	0.8	M-H
5	provides the necessary technical training to the staff to support his management approach	38	40	15	5		4.13	0.83	H
6	Focus on a directive rather than a supervisory approach.	47	25	16	5	5	4.06	0.81	H
7	Proficient in managing project time and budget.	50	25	15	4	4	4.15	0.83	H
8	Capable of project quality control	45	36	10	5	2	4.19	0.84	H
9	Knowledge of risks affecting time, cost, or scope of work.	46	37	9	3	3	4.21	0.84	H
10	Excellent at delegating and assigning tasks.	44	35	14	5		4.20	0.84	H
11	Ability to monitor performance and motivate employees.	40	42	13	3		4.21	0.84	H

Regarding this Table 1, all the traits in it got high ratings of H with respect to RII except for the trait 4 that got the estimate of H-M and the sequence of traits was as follows:

No.	Adjective	RII	RII-Level	Mean
1	2-Capable of successful planning	0.91	H	4.55
2	3- Knowing the team's ability and progress	0.91	H	4.55
3	1-He Is able to segment the work	0.87	H	4.34
4	9-Knowing all the risks that may affect time, cost, or scope	0.84	H	4.21
5	11-he is Skilled at performance monitoring and motivation	0.84	H	4.21
6	10-He is skilled in delegating work	0.84	H	4.20
7	8-Capable of project quality control	0.84	H	4.19
8	7-Capable of controlling project time and budget	0.83	H	4.15
9	5-provides the technical training necessary to the staff to support its management approach	0.83	H	4.13
10	6-He uses the manner of guidance, not monitoring	0.81	H	4.06

Table 2. The possibility of availability of Micromanager Characteristics in the sample population

No.	Specifications	Available	Sometimes available	Not available	Mean	RII	RII Level
1	He Is able to segment the work	34	55	9	2.26	0.75	H
2	Capable of successful planning	30	50	18	2.12	0.7	H
3	Knowing the team's ability and progress	33	50	15	2.18	0.72	H
4	Provides the necessary training for employees in the management approach	28	45	25	2.03	0.67	M
5	provides the technical training necessary to the staff to support its management approach	28	48	22	2.06	0.68	H
6	He uses the manner of guidance, not monitoring	38	45	15	2.23	0.74	H
7	Capable of controlling project time and budget	28	50	20	2.08	0.69	H
8	Capable of project quality control	33	45	20	2.13	0.7	H
9	Knowing all the risks that may affect time, cost, or scope	28	52	18	2.10	0.69	H
10	He is skilled in delegating work	35	48	15	2.20	0.73	H
11	he is Skilled at performance monitoring and motivation	35	47	16	2.19	0.72	H

Table 2 is the possibility of the availability of each attribute, all the traits obtained RII-LEVEL = H except for the trait (4) obtained the estimate of RII-LEVEL=M, so the sequence of traits became as follows:

No.	Adjective	RII	RII-Level	Mean
1	1- He Is able to segment the work	0.75	H	2.26
2	6- He uses the manner of guidance, not monitoring	0.74	H	2.23
3	10- He is skilled in delegating work	0.73	H	2.20
4	11- he is skilled at performance monitoring and motivation	0.72	H	2.19
5	3- Knowing the team's ability and progress	0.72	H	2.18
6	8- Capable of controlling project time and budget	0.7	H	2.13
7	2- Capable of successful planning	0.7	H	2.12
8	9- Knowing all the risks that may affect time, cost, or scope	0.69	H	2.10
9	7- Capable of controlling project time and budget	0.69	H	2.08
10	5- provides the technical training necessary to the staff to support its management approach	0.68	H	2.06

Table 3. The main factors of Micromanagement and influencing its application.

No.	Factors	possible	impossible	Sometimes possible	Mean	RII	RII-LEVEL
1	Administrative style	66	7	25	2.60	0.86	H
2	Organizational culture	49	20	29	2.30	0.76	H
3	good and sober micromanagement behavior	36	20	42	2.16	0.71	H
4	Micromanager and its aforementioned attributes	43	22	33	2.21	0.73	H
5	The employer's acceptance of the effects that occur in the following:						
A	The benefit derived from the project, which is affected by business decisions and its results	41	18	39	2.21	0.73	H
B	the legal and moral rights of the employer	40	19	39	2.31	0.76	H
C	Specialized and organizational knowledge	45	15	38	2.20	0.73	H
D	The time for providing resources, allocating and providing funding	40	20	38	2.27	0.75	H
E	His ownership of a specific property	43	17	38	2.19	0.72	H
6	micromanagement aligns with the company's projects methodology	39	20	39	2.21	0.73	H
7	Employees accept the micro-management methodology	40	19	39	2.60	0.86	H

The researcher studied the possibility of their availability in the sample community. The highest to the lowest is as follows:

No.	Factor	RII	RII-Level	Mean
1	1-Administrative style	0.86	H	2.60
2	7-Employees accept the micro-management methodology	0.86	H	2.60
3	(5-B)- the legal and moral rights of the employer	0.76	H	2.31
4	2-Organizational culture	0.76	H	2.30
5	(5-D)- The time for providing resources, allocating and providing funding	0.75	H	2.27
6	(5-A)- The benefit derived from the project, which is affected by business decisions and its results	0.73	H	2.21
7	4-Micromanager and its aforementioned attributes	0.73	H	2.21
8	6- micromanagement aligns with the company's projects methodology	0.73	H	2.21
9	(5-C)- Specialized and organizational knowledge	0.73	H	2.20
10	(5-E)- His ownership of a specific property	0.72	H	2.19
11	3-good and sober micromanagement behavior	0.71	H	2.16

4. Conclusions

The researcher's findings in this research of factors differ from what the rest of the researchers have found, since the aspects dealt with by the rest of the researchers differ from what was dealt with in this research if all previous research did not go to the effect of micro-management in the management of construction contracting companies, where work was previously done on companies Administrative but not constructional

From the research on the factors affecting the application of micro-management, it was found that:

Note that the RII range is very close, meaning the researcher relied on factors used in previous studies and research, all of which were discussed with experts and have a high impact. It is possible that most of the sample was influenced by previous readings due to the novelty of the methodology.

The researcher found that the most important characteristic of a micromanager is the ability to plan successfully and understand the team's capabilities and progress..

1. The most needed and common micromanager trait in construction companies is the ability to delegate work.
2. The success of a detail-oriented manager is more crucial in financial management than in technical management.
3. The absence of a manager during the design phase, while their importance increases during the implementation and project financing phases.

Abbreviations

RII	Relative Importance Index
H	High
M	Medium
L	Low

Conflict of interest

The authors declare no conflicts of interest concerning this research.

Funding

No funding was received for conducting this study.

Author Contribution

T.A. Obaid proposed the research problem and developed the theoretical framework. H.K. Breesam verified the analytical methods. T.A. Obaid and H.K. Breesam authors participated in the discussion of the results and contributed to writing the manuscript.

AI Declaration Statement

The authors confirm that the manuscript has been written without the assistance of generative AI or AI-based writing tools.

References

- [1] L. P. Raknes, "Prosperous," M.Sc. thesis, BI Norwegian Business School, Oslo, Norway, 2016.
- [2] E. Gnospelius, "Micro-management vs. macro-management: Striking a balance," 2014. [Online]. Available: <https://www.linkedin.com/.../20140417140436-15219272-micro-management-vs-ma>
- [3] N. Angelovska, "Micromanagement and leadership," Ph.D. dissertation, Ss. Cyril and Methodius Univ., Skopje, North Macedonia, 2017.
- [4] R. F. Wright, "Strategies for avoiding the micromanagement trap," *Manag. Decis.*, vol. 38, no. 5, pp. 362–364, 2000. <https://doi.org/10.1108/00251740010340544>
- [5] R. D. White, "The micromanagement disease: Symptoms, diagnosis, and cure," *Public Pers. Manag.*, vol. 39, no. 1, pp. 71–76, 2010. <https://doi.org/10.1177/009102601003900105>
- [6] B. Y. Shuford and J. A. Shuford, "Micromanagement: The enemy—Identifying micromanagement," pp. 36–41, Oct. 2019.
- [7] M. J. Miller, "Alleviating stress induced by workplace micromanagement through

mindfulness applications,” [Unpublished manuscript].

- [8] S. K. V., “Dilemmas of IT professionals with special emphasis on micromanagement,” *Int. J. Adv. Res.*, vol. 4, no. 11, pp. 794–800, 2016.
<https://doi.org/10.21474/IJAR01/2149>
- [9] J. Li and U. Khalid, “Implementing an effective change,” 2015.
- [10] G. A. Castillo, “Micromanagement behavior: A qualitative empirical phenomenological study,” *Int. J. Bus. Manag.*, vol. 6, no. 2, pp. 1057–1067, 2018.
- [11] N. Mishra, M. Rajkumar, and R. Mishra, “Micromanagement: An employers’ perspective,” *Int. J. Sci. Technol. Res.*, vol. 8, no. 10, pp. 2949–2952, 2019.
- [12] M. Sambasivan and Y. W. Soon, “Causes and effects of delays in Malaysian construction industry,” *Int. J. Project Manag.*, vol. 25, no. 5, pp. 517–526, 2007.
<https://doi.org/10.1016/j.ijproman.2006.11.007>

Blank Page



IRAQI
Academic Scientific Journals



Optimization of ESP Performance Using Pump Frequency and Wellhead Pressure Sensitivity Analysis in the Rmelan Oil Field (PIPESIM-Based Study)

Ahmed M. Hussein^{1*} ✉, Abu Zied Ahmed², Tarek M. Aboul-Fotouh³, Sayed Gomaa³

¹ Department of Petroleum Engineering, the Institute of Science and Modern Technology, Rojava University, Qamishli, Syrian Arab Republic.

² Mining and Petroleum Engineering Department, Faculty of Engineering, Al-Azhar University, Cairo, Egypt.

Article Info	ABSTRACT
<p>Received: 14 March 2026 Revised: 28 March 2026 Accepted: 29 March 2026 Available online: 31 March 2026</p> <p>Keywords: Artificial lift; Electrical Submersible Pump; PIPESIM software; Nodal analysis; Optimization; Rmelan field.</p>	<p>The aim of this study is to optimize ESP performance by evaluating the current conditions and the performance optimization of the electrical submersible pump (ESP) for six oil wells in the Rmelan oil field. fluid and reservoir properties (API = 23, T = 78 C°, pressure of reservoir = 160 atm and the WC is 70%). This paper presents a sensitivity assay conducted by Nodal Analysis (Using PIPESIM Software) on the pump frequency and wellhead pressure. The outflow tubing performance and inflow performance relationship were generated and plotted for each well. The curves are investigated, indicating problems in some wells (W-12R, W-21KH, and W-21SH). The results of this study show that we can increase the flow rate by optimizing the ESP performance by decreasing the wellhead pressure to 71.58 psi and raising the frequency of ESP to a specific value of about 65 Hz based on the limites of production of each types pump capacity . Increasing the frequency from 55 to 65 Hz resulted in increasing the production from 634 to 1092 bbl/day for W-12R, from 1928 to 2806 bbl/day for W-21KH, and from 1722 to 2279 bbl/day for W-21SH.</p>

1. Introduction

At first, natural flow of fluids occurring hydrocarbons from the reservoir can flow toward the surface without pumps (natural flow); however, this state is not stable. There will come a point in time when the reservoir pressure drops, which may result in the well closing or producing less [1]. The production of oil wells frequently uses artificial lift techniques. It is applied to maximize production [2]. For productivity to be displayed effectively, production performance must be thoroughly understood. When the reservoir driving energy is insufficient to produce oil to the surface, this technique decreases the bottom hole flowing pressure and increases the pressure difference to bring the oil up to the

surface. Bottom-hole pressure is overcome with this technique. The new primary issue facing a field is choosing the best lift technique for each well or the field as a whole. A poor choice may result in excessive production costs [3].

Artificial lift is a crucial technique used in the oil and gas industry to maintain optimal hydrocarbon production as reservoirs mature [4]. It involves employing various methods, such as pumps and gas lift valves, to increase reservoir pressure or reduce wellbore backpressure by installing lift mechanisms down hole. Artificial lift systems efficiently raise fluids to the surface, counteracting declining flow rates. The choice of artificial lift method depends on reservoir characteristics, well conditions, and production requirements. Common methods include



Electrical Submersible Pump (ESP), Progressive Cavity Pump (PCP), Sucker Rod Pump (SRP), Gas Lift (GL), Plunger Lift (PL), and Hydraulic Jet Pump (HJP) [5]. These systems play a vital role in sustaining production rates from oil and gas fields. This study mainly focuses on artificial lift using ESP, which is introduced in detail in this chapter. Other artificial lift methods are briefly reviewed.

2. Literature Review

Electric Submersible Pump (ESP) uses multiple centrifugal pump stages mounted in series within a housing mated closely to a submersible electric motor on the end of the tubing and connected to surface controls and electric power by an arm or protected cable as shown in Figure 1. Submersible systems have a wide performance range and are one of the more versatile lift methods. Standard surface electric drives power outputs from 100 to 30,000 B/ D [16 to 4770 m³/ d] and variable-speed drives add pump rate flexibility [6]. High GOR (Gas oil Ratio) fluids can be handled, but large gas volumes can lock up and destroy pumps.

The advantages are that high water cut is not restricted, can lift extremely high volume, can handle rates from 50 to 60,000 bbl/day, flexibility quick restart after shutting down. The disadvantages: not applicable in case of high GOR and sand production, tubing has to be pulled to replace the pump, high voltage (1000 V) electrical powers required, no suitable for low volume wells: <150 bbl/day, viscous crude reduce pump efficiency, and high temperature can degrade the electrical motor. [7]

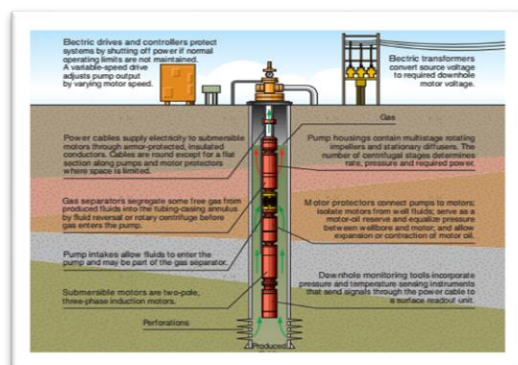


Figure 1. Electric Submersible Pump [2]

Saurabh and Dr. Tej Singh studied artificial lift to boost oil production [8]. Artificial lifts

improved profitability and efficiency by improving the production cycle of oil and gas reservoirs and raising flow rates. The purpose of artificial lift solutions was to reduce bottom-hole pressure and enable a well to produce at the desired flow. Usually, this included pumping gas or using a pump to decrease the hydrostatic pressure to give more lift pressure downhole. The authors of this study found that artificial lifts were a practical way to increase oil production, and they were also the most efficient by increasing the natural well flow and allowing the reservoir to accelerate production while delaying the operator's option to abandon a producing well, artificial lifts offered a chance to decrease back pressure on the well.

Hamdi Youcef studied an artificial lift ESP well on the BRN field (a case study of SFNE 13 oil well in Algeria) to raise the production [7] 2018). The study has been separated into three sections: the first discussed the advantages and disadvantages of each artificial lift method as well as the criteria to be used when choosing between them; the second part gave general information about ESP; and the last part focused on the design investigation and action evaluation of ESP on oil wells with high salinity and high WC using nodal analysis software (Prosper). The work finished by mentioning a few issues of ESP wells on BRN fields. The results showed the ESP's flexibility 100% WC handling capacity, and it could be used for both vertical and horizontal wells. It also offered us roughly 60% of the oil rate from a single well (SFNE 13). In addition, the disadvantage of the ESP system was the significantly short-run life (2 years) which made it the most cost-effective artificial lift method.

Wang et al 2023. studied the optimization of the well start-up procedure and operating parameters for ESP gas well dewatering [9]. Two gas wells had Electrical Submersible Pump (ESP) systems installed in to remove the gas from the wells. The well start-up operation recorded for the first problem showed that the ESP noticed gas locking. To prevent this, an accordingly suggested optimization method for the ESP well's start-up process with a check valve was designed. In the second, a set of optimization techniques for ESP operating parameter changes was provided in the nodal analysis method. The results showed a new well start-up technique for ESP removed the gas

from wells by a check valve with the use of this process, workover procedures can be avoided to prevent ESP start-up failure, saving the operators money, time, and effort. Furthermore, an optimization technique for production rate and ESP operating frequency was offered based on the nodal analysis method. The well's production capacity was increased through hydraulic fracturing. In addition, the computation results showed that the optimal pump efficiency might be achieved by an increase of 12.2–33% over the prior value.

Carlos Andrés et al studied the optimization of an electrical submersible pump artificial lift system for extra heavy oils through an analysis of the bottom dilution scheme [10]. To analyze the unknown behavior of the variables through their responsiveness in the vertical flow modeling used for a Chi Chimene Field well, this study presented the analysis of the variables that had the greatest effect on the energy requirements for an artificial lift system applied to extra heavy crude oils. The well depth, the flow rate of produced fluids, the reduction percentage, the viscosity and fluid density, and the necessary artificial lift system pressure difference were the variables that had been chosen. The results of this study showed that, for the extra heavy oil, the Modified correlations were more suitable for the calculations of the PVT parameters. Representing the computation of the GOR in solution and the bubble pressure, as well as the adjusted Vázquez-Beggs for the calculation of the oil compressibility including the adjustment of the IPR curve had been studied. Additionally, the oil had a high GOR value in solution when compared to the forecast made using correlations from traditional usage, suggesting that the oil might reach supersaturating conditions. Furthermore, the most important consideration in estimating the system's energy need was the dilution's effect on the oil density's drop. The concept considers a primary system such as rod pumping or ESP combined with gas lift as a secondary system. The design provided a wide operating range, allowing individual operation of the primary, the secondary, and the combined system, reaching the optimal technical and economic performance while the combined system was operating. The operating envelope was framed in terms of production rate and power consumption.

Weny and Wahyu Tri investigated the production optimization in well A and well B using an electric submersible pump (ESP) in the field of West Java, Indonesia [11]. Their research discussed the optimization of production carried out in Well A and Well B. The two wells were production wells with three production layers (multilayer) that had different characteristics for each layer. Based on the performance evaluation of the production well, well A and well B were no longer able to produce naturally (natural flow). They used an electric submersible pump. The results showed that an electric submersible pump was used for the two wells to achieve the production target of 4088 stb/d for well A and 2712 stb/d for well B. In addition, the best scenario for well A was to use the REDA D4300 pump which was operated at a frequency of 60 Hz and 156 stages, while well B used the REDA DN3100 pump which was operated at a frequency of 70 Hz and 188 stages. Furthermore, with the pump used, well A could produce a liquid of 4087.42 stb/d with a pump efficiency value of 70.04%. Then, well B could produce a liquid of 3163.37 stb/d with a pump efficiency value of 67.04%.

Dyah Rini R. researched the selection & optimization of artificial lift using Delphi, TOPSIS, and SAW methods for natural flow oil wells at HAS Field 2022 [12]. The Reduced oil production and increased water production were detrimental to the HAS field. The increased production of water is the cause of the production decline. A higher water cut and a decrease in reservoir pressure were the main causes of the production decline. The Delphi methodology, which merged the Topsis method with 21 screening characteristics, was employed in the artificial lift selection process. The electrical submersible pump (ESP) was the artificial lift technique employed at the HAS Field. The result showed that by optimizing the number of stages and setting the frequency to 45 Hz, they achieved an increase in production with the electric submersible pump (ESP). The results were encouraging. Another method of optimization involved gradually increasing the pump frequency to 60 Hz, without any modifications to the type of pump. Also, the HAS field's economic analysis determined that the most advantageous option was to employ an ESP pump.

Abbas Khaksar studied oil production optimization via optimum artificial lift design [13] (et al. 2017). That study presented optimization of the production conditions of three wells by using artificial lift method ESPs (Electric Submersible Pump). For that purpose, the single well model was created to predict future production conditions in the well drainage area and the recommended optimum production conditions. According to the results of that study, a total gas of 4.75 MMscf/day at a high pressure of 2000 psig could increase the total production of these three wells from 1032 to 6000 stb/day. Furthermore, the total power of 350 HP was required to run ESP for these wells to achieve the same oil production rate as that was considered in the gas lift design. In addition, for the effect of gas injection pressure and the gas specific gravity the authors referred that an increase in the injection pressure was not always beneficial for gas-lift operation if it exceeded the limit wanted, it might increase the compression cost and at a constant gas injection rate, the higher the gas specific gravity was not always good too, it might cause the lower oil production rate if it exceeded the limit wanted because it caused an increase in the bottom hole pressure.

Angung Wahyudi and Bambang studied the performance analysis of DN1750 and DN1800 electric submersible pumps for production optimization on the oil well [14]. In their research, an analysis of pump performance and optimization of ESP pumps were carried out using the Nodal Variable Speed Drive to determine the production capacity of the oil well and the pump speed according to the desired flow rate at frequency changes. The results showed the DN1750 pump at a frequency of 50 Hz with a pump speed of 3000 rpm and a frequency of 55 Hz with a pump speed of 3300 rpm worked under the desired optimum production rate. The DN1750 pump at a frequency of 60 Hz with a pump speed of 3600 rpm, a frequency of 65 Hz with a pump speed of 3900 rpm, and a frequency of 70 Hz with a pump speed of 4200 rpm operating above the optimum limit of the desired production rate. The DN 1750 Pump was not good capability of the oil well because it worked under conditions that were not optimal. In addition, the DN 1800 Pump at a frequency of 55 Hz with a speed of 3300 rpm was in the range of fluid flow rates desired by the oil well, which was 1936,698 Barrels Per Day (BPD) with a wellbore

pressure (PWF) of 629 psi by the production capacity of the oil well so a suitable pump was obtained and expected to work at optimum conditions.

Mohammed A. Al-Hejjaj et al. studied a review of the electrical submersible pump development chronology [15]. The main objective of this study was to deliver a general review of the development of the ESP Optimization problem and the available studies and applications to solve the problem at hand. After reviewing a fair number of studies and papers on the problem of ESP Optimization the following conclusions were made: The solutions available for the ESP optimization problem evolved rationally with the rising computational power and the computer abilities that were available to be utilized to the solution of the problem. Moreover, under gassy flow conditions with different amounts of surfactants, extensive experimental evaluations of ESP stage pressure increment should be done.

Njeudjang studied the optimization of field X's eruptive well X-1 by using the nodal analysis and PIPESIM software [16]. Achieving a production rate that is profitable economically was the aim of this article. The well X-1's production was increased by using the nodal analysis and PIPESIM software, completion data, pressure-volume-temperature (PVT) data, and reservoir data. By making changes, several optimization options were considered, including the tubing diameter, wellhead pressure, water cut, and flow line diameter. The main findings showed that by raising the flow line's diameter from 2.5 to 4 inches and lowering the wellhead pressure from 350 to 100 psia, the production flow rate could have increased from 850 to 2030.472 barrels per day.

Mohammed Saeed Mohammed et al. studied the comparison of the productivity of the gas lift and Electrical submersible pump (ESP) in Mishrif formation in Rami Ali Altam studied production optimization by nodal analysis [17]. It was important to make sure that every component of the production system, from the separator to the downhole completion, was running as efficiently as possible given the high cost of developing gas fields. Field optimization was intended to determine the ranges of operational parameters that would enable and help the operator reach the desired result, such as maximizing the field's total

production rate. Nodal analysis offered a practical means of helping in the decision-making process for optimization. The initial step was to optimize each well's tubing size. After that, the wells and surface facilities were integrated into a field-wide network model. The "X" field was critically analyzed using the available field data, and the following conclusions were reached when modeling every well using nodal analysis using a 2.75-inch tubing size was less advantageous than 3.5" tubing size when reservoir pressure and flow rate dropped; as a result, 3.5" tubing size was suggested. The duration of the perfect gas rate could also be extended by employing a compressor to decrease the minimum allowed backpressure at the wellhead. In addition, drilling new wells increased the gas recovery factor by around 14% and produced a longer and more stable production rate.

Sardam Ahmed et al. studied the optimization of oil and gas production using nodal analysis techniques in the Kurdistan field [18]. The authors observed that the petroleum production optimization was managed through well deliverability analysis that was determined by the combination of well inflow performance and wellbore flow performance. Using nodal analysis to find the effect of each parameter on the pressure drop and flow rate at different nodes in the production system. Examination of the inflow performance relationship with vertical flow performance will be carried out for steady-state flow regimes. The results showed that increasing the value of the reservoir temperature led to an increase in the production rate. Moreover, decreasing the value of the skin led to an increase in the production rate, and having a higher tubing diameter led to an increase in the production rate. In addition, increasing the value of the reservoir permeability led to an increase in the production rate, and decreasing the value of the tubing roughness led to an increase in the production rate. Finally, increasing the value of the perforation interval led to an increase in the production rate.

Muhab Abeed and Maamar Khalleefah investigated Nodal analysis calculation for the estimation of the best operating conditions using two wells Z1&Z2 in Libya 2023 [19]. In that study, two wells (Z1 and Z2) in the AL_Nafoora field in Libya were tested with a sensitivity analysis to simulate the IPR and OPR model using

PIPESIM software. This enabled researchers to determine the optimal operating conditions for flow rate and flowing bottom hole pressure, the maximum water cut ratio, and the maximum wellhead pressure value that should not be exceeded to preserve the natural flowing phase for as long as possible. The findings demonstrated that a higher productivity index, which raised the flow rate, relates to a larger pressure differential between the reservoir's pressure and the bottom hole pressure. Additionally, the flow rate value increases with decreasing pipe diameter for inner diameters. Furthermore, the productivity value increased with decreasing wellhead pressure. Finally, a drop in flow rate results from a higher bottom hole pressure value matching with a larger water cut value.

The use of artificial lift techniques in an oil field in the Rmelan field is examined in this study. Electrical submersible pumps (ESP) are one useful method in this field because of their high production compared with other artificial lift methods[4]. Six oil field wells are examined for this purpose based on what is currently known in this field. Water drive is the primary reservoir energy source. Therefore, a quick pressure reduction will take place in the well drainage area as a result of oil production. Many parameters are involved in a successful artificial lift operation. This study uses the PIPESIM Software as an attempt to specify these parameters in such a way that the production and the operation's net present values are maximized by changing the frequency of the ESP pump and decreasing the wellhead pressure between the wells and the facilities to find the best operating condition for each tested well.

3. Results and Discussion

3.1 The specification of ESP used in the Rmelan field.

The use of artificial lift techniques in an oil field in the Rmelan field is examined in this study. Because the pressure in this field became less to raise the fluid at the surface and the water cut is large about 70%.

Electrical submersible pumps (ESP) are one useful method in this field because of their high production compared with other artificial lift methods and useful for high water cut. In this paper, we are trying to evaluate the current well

performance of the tested wells operated by ESP at 50 HZ and trying to optimize the flow rate of the ESP pump through the sensitivity analysis on the pump frequency and wellhead pressure using PIPESIM Software version 2022.1. We selected six wells artificially lifted and operated with ESP pumps in the Rmelan field. The specification of ESP used in the Rmelan field is not included in PIPESIM software so, we selected the nearest specifications of pumps in PIPESIM to represent, evaluate, and optimize the ESP used in the Rmelan field as presented in Table 1.

Table 1: Specifications of ESP used in the Rmelan field.

Pump in Rmelan field	Pump in PIPESIM software
H-300/167stages	(1500-2500 bbl/day) ODI-RA22/167stages
H-200/148stages	(600-1800 bbl/day) (Alkhorayef /WG1600/) and (centre lift P16) (148 stages)

So, all tested runs on PIPESIM software were carried out on the selected pumps from PIPESIM manufacturers. The current operating conditions for the tested wells are listed in Table 2. This table shows the tested wells operated at a constant current pump frequency of 50 Hz, wellhead pressure changed from one well to another and the actual flow rate wasn't constant for the tested wells.

Table 2: Current Conditions for the Tested Wells

Well	No. of Stages	Frequency (Hz)	wellhead pressure(psi)	Actual flow rate (bbl/day)
7SV	167	50	142.71	1228
12RV	167	50	171.15	515
21KH	167	50	185.3	2020
21SH	148	50	142.71	1730
32KV	148	50	228.05	1375
155KV	148	50	199.6	1139

3.2 Well Modelling.

Two parameters control the well performance: Inflow performance relationship (IPR) and Vertical Lift Performance (VLP). IPR is known as the relationship between well-flowing bottom-hole pressure (Pwf) and production rate so it represents the flow from the reservoir to the inside wellbore[20].

Many correlations and methods can be used to describe the reservoir performance. Each correlation has specific conditions to be applied according to reservoir characteristics and flow type. The most important methods that could be used for black oil reservoirs are Vogle, Darcy, and Fetkovich methods. In this work, the productivity index (PI) is already calculated from PLT data of

the tested wells, therefore it can be used directly in Nodal analysis[21].

The VLP depends on many parameters such as fluid PVT properties, tubing inside diameter, surface pressure, well depth, water cut, and gas oil ratio.

ESP components are key parameters in ESP design. Any change in one or more of them will affect the overall ESP performance. ESP components are motor frequency which is the system prime mover and electric motor with different types and sizes of ESP motors that give different values of horsepower required.

The objectives of well modeling & analysis in this research are as follows:

1. To evaluate the current well conditions and when it might be ceased to produce. This could be due to the timing of reservoir pressure depletion or ESP problems such as up-thrust and down-thrust conditions (the pump works outside the range of pump performance).
2. To determine the optimum flow rate at which the well will flow with known wellbore conditions and completion.
3. To study the effect of changing the motor frequency and wellhead pressure on the well productivity.
4. To evaluate the well completion to determine if there is any restriction to flow unnecessarily.
5. To make a sensitivity analysis of motor frequency and wellhead pressure and choose the best controlling one for each tested well.

3.3 Nodal analysis for the Current system

The systems analysis approach represents a method for analysing the tested wells that allow the determination of the producing capacity for any combination of components (reservoir pressure, well productivity, wellbore completion, tubing string, surface choke). The essential principle of this method is to determine the location of the studying node. In this study, it is preferred to select the bottom hole pressure (Pwf) as the studying node to divide the production system into two parts: the piping system as the outflow curve and reservoir performance as the inflow curve. The initial node is the reservoir, and

the final node in this study is the wellhead pressure (WHP).

Figures 2 to 7 illustrate the IPR (representing what the reservoir can deliver in terms of oil quantity) versus the VFD (Variable frequency drive) relationship.

In these Figures, the blue line represents the inflow performance, and the red one represents the well vertical flow performance. The intersection point of those two lines represents the operating point for the tested well, which represents the flow rate the well can deliver. The analysis shows that well-7SV, well-12R, well-21Kh, well-21SH, well-32K, and well-155K have production rates of 1228,515,2020,1730,1375 and 1139 STB/Day respectively as presented in Table (2).

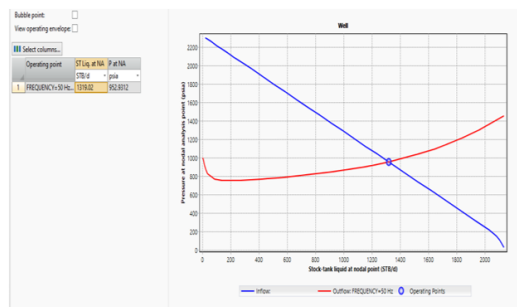


Figure 2: VLP/IPR relationship for the existing system for Well 7SV

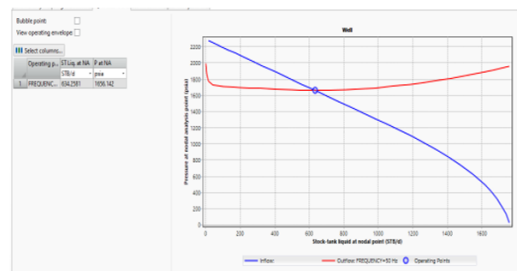


Figure 3: VLP/IPR relationship for the existing system for Well-12R

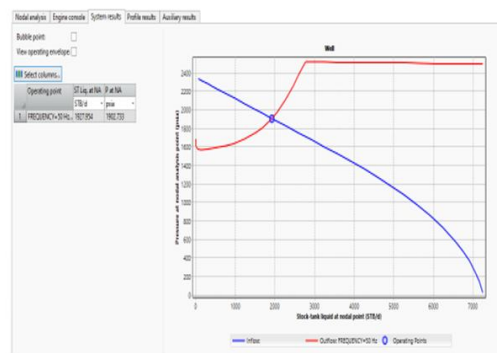


Figure 4: VLP/IPR relationship for the existing system for Well-21KH

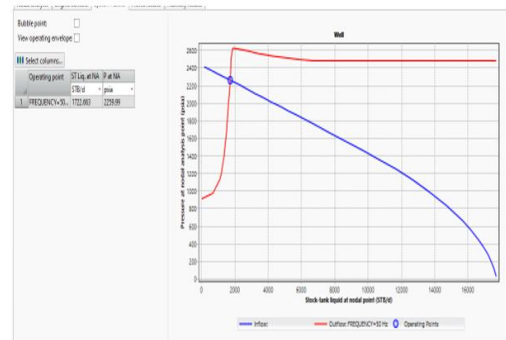


Figure 5: VLP/IPR relationship for the existing system for Well-21SH

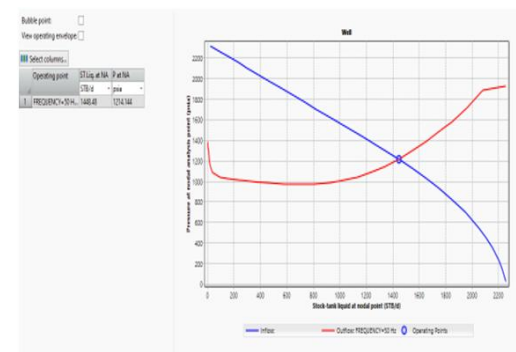


Figure 6: VLP/IPR relationship for the existing system for Well 32K

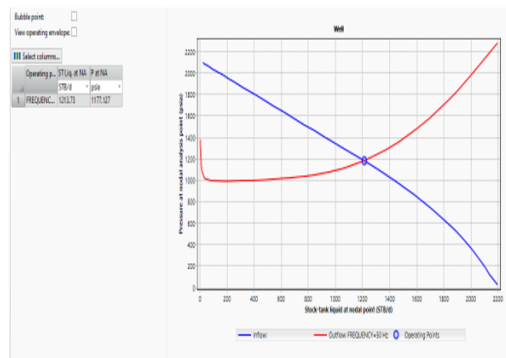


Figure 7: VLP/IPR relationship for the existing system for Well 155K

Figures 4 and 5 show that the intersection points (operating points) are close to the Y-axis. This means that the tubing sizes in these wells are too small to meet the reservoir production. Even though the reservoir may be capable of producing a large amount of fluid, if too much pressure drop occurs in the tubing, the well performance suffers. So, it is recommended to use PIPESIM software to optimize the tubing size to a large one relative to reservoir conductivity.

3.4 Sensitivity on Pump Frequency:

ESP is one of the artificial lift methods for the production of large production rates as well as

for deep wells. ESP regulates the production rate by operating frequency of electricity supplied to pump operation[22].

The frequency of electricity supplied can be changed by VSD (Variable Speed Drive) or VFG (Variable Frequency Drive) devices. Pump rate and pump power are proportional to the operating frequency[23]. When the operating frequency of the pump increases, the pump rate and capacity will also increase, which is clearly shown in the equations. (1) and (2).

In addition, the decrease in pressure discharge of the pump means that the pump power is reduced, so the friction of the IPR curve or the VLP curve depends on the selected node position concerning the selected node intake or discharge of the pump. Thus, determining the optimal operating frequency is very important in order to produce the maximum oil flow without affecting the life cycle of the ESP and this section will detail the optimization of operating frequency in this section. The relationship between the well production and the pump frequency may be expressed as:

$$\frac{Q_1}{Q_2} = \frac{F_1}{F_2} \tag{1}$$

Q_1 (STB/D): Production well at frequency F_1 (Hz)

Q_2 (STB/D): Production well at frequency F_2 (Hz)

Figures 8 to 13 represent the relationship between productivity and pressure at the point of nodal analysis at different frequencies for the tested wells. It is observed from these figures that, in general, as the frequency increases, productivity also increases. Also, the change in frequency has a good influence on the productivity for all tested wells except Well 21 SH as shown in Figure 11. It is observed from this Figure that, the operating points are close to each other this explains that the change in frequency has little effect on the productivity for this well.

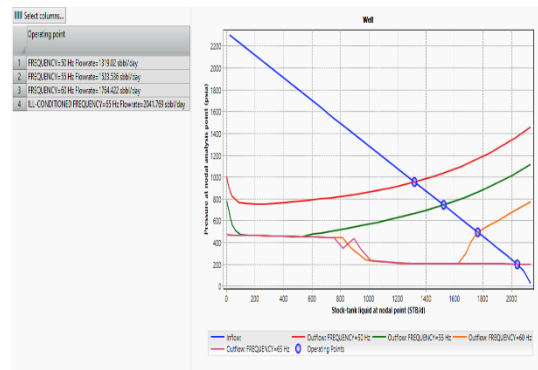


Figure 8: Sensitivity on pump frequency for well 7SV

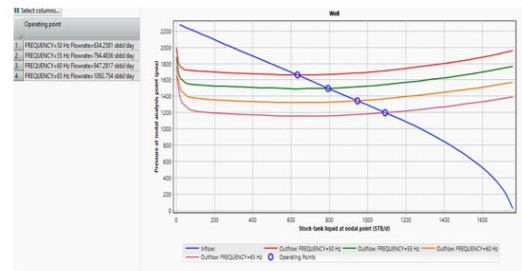


Figure 9: Sensitivity on pump frequency for well 12RV

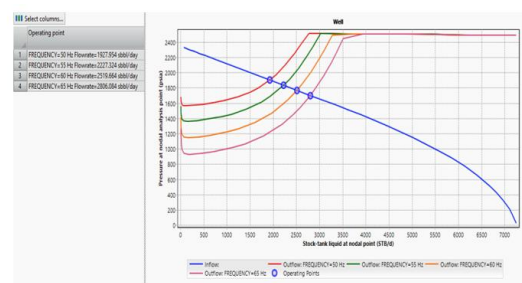


Figure 10: Sensitivity on pump frequency for well 21KH

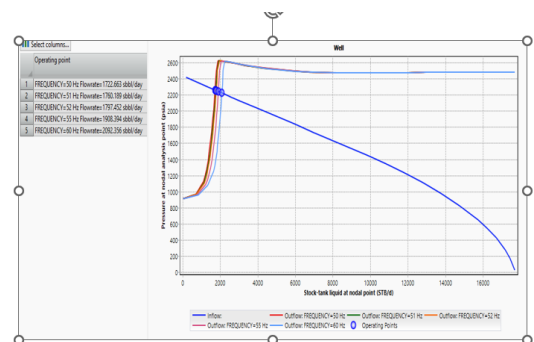


Figure 11: Sensitivity on pump frequency for well 21SH

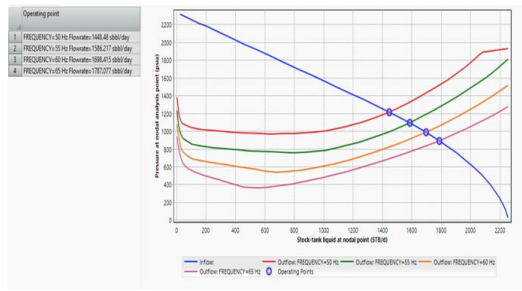


Figure 12: Sensitivity on pump frequency for well 32KV

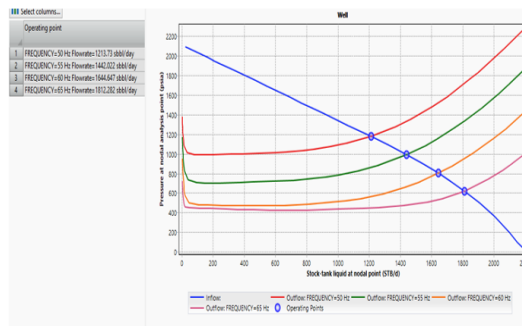


Figure 13: Sensitivity on pump frequency for well 155KV

For the same number of stages of ESP, the production rate increases when frequency increases this means that there is a direct relation between production rate and pump frequency as the pump will rotate more with high frequency. For example, the well 7SV produced 1319 STB/Day with 50 Hz then the flow rate increased to 2041.76 STB/Day with 65 Hz (number of stages equal to 167 stages). For the same frequency, well-155KV produces less fluid when the number of stages decreases. For the same frequency equal to 50Hz, the well produces 1448 STB/Day with 148 stages then the production rate increases to 1812 STB/Day with 65 Hz.

Increasing flow rate due to changing the frequency calculated from Eq. (2) and illustrated in Figure 14.

$$IR = \frac{Q_{\text{tested frequency}} - Q_{\text{current frequency}}}{Q_{\text{current frequency}}} \% \quad (2)$$

Where:

IR: Percent in increasing flow Rate due to change of frequency

$Q_{\text{tested frequency}}$: Flow rate at tested frequency, Hz

$Q_{\text{current frequency}}$: Flow rate at current frequency, Hz

Figure 14 illustrates the relationship between changing the frequency and increasing the production rate for tested wells. It is noticed from this figure that, the increasing flow rate for Well-12RV is the highest one for all tested frequencies. This means that the productivity of the well is affected more by changing the pump frequency.

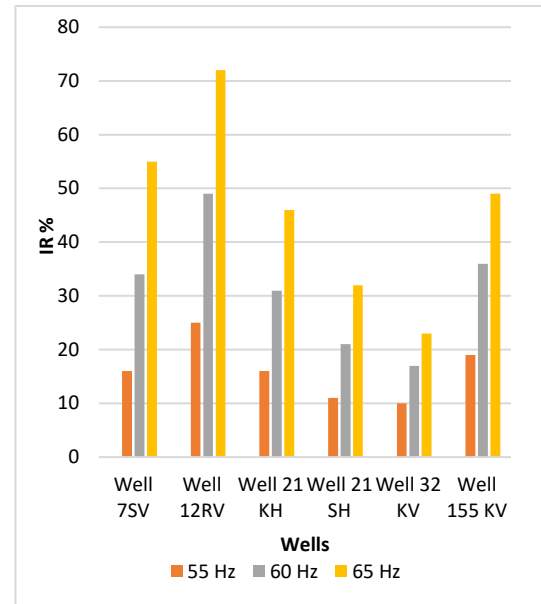


Figure 14. Effect of frequency change on productivity

3.5 Sensitivity on wellhead pressure:

The wellhead pressure has a direct influence on bottom hole pressure by the hydrostatic pressure. Figures 15 to 20 showed the relationship between the wellhead pressure and the well productivity.

According to these Figures, it instantly appears that the wellhead pressure is inversely proportional to the overall production rate. This can be explained by the fact that increasing wellhead pressure implies an increase in bottom-hole pressure. An optimal flow rate requires a significant drawdown (difference between reservoir pressure and bottom-hole pressure). The best value of interest on wellhead pressure here differs from one well to another. Also, it is observed that. The production rate decreases when wellhead pressure increases and this is due to more WHP, leading to more Pwf and less pressure drop across the reservoir causing a low production rate. The change in wellhead pressure has little effect on the productivity of Well-7SV and Well-21KH.

It is noticed also that, the operating point in Figure 18 is the same for all tested wellhead pressures this means that any change in wellhead pressure does not affect the well productivity for well-21SH.

It is obvious from these figures that, there is an inverse relationship between the wellhead pressure and IR. As the wellhead pressure decreases, the IR increases. The percentage of IR varies from one well to another as shown in these tables. For example, for well-12RV the production increased by 5.4 % when WHP decreased to 128.41 psi then increased to 12.9 % when WHP decreased to 71.58 psi. Well-21SH is less influenced by the change in wellhead pressure than the other wells. The increase in production rate is expressed as equation 3:

$$IR = \frac{Q_{\text{tested value (psi)}} - Q_{\text{current condition (psi)}}}{Q_{\text{current condition (psi)}} \% \quad (3)$$

Where:

IR: Percent in increasing flow rate due to change wellhead pressure %.

$Q_{\text{tested value (psi)}}$: Flow rate at tested wellhead pressure, bbl/day.

$Q_{\text{current condition (psi)}}$: Flow rate at the current operating well head, bbl/day.

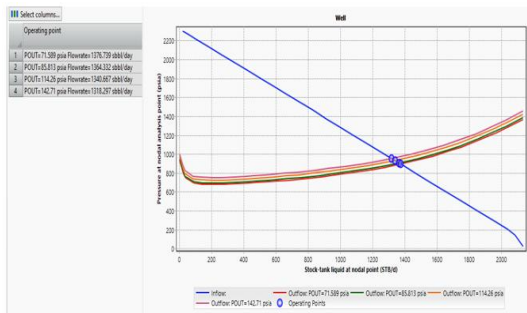


Figure 15: Sensitivity on wellhead pressure for well 7 SV

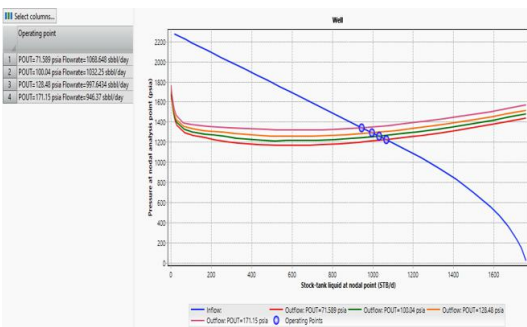


Figure 16: Sensitivity on wellhead pressure for well 12RV

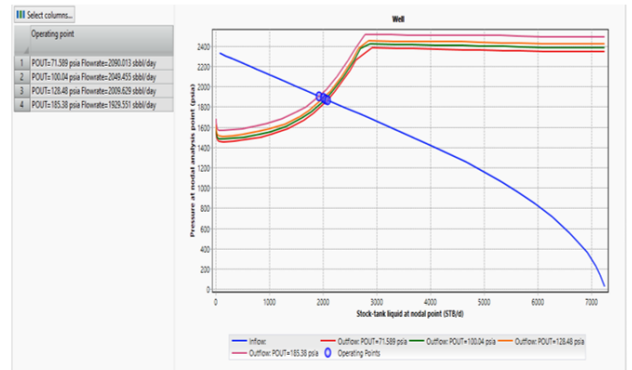


Figure 17: Sensitivity on wellhead pressure for well 21KH

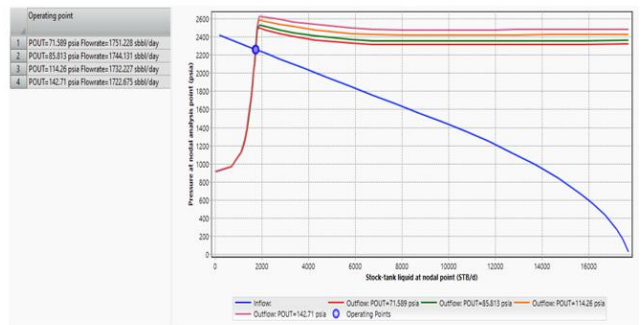


Figure 18: Sensitivity on wellhead pressure for well 21SH

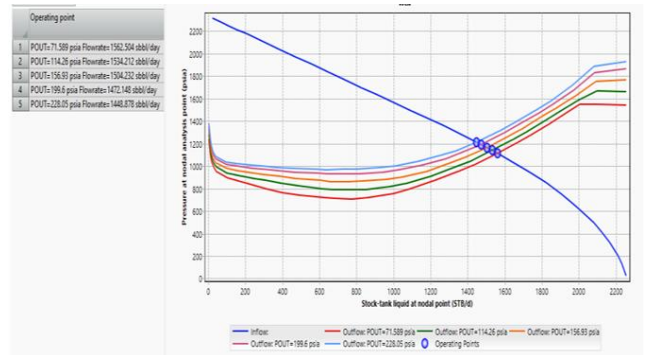


Figure 19: Sensitivity on wellhead pressure for well 32KV

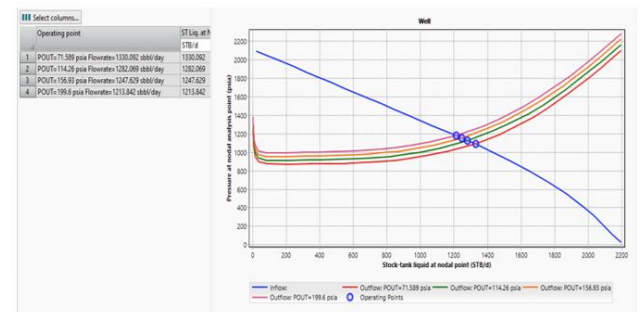


Figure 20: Sensitivity on wellhead pressure for well 155KV

ESP regulates the production rate by the operating frequency of electricity supplied to pump operation so this study suggests that the operating company can install one of the following devices to control the electricity to the pump and consequently change the frequency:

1- Variable frequency drive (VFD) device. The pump rate and pump power are proportional to the operating frequency. When the operating frequency of the pump increases, the pump rate and capacity will also increase.

2- Setting up a variable speed drive (VSD) with the submersible pump (ESP) on the wellhead to control the supply power to the motor and then control the frequency and the revolution per minute (RPM) of the pump [24].

Variable speed drives (VSDs) are used to control electrical ESP systems. They enable adjustments to be made to production parameters and ESP output when downhole conditions change. Increasing and decreasing motor speed may be used to optimize the pump performance, speed, or slow production, and avoid gas locking and system cycling. VSDs setting up have another advantage of protecting the pumps and motors by reducing electrical stress on startup and by adjusting to dynamic conditions as they change.

For this to be achieved, the operating company must use the appropriate method for each well according to the type of crude oil from the methods mentioned in the literature review (Section 2.5) to reduce the pressure drop in flow lines and thus lead to reducing the wellhead pressure for each well and consequently increasing the production rate.

4. Conclusions

From this study, the following conclusions may be drawn:

- The production rate increases when wellhead pressure decreases for the most tested wells.
- The wellhead Pressure can be decreased to the value that allows the fluid to flow through the flow line to process facilities.
- For ESP well, the production rate increases when ESP frequency increases and/or the number of stages increases.
- The change in ESP frequency differs from one well to another according to the well conditions and number of stages of ESP and the range between 55-65Hz.
- Some wells such as Well-21SH don't respond to changing pump frequency or the reduction of wellhead pressure may be due to any restrictions in well completion or organic or inorganic deposits.

Acknowledgment

We would like to thank colleagues who supported us.

Abbreviations:

AL: Artificial Lift.
 API: American Petroleum Institute.
 D: Darcy.
 ESP: Electric Submersible Pump.
 GL: Gas Lift.
 GOR: Gas Oil Ratio (SCF/STB).
 HJP: Hydraulic Jet Pump.
 IPR: Inflow Performance Relationship.
 IR: Percent in Increasing Flow Rate %.
 P/T: Pressure (Psi)/Temperature (F°).
 PCP: Progressing Cavity Pumps.
 PI: Production Index (STB/day.psi).
 PL: Plunger Lift.
 Pr: Reservoir Pressure (psi).
 PVT: Pressure, Volume and Temperature.
 Pwf: Wellbore Flow Pressure (psi).
 Qo(max): Max Oil Production Rate (STB/Day).
 Qo: Oil Production Rate (STB/Day).
 RPM: Revolution Per Minute.
 SRP: Sucker Rod Pump.
 SSSV: Subsurface Safety Valve.
 TVD: Total Vertical Depth, ft.
 VFD: Variable Frequency Drive.
 VLP: Vertical Lift Performance.
 VSD: Variable Speed Drive.
 VSD: Variable Speed Drives.
 WC: Water Cut %.
 WHP: Well Head Pressure (Psi).

Conflict of interest

The authors declare no conflicts of interest concerning this research.

Funding

No funding was received for conducting this study.

Author Contribution

A.M. Hussein and A.Z. Ahmed proposed the research problem. A.M. Hussein and T.M. Aboul-Fotouh developed the theoretical framework. S.

Gomaa verified the analytical methods. All authors participated in the discussion of the results and contributed to writing the manuscript.

AI Declaration Statement

The authors confirm that the manuscript has been written without the assistance of generative AI or AI-based writing tools.

Appendix A

A.1 Types of used pumps: H-300(1500-2500STB/Day) (ODI RA22/167stages):

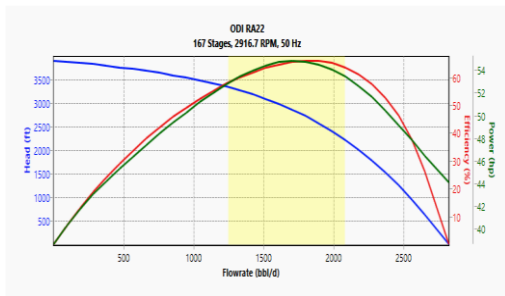


Figure A.1. Performance curve of the pump H-300(1500-2500STB/Day)(ODI RA22/167stages):

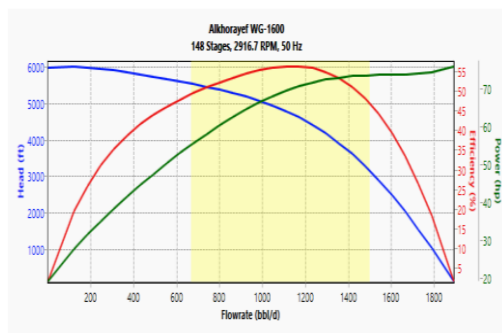


Figure A.2. Performance curve of the pump H-200(600-1800STB/Day)(WG1600/148stages):

References

- [1] H. D. Beggs, *Production Optimization Using Nodal Analysis 2nd Edition*, 1st ed. New York: Oil & Gas Consultants Intl, 2008, p. 411.
- [2] R. Fleshman and H. O. Lekic, "Artificial lift for high-volume production," *Oilfield review*, vol. 11, no. 1, pp. 49-63, 1999.
- [3] W. Astuti and W. T. J. J. o. E. E. E. Mulyono, "Production optimization in Well A and Well B using electric submersible pump (ESP)," *Journal of Earth Energy Engineering*, vol. 12, no. 2s, pp. 16-26, 2023, doi: <https://doi.org/10.25299/jeeec.2023.13957>.
- [4] H. Sucipto, S. S. Wiwaha, and I. Ridzki, "Instalasi Esp (Electric Submersible Pump) Sistem Tandem Pada Sumur Minyak Dengan Variable Speed Drive," *Jurnal Eltek*, vol. 16, no. 1, pp. 51-63, 2018, doi: <https://doi.org/10.33795/eltek.v16i1.86>.
- [5] K. E. Brown, "Overview of artificial lift systems," *Journal of Petroleum Technology*, vol. 34, no. 10, pp. 2384-2396, 1982, doi: <https://doi.org/10.2118/9979-PA>.
- [6] E. P. Kanu, J. Mach, and K. E. Brown, "Economic approach to oil production and gas allocation in continuous gas lift (includes associated papers 10858 and 10865)," *Journal of Petroleum Technology*, vol. 33, no. 10, pp. 1887-1892, 1981, doi: <https://doi.org/10.2118/9084-PA>.
- [7] Y. Hamdi and S. Latreche, "Artificial Lift: Esp Well on Brn Field (Case Study of SFNE 13 Oil Well)," M.Sc. M.Sc., Department of Hydrocarbons Production, University of Kasdi Merbah Ouargla, Ouargla, Algeria, 2018.
- [8] S. Goswami and D. Chouhan, "Artificial Lift to Boost Oil Production," *International Journal of Engineering Trends and Technology*, vol. 26, no. 1, pp. 1-5, 2015, doi: <https://doi.org/10.14445/22315381/IJETT-V26P201>.
- [9] X. Wang et al., "Optimization of the Well Start-Up Procedure and Operating Parameters for ESP Gas Well Dewatering," *Sustainability*, vol. 15, no. 2, p. 1498, 2023, doi: <https://doi.org/10.3390/su15021498>.
- [10] C.-A. Díaz-Prada, F. Guarín-Arenas, J.-E. González-Barbosa, C.-A. García-Chinchilla, E. d. J. Cotes-León, and C. Rodríguez-Walteros, "Optimization of electrical submersible pump artificial lift system for extraheavy oils through an analysis of bottom dilution scheme," *CT&F-Ciencia, Tecnología y Futuro*, vol. 4, no. 1, pp. 63-73, 2010, doi: <https://doi.org/10.29047/01225383.439>.
- [11] W. Astuti and W. T. Mulyono, "Production optimization in Well A and Well B using electric submersible pump (ESP)," *Journal*

- of *Earth Energy Engineering*, vol. 12, no. 2s, pp. 16-26, 2023, doi: <https://doi.org/10.25299/jeece.2023.13957>.
- [12] D. Kristanto, D. R. Ratnaningsih, H. S. Anshari, and D. S. Wicaksono, "Selection & Optimization of Artificial Lift Using Delphi, TOPSIS, and SAW Methods for Natural Flow Oil Wells at HAS Field," *Journal of Petroleum and Geothermal Technology*, vol. 3, no. 1, pp. 12-23, 2022.
- [13] A. K. Manshad, M. Jabbari, and A. H. Mohammadi, "Oil Production Optimization via Optimum Artificial Lift Design," in *Heavy Oil: Characteristics, Production and Emerging Technologies*, 1st ed. New York, USA: Nova Science Publishers, Inc., 2017, ch. Ch 3.
- [14] A. W. Biantoro, B. Darmono, and H. Pranoto, "Performance Analysis of DN1750 and DN1800 Electric Submersible Pump for Production Optimization on the Oil Well," *Institute for Research on Innovation and Industrial System (IRIS)*, vol. 3, no. 1, pp. 39-52, 2022, doi: <https://doi.org/10.37869/ijatec.v3i1.55>.
- [15] M. A. Al-Hejjaj, D. J. Sadeq, and O. Al-Fatlawi, "A Review of the Electrical Submersible Pump Development Chronology," *Iraqi Journal of Chemical and Petroleum Engineering*, vol. 24, no. 2, pp. 123-135, 2023, doi: <https://doi.org/10.31699/IJCPE.2023.2.14>.
- [16] K. Njeudjang, L. Karga, A. Chamgoue, J. Bawane, K. Njeudjang, and L. M. Ngueyep, "Production optimization of an eruptive well by using nodal analysis," *Journal of Ecology & Natural Resources*, vol. 6, no. 2, p. 000282, 2022, doi: <https://doi.org/10.23880/jenr-16000282>.
- [17] M. S. Mohammed, A. A. Al Dabaj, and S. A. Lazim, "Artificial lift design of Mishrif formation in Nasiriyah oil field," *Journal of Petroleum Research and Studies*, vol. 9, no. 2, pp. 1-21, 2019, doi: <https://doi.org/10.52716/jprs.v9i2.288>.
- [18] A. Sardam, K. Khalid, and A. Las, "Optimization of Oil and Gas Production Using Nodal Analysis Technique, Design Project Engineering," M.Sc., Department of Energy & Mechanical Engineering, American University of Iraq, Sulaimani, Iraq-Sulaimani, 2019.
- [19] H. B. Mahmud and A. Abdullah, "Investigate a gas well performance using nodal analysis," in *IOP Conference Series: Materials Science and Engineering*, 2017, vol. 217, no. 1: IOP Publishing, p. 012022, doi: <https://doi.org/10.1088/1757-899X/217/1/012022>.
- [20] H. D. Beggs, *Production Optimization Using Nodal (TM) Analysis*, 1st ed. New York: Oil & Gas Consultants Intl, 2008.
- [21] I. Salaudeen, D. Bopbekov, and A. Abdulkarim, "Optimization of petroleum production system using Nodal Analysis Program," *Nigerian Journal of Technological Development*, vol. 19, no. 1, pp. 1-8, 2022, doi: <https://doi.org/10.4314/njtd.v19i1.1>.
- [22] A. Al-Qasim, F. Almudairis, Z. AlAbdulatif, and M. Alsubhi, "Optimizing Production using Nodal Analysis Applications," in *SPE Kuwait Oil and Gas Show and Conference*, Mishref, Kuwait, 2019: SPE, p. D043S026R007, doi: <https://doi.org/10.2118/198136-MS>.
- [23] P. M. Lingom, J. Song-Manguelle, M. L. Doumbia, R. C. C. Flesch, and T. Jin, "Electrical submersible pumps: a system modeling approach for power quality analysis with variable frequency drives," *IEEE Transactions on Power Electronics*, vol. 37, no. 6, pp. 7039-7054, 2021, doi: <https://doi.org/10.1109/TPEL.2021.3133758>.
- [24] C. Schmehl, M. McKinley, W. McBride, J. Kavanaugh, and R. Paes, "Adjustable speed drive selection for electric submersible pumps," in *2014 IEEE Petroleum and Chemical Industry Technical Conference (PCIC)*, San Francisco, CA, USA, 2014: IEEE, pp. 201-216, doi: <https://doi.org/10.1109/PCICon.2014.6961885>.

Blank Page



Effect of Solar Module Operating Temperature on Electric Parameters of Photovoltaic Monocrystalline Module

Nadeem F. Kadhum ¹ , Emad T. Hashim ¹  

¹ Energy Department, College of Engineering, University of Baghdad, Baghdad, Iraq.

Article Info	ABSTRACT
<p>Received: 04 March 2026 Revised: 30 March 2026 Accepted: 30 March 2026 Available online: 31 March 2026</p> <p>Keywords:</p> <p>Current; Open; Temperature; Short; voltage</p>	<p>50W monocrystalline silicon solar module performance is tested with experimental measurements conducted at Baghdad city /Al-Jaderia (33.26 N, 44.21E). Solar irradiance striking is subjected to more losses which after the experiments conducted resulted approximately in 15% of the total energy which is converted into electric power energy. To study the effect of temperature variations on solar performance, solar irradiance must be kept constant and vice versa. Therefore, to have of the temperature range and for more accuracy, the measurements was done for tested module with three solar radiations levels; 500, 750 and 1000 W/m². The maximum value of power (P_{max}) at solar radiation intensity 1000W/m² was 46.34 W on January 2025 at cell temperature 24.1 °C, with the corresponding the maximum open voltage, and open circuit current 18.28 V, and 2.944 A respectively. The highest value of efficiency was 13.5 % January 2025 at solar radiation 500W/m². Consequently, the minimum value of power (P_{max}) at solar radiation intensity 500W/m² was 27.54 W on October 2024 at cell temperature 40.5 °C, with the corresponding the maximum open voltage, and open circuit current 18.01 V, and 1.752 A respectively. The lowest value of efficiency was 6.9 % October 2024 at solar radiation 1000W/m². In general, the results showed slightly decrease in short circuit current with temperature increasing. With temperatures change great influence on the output voltage especially on open circuit voltage while very small decrease in the output current has been noticed.</p>

1. Introduction

Solar energy is one of the major renewable energy resources since it is silent and an environmental-friendly power-generating process. Solar module is a process to convert solar energy to electrical power using semiconducting materials [1]. Solar module power outlet is measured at room temperature and pressure; irradiance 1000 W/m², temperature 25 °C, and standard earth spectrum AM 1.5 G, where G stands for global and includes both direct and diffuse radiation [2,3,4]. Actually, part of incident light that falls on solar panel is reflected or transmitted instead of being absorbed. Such losses are referred to as optical

losses [5,6,7,8,9]. The reflection losses directly reduce the I_{sc} of solar cells. Similarly, the finite thickness or geometry of the solar cell contributes to transmission losses in a PV cell. Furthermore, the application in this field need more work in design, sizing and dimensions. This technology needs more work and information on atmospheric conditions and weather parameters; atmospheric temperature, solar irradiance, and wind speed. New research work concerned with improvement of solar module performance and efficiency. These studies need more data about solar radiation and solar module operating temperature, were carried out by many researchers [10,11]. Operating solar module temperature is considered a major parameter effect on solar cell



performance [12]. They also stated that there is a linear proportionality between outlet power and solar module operating temperature. Previously, researchers found that solar cells differed in output depending on temperature changes. Skoplaki et al. [13] stated that the power output of PV modules was seen to lessen by 0.4 - 0.5% for each degree Celsius increase in temperature beyond the predetermined operational temperature, depending on the temperature coefficient of the power of the module. It was also discovered that the desired efficiency of a PV module could be influenced by varying the temperature around it [14]. Bonkaney et al. [15] studied the influence of ambient temperature over PV efficiency and power production, the study showed that when PV temperature raises by one degree Celsius the electrical performance and power output will reduce by 0.49% and 2.6 W respectively. Al-Damook, et al., 2022 [16] Studied the photovoltaic performance in Iraq under hazardous weather, and the results showed that with the lower ambient temperature would lead to higher power production. In this paper, it will review several important studies on the impact of environmental effect on the photovoltaic cell [17,18,19]. Operating solar module temperature is considered a major parameter effect on solar cell performance. Hashim, et al., 2016 [20] found the four-parameter model using different methods: slope method, and explicit simplified method. The accuracy of these methods as it's compared with the measured data are 5%, 7.9%, and 9.3% respectively An extensive work was done on impact of temperature on solar panel performance [21,22,23,,24]. Many literatures have been examined solar module performance and power output [25,26,27,28,29]. They also stated that there is a linear proportionality between outlet power and solar module operating temperature. Katee et al., 2022 [30] made experimental measurements for current, voltage, and power for two type of solar modules. These data were used to extract four parameters model using two different extracting methods. For monocrystalline solar panel the percentage errors 5%, and 8% for iterative method and simplified explicit, while for the corresponding copper indium gallium di-selenide one are 10% and 9%. More work concerned with modeling solar module are available in these references [17,31]. More recent work was done by Abdulhadi et al.,

2025 [32] on floating Photovoltaic Solar System of of some Iraq water infrastructure and also solar photovoltaic Systems a 100 MW system done by Faisal et al., 2025 [33]. The aim of this study is to study the effect of operating solar temperature on module electric parameters; open circuit voltage and short circuit current.

2. Experimental work

Monocrystalline solar module had been examined, which is from the first-generation solar module family. Table 1 gives the panel properties at reference Standard Test Conditions STC. The solar module is calibrated in fixed procedure in Energy Department Laboratory. The Wireless Weather Sensor have 19 measurements; weather, light, and GPS. More details for The Wireless Weather Sensor are available in Figure 1 and Table 2.

Table 1. Mono crystalline silicon solar panel properties

Area, m ²	V _{oc} , V	I _{sc} , A	Peak power, W	Peak voltage, V	Peak current, A	No. of cells
0.46	21.8	3.25	50	17.2	2.9	36



Figure 1. Wireless Weather Sensor with 19 measurements.

Solar module analyzer PROVA 210A is used to test the characteristics solar panel electric parameters (V_{oc} , I_{sc} , V_m , I_m and P_m). PROVA 210A generates the I-V curve by variable internal resistive load in ohm (Ω) (0 to ∞) with time (10sec) therefore for each value of load there is a value for voltage and current from (0, I_{sc}) to (V_{oc} , 0). The device has an option to setup the values of both solar radiation and the area of the solar module (Figure 2).



Figure 2. Prova 210A Solar Module Analyzer .

The present work was done during July 2024 to April 2025. The experimental work was obtained under the outdoor exposure in Baghdad-Al-Jaderia. The readings were taken in a selected days, where the atmospheric conditions of clear sky. To study the effect of temperature variations on solar performance, solar irradiance must be kept constant and vice versa. Therefore, to have the temperature range and for more accuracy, the measurements was done for tested module with three solar radiations levels; 500, 750, and 1000 W/m²

The solar module is cleaned before the tests. The solar module is fixed to the south direction with tilted angle 33° then recording the temperature of the back side of the module (using thermocouple) and start the IV scanning process which is done by the Solar Module Analyzer then save the data in the computer (see Figure 3).



Figure 3. Setup of the experiment

3. Result and discussions

3.1 Solar module electrical parameters

Tables 2-4 show solar module parameters (T_c (°C), V_{oc} (V), I_{sc} (A), P_{max} (W), V_{max} (V), I_{max} (A), η (%), and FF) with measured solar module operation temperature for solar irradiance of 500, 750 and 1000 W/m² respectively. Tables 3-5 also some contain environment conditions; ambient temperature (T_a) and wind velocity. The module operating temperature is usually determined by the heat balance between the heat generated in the bulk material of the module and the heat lost to the surrounding. The heat generated in the module depends on the amount of solar radiation incident on the module, conversion efficiency.

The maximum value of power (P_{max}) at solar radiation intensity 1000W/m² was 46.34 W on January 2025 at cell temperature 24.1 °C, with the corresponding the maximum open voltage, and open circuit current 18.28 V, and 2.944 A respectively. The highest value of efficiency was 13.5 % January 2025 at solar radiation 500W/m². Consequently, The minimum value of power (P_{max}) at solar radiation intensity 500W/m² was 27.54 W on October 2024 at cell temperature 40.5 °C, with the corresponding the maximum open voltage, and open circuit current 18.01 V, and 1.752 A respectively. The lowest value of efficiency was 6.9 % October 2024 at solar radiation 1000W/m².

Table 2. Solar module parameters with module operation temperature for solar irradiance of 500 W/m²

T _{am} , °C	v, m/s	T _c , °C	V _{oc} , V	I _{sc} , A	P _{max} , W	V _{max} , V	I _{max} , A	η, %	Date
40.5	2.3	42.3	18.01	1.752	27.54	15.85	1.738	11.7	10/2024
24.7	4.1	25.8	19.85	1.821	29.20	16.88	1.730	12.7	11/2024
18.6	3.6	20.4	20.37	1.852	30.78	17.52	1.757	13.4	12/2024
15.9	1.5	18.7	20.76	2.019	31.00	18.06	1.716	13.5	1/2025
23.2	2.2	24.0	20.22	1.847	30.69	17.05	1.707	13.3	2/2025
27.0	5.2	28.3	19.62	1.810	29.07	15.53	1.871	12.6	3/2025
28.5	4.5	30.8	19.00	1.796	28.41	16.41	1.731	12.4	3/2025

Table 3. Solar module parameters with module operation temperature for solar irradiance of 750 W/m²

T _{am} , °C	v, m/s	T _c , °C	V _{oc} , V	I _{sc} , A	P _{max} , W	V _{max} , V	I _{max} , A	η, %	Date
40.5	2.3	43.9	19.04	2.188	31.76	16.34	1.944	9.2	10/2024
24.7	4.1	28.0	19.96	2.192	35.83	17.59	2.037	10.4	11/2024
18.6	3.6	22.7	20.34	2.200	36.22	17.88	2.025	10.5	12/2024
15.9	1.5	20.3	20.86	2.220	36.36	18.30	1.987	10.5	1/2025
23.2	2.2	26.0	20.65	2.192	35.98	17.42	2.065	10.4	2/2025
27.0	5.2	30.4	20.11	2.171	35.78	17.22	2.078	10.4	3/2025
28.5	4.5	32.9	20.20	2.179	32.52	16.76	1.940	9.4	3/2025

Table 4. Solar module parameters with module operation temperature for solar irradiance of 1000 W/m²

T _{am} , °C	v, m/s	T _c , °C	V _{oc} , V	I _{sc} , A	P _{max} , w	V _{max} , v	I _{max} , A	η, %	Date
40.5	2.3	47.0	19.20	2.702	36.95	16.44	2.247	6.9	10/2024
24.7	4.1	31.1	20.83	2.811	43.86	17.62	2.489	9.5	11/2024
18.6	3.6	27.0	21.00	2.902	44.87	17.98	2.495	9.7	12/2024
15.9	1.5	24.1	21.64	2.944	46.34	18.28	2.535	10.1	1/2025
23.2	2.2	29.7	21.13	2.890	45.81	17.37	2.637	10.0	2/2025
27.0	5.2	32.9	20.31	2.785	43.20	17.25	2.504	9.4	3/2025
28.5	4.5	35.5	20.29	2.738	37.95	16.78	2.261	8.3	3/2025

3.2 Open circuit voltage and short circuit current changes with temperature

Solar module operating temperature sensitivity of photovoltaic panel is critical aspects of module electric output performance. When solar module operates a part of solar isolation will be converted to useful electric power, typically around 15%, and the remainder is dissipated as heat. This dissipated heat will increase module operating temperature, which in turn affects the module's electrical parameters, particularly the open-circuit voltage (V_{oc}). An elevated operating temperature can have detrimental effects on the performance of PV modules. Higher temperatures generally reduce the V_{oc} , which is an essential parameter for optimizing the system's power output. A lower V_{oc} means that the module needs to apply more voltage to initiate electricity generation, leading

to a decrease in overall power output. This reduction in power output can significantly impact the efficiency and profitability of solar energy systems. Moreover, the temperature variation also affects other electrical parameters of monocrystalline silicon solar modules, such as short-circuit current (I_{sc}) and fill factor (FF).

To analyze the data a scatter plot used between V_{oc} and I_{sc} for different solar irradiances: 500, 750, and 1000 W/m² and the corresponding module temperatures (available in Figure 1 and 2). It will be seen that there is a linear relation, so a linear regression was used to find a relation between them and the temperature.

The open circuit voltage has a logarithmic relationship with the solar radiation and has a little change with radiation variation at high radiation levels. The negative slope of the linear

fitting in Figure 4 represents the temperature coefficient (TCO) of V_{oc} . In general, the results showed decrease in short circuit current with temperature increasing.

PROVA 210A measures the short circuit current of a solar module at the beginning of the I-V curve where the resistive load is zero. The short circuit current is linearly proportional with the solar radiation and occasionally it is considered to be equal to the photo-generated current. A scatter plot illustrates the linear relationship represented by a linear regression equation where the positive slope is TCO of I_{sc} (see Figure 5). In general, the results showed slightly decrease in short circuit current with temperature increasing.

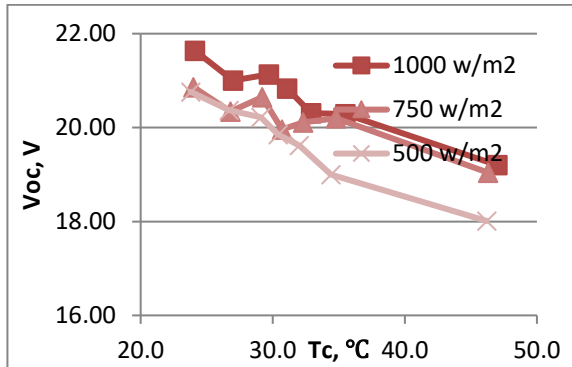


Figure 4. Variation of open circuit voltage with solar module operating temperature.

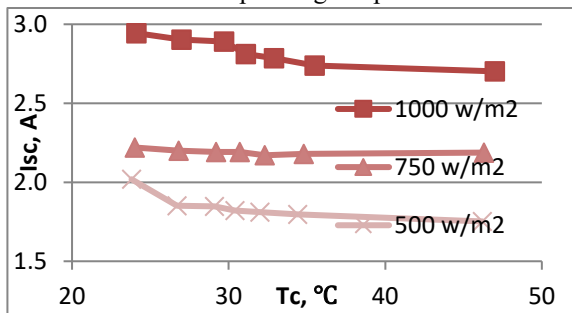


Figure 5. Variation of short circuit current with solar module operating temperature.

With temperatures change great change on the outlet voltage especially on open circuit voltage while very small decrease in the outlet current has been recognized. A plot is used to analyze the practical measurements of the open circuit voltage and short circuit current with panel temperatures. A linear regression analysis between V_{oc} and I_{sc} with the corresponding operating panel temperature. The major power drop in voltage values had been happen with

increasing operating panel temperature. The temperature coefficient (TCO) is defined as the amount of change in, or with temperature. TCO considered being equal to the slope of the linear equation as given in Equations 1 and 2, the value of the slope of each straight line equation is calculated. The TCOs of, or are symbolized as the following:

$$TCO_{V_{oc}} = \frac{\Delta V_{oc}}{\Delta T} \quad (1)$$

$$TCO_{I_{sc}} = \frac{\Delta I_{sc}}{\Delta T} \quad (2)$$

Where $TCO_{V_{oc}}$ and $TCO_{I_{sc}}$ are temperature coefficients of open circuit voltage and short circuit current respectively, ΔV_{oc} is the open circuit voltage difference, ΔI_{sc} : short circuit current difference and ΔT : temperature difference in $^{\circ}\text{C}$.

The measured data explain that monocrystalline module showed a decrease in open circuit voltage by $-0.1140 \text{ V}/^{\circ}\text{C}$ (average value). The outlet results showed a slightly decrease in short circuit current with temperature increasing about $-0.0065 \text{ A}/^{\circ}\text{C}$ (average value).

4. Conclusions

The temperature sensitivity of PV modules is a critical aspect of their electrical output performance. Higher temperatures generally reduce the V_{oc} , which is an essential parameter for optimizing the system's power output. The temperature variation also affects other electrical parameters of monocrystalline solar module, such as short-circuit current (I_{sc}) and fill factor (FF). Reduction in power output can significantly impact the efficiency and profitability of solar energy systems, this reduction in outlet power of solar module is function of decreasing of solar irradiance values. It is proved that increasing solar irradiance will increase module temperature at constant ambient temperature and also increased value of module temperature with increasing ambient temperature at constant solar irradiance.

Acknowledgements

The authors acknowledge the lab team at the Energy Department, College of Engineering, University of Baghdad for their assist.

Conflict of interest

The authors declare no conflicts of interest concerning this research.

Funding

No funding was received for conducting this study.

Author Contribution

N.F. Kadhun proposed the research problem. E.T. Hashim developed the theoretical framework. N.F. Kadhun, E.T. Hashim verified the analytical methods and participated in the discussion of the results and contributed to writing the manuscript.

AI Declaration Statement

The authors confirm that the manuscript has been written without the assistance of generative AI or AI-based writing tools.

References

- [1] R. Hill, "Prospects for photovoltaic," *Energy World*, no. 208, pp. 8–11, 1999.
- [2] A. S. Joshi, I. Dincer, and B. V. Reddy, "Thermodynamic assessment of photovoltaic systems," *Solar Energy*, vol. 83, no. 7, pp. 1139–1149, 2009. <https://doi.org/10.1016/j.solener.2009.02.007>
- [3] J. Wei, Q. Wang, J. Huo, F. Gao, Z. Gan, Q. Zhao, and H. Li, "Mechanisms and suppression of photoinduced degradation in perovskite solar cells," *Advanced Energy Materials*, vol. 11, no. 3, 2002326, 2021. <https://doi.org/10.1002/aenm.202002326>
- [4] W. Lipiński et al., "Progress in heat transfer research for high-temperature solar thermal applications," *Applied Thermal Engineering*, vol. 184, 116137, 2021. <https://doi.org/10.1016/j.applthermaleng.2020.116137>
- [5] B. Lorenzi, M. Acciarri, and D. Narducci, "High temperature behavior of solar materials," *Journal of Materials Research*, vol. 30, no. 18, pp. 2663–2672, 2015. <https://doi.org/10.1557/jmr.2015.212>
- [6] O. Dupré, R. Vaillon, and M. A. Green, "Thermal behavior of photovoltaic devices: Physics and engineering," *Solar Energy*, vol. 140, pp. 73–88, 2016. <https://doi.org/10.1016/j.solener.2016.11.017>
- [7] K. P. Sarath et al., "Advances in heat transfer physics in latent heat storage systems," *Thermal Science and Engineering Progress*, vol. 38, 101886, 2023. <https://doi.org/10.1016/j.tsep.2023.101886>
- [8] S. K. Sharma et al., "Nanoparticles-based magnetic and photo-induced hyperthermia for cancer treatment," *Nano Today*, vol. 29, 100795, 2019. <https://doi.org/10.1016/j.nantod.2019.100795>
- [9] S. Fang et al., "Turning dead leaves into an active multifunctional material as evaporator, photocatalyst, and bioplastic," *Nature Communications*, vol. 14, no. 1, p. 1203, 2023. <https://doi.org/10.1038/s41467-023-36848-8>
- [10] E. T. Hashim and Z. R. Talib, "Study of the performance of five parameter model for monocrystalline silicon photovoltaic module using reference data," *FME Transactions*, vol. 46, no. 4, pp. 585–594, 2018. <https://doi.org/10.5937/fmet1804585H>
- [11] S. T. Mohammad, H. H. Al-Kayiem, M. A. Aurybi, and A. K. Khelif, "Measurement of global and direct normal solar energy radiation in Seri Iskandar and comparison with other cities of Malaysia," *Case Studies in Thermal Engineering*, vol. 18, 100591, 2020. <https://doi.org/10.1016/j.csite.2020.100591>
- [12] A. Cavaco, P. Canhoto, and M. C. Pereira, "Corrigendum to 'Procedures for solar radiation data gathering and processing and their application to DNI assessment in southern Portugal'," *Renewable Energy*, vol. 168, p. 1405, 2021. <https://doi.org/10.1016/j.renene.2020.10.075>

- [13] J. Fesharaki, M. Dehgani, J. Fesharaki, and H. Tavasoli, "Effect of temperature on photovoltaic cell efficiency," in Proc. 1st Int. Conf. Emerging Trends in Energy Conservation, Tehran, Iran, Nov. 20–21, 2011.
- [14] E. Skoplaki and J. A. Palyvos, "On the temperature dependence of photovoltaic module electrical performance: A review of efficiency/power correlations," *Solar Energy*, vol. 83, no. 5, pp. 614–624, 2009. <https://doi.org/10.1016/j.solener.2008.10.008>
- [15] A. H. Al-Waeli et al., "Photovoltaic solar thermal (PV/T) collectors past, present and future: A review," *International Journal of Applied Engineering Research*, vol. 11, no. 22, pp. 10757–10765, 2016.
- [16] A. L. Bonkaney, S. Madougou, and R. Adamou, "Impact of climatic parameters on the performance of solar photovoltaic (PV) module in Niamey," *Smart Grid and Renewable Energy*, vol. 8, no. 12, pp. 379–393, 2017. <https://doi.org/10.4236/sgre.2017.812025>
- [17] M. Al-Damook et al., "Photovoltaic module efficiency evaluation: The case of Iraq," *Alexandria Engineering Journal*, vol. 61, no. 8, pp. 6151–6168, 2022. <https://doi.org/10.1016/j.aej.2021.11.046>
- [18] E. T. Hashim and Z. R. Talib, "Modeling and simulation of solar module performance using five parameters model by MATLAB in Baghdad city," *Journal of Engineering*, vol. 24, no. 10, pp. 15–31, 2018. <https://doi.org/10.31026/j.eng.2018.10.02>
- [19] S. A. Mohammed and E. T. Hashim, "Synchronous buck converter with perturb and observe maximum power point tracking implemented on a low-cost Arduino microcontroller," *Journal of Engineering*, vol. 24, no. 2, pp. 16–33, 2018. <https://doi.org/10.31026/j.eng.2018.02.02>
- [20] S. A. Mohammed and E. T. Hashim, "Designing a maximum power point tracking system for a monocrystalline silicon solar module using the Arduino microcontroller and synchronous buck converter," *FME Transactions*, vol. 47, no. 3, pp. 524–533, 2019. <https://doi.org/10.5937/fmet1903524M>
- [21] E. T. Hashim and A. A. Abbood, "Temperature effect on power drop of different photovoltaic module," *Journal of Engineering*, vol. 22, no. 5, pp. 126–143, 2016. <https://doi.org/10.31026/j.eng.2016.05.09>
- [22] Y. Sanusi, G. Fajinmi, and E. Babatunde, "Effects of ambient temperature on the performance of photovoltaic solar systems in a tropical area," *The Pacific Journal of Science and Technology*, vol. 12, no. 1, pp. 176–180, 2011.
- [23] J. Zhou, Q. Yi, Y. Wang, and Z. Ye, "Temperature distribution of photovoltaic module based on finite element simulation," *Solar Energy*, vol. 111, pp. 97–103, 2015. <https://doi.org/10.1016/j.solener.2014.10.040>
- [24] P. S. Rani, M. S. Giridhar, and S. Prasad, "Effect of temperature and irradiance on solar module performance," *IOSR Journal of Electrical and Electronics Engineering*, vol. 13, no. 2, pp. 36–40, 2018. <https://doi.org/10.9790/1676-1302033640>
- [25] M. K. S. Al-Ghezi, R. T. Ahmed, and M. T. Chaichan, "The influence of temperature and irradiance on performance of the photovoltaic panel in the middle of Iraq," *International Journal of Renewable Energy Development*, vol. 11, no. 2, pp. 501–513, 2022. <https://doi.org/10.14710/ijred.2022.43713>
- [26] W. Luo et al., "Potential-induced degradation in photovoltaic modules: A critical review," *Energy & Environmental Science*, vol. 10, no. 1, pp. 43–68, 2017. <https://doi.org/10.1039/c6ee02271e>
- [27] J. Lindahl, M. R. Dahlberg, and A. O. Westerberg, *National Survey Report of PV Power Applications in Sweden 2019: Task 1 Strategic PV Analysis and Outreach*. International Energy Agency, 2019.

- [28] S. Kurpaska et al., "Efficiency of solar radiation conversion in photovoltaic panels," *BIO Web of Conferences*, vol. 10, no. 02014, pp. 1–10, 2018. <https://doi.org/10.1051/bioconf/20181002014>
- [29] S. R. Depuru and M. Mahankali, "Performance analysis of a maximum power point tracking technique using silver mean method," *Advances in Electrical and Electronic Engineering*, vol. 16, no. 1, pp. 25–35, 2018. <https://doi.org/10.15598/aece.v16i1.2249>
- [30] B. Bora, O. S. Sastry, A. Kumar, et al., "Estimation of most frequent conditions and performance evaluation of three photovoltaic technology modules," *Journal of Solar Energy Engineering*, vol. 138, no. 5, pp. 054504, 2016. <https://doi.org/10.1115/1.4034202>
- [31] N. S. Katee, I. B. Abdullah, and E. T. Hashim, "Extracting four solar model electrical parameters of mono-crystalline silicon (mc-Si) and thin film (CIGS) solar modules using different methods," *Journal of Engineering*, vol. 27, no. 4, pp. 16–32, 2021. <https://doi.org/10.31026/j.eng.2021.04.02>
- [32] N. J. Kadia, E. T. Hashim, and I. B. Abdullah, "Performance of different photovoltaic technologies for amorphous silicon (A-Si) and copper indium gallium diselenide (CIGS) photovoltaic modules," *Journal of Engineering and Sustainable Development*, vol. 26, no. 1, pp. 95–105, 2022. <https://doi.org/10.31272/jeasd.26.1.10>
- [33] Z. A. Abdulhadi, E. T. Hashim, and M. H. Tolephih, "Investigation of some key factors impacting floating photovoltaic solar system performance on major Iraq water bodies," *Journal of Engineering*, vol. 31, no. 3, pp. 63–80, 2025. <https://doi.org/10.31026/j.eng.2025.03.04>
- [34] S. S. Faisal and E. T. Hashim, "An approach to solar photovoltaic systems simulation utilizing builder block: A case study of a 100 MW system," *Journal of Engineering*, vol. 31, no. 1, pp. 98–119, 2025. <https://doi.org/10.31026/j.eng.2025.01.06>
-



Simulation Approaches for Polyurethane Materials: A Multiscale Review

Ahmed K. Al-Kamal^{1*}  

¹ University of Duisburg Essen - Campus Duisburg, Germany.

Article Info	ABSTRACT
<p>Received: 14 March 2026 Revised: 28 March 2026 Accepted: 29 March 2026 Available online: 31 March 2026</p>	<p>Polyurethane (PU) products enjoy remarkable versatility due to their tunable chemistry, segmented structure, and a wide range of mechanical properties, making them useful in flexible foam products, structural systems, and biomedical applications. However, the complex multiphase morphology and the strong interaction between reaction and processing processes make experimental characterization incomprehensible on its own. In turn, computational studies have become essential to study and design PU systems at a range of spatial and temporal scales. The current review provides an overview of simulation methodologies that are relevant to polyurethane, including atomistic molecular dynamics (MD), coarse-grained (CG), and mesoscale simulations, including dissipative particle dynamics (DPD), finite element method (FEM) modeling, and computational fluid dynamics (CFD) simulations. Atomistic models provide data on molecular interactions, hydrogen bonding, and thermomechanical behavior, and CG and mesoscale methods on phase separation and morphological evolution. At the bigger length scale, nonlinear mechanical response can be predicted using FEM, whereas foaming and mold-filling processes can be predicted using CFD that is coupled with reaction kinetics and population balance equations. Its focus is on multiscale modeling strategies, which combine these apparently different approaches, hence allowing the explanation of structure-property-process links. New trends and modern issues, including the integration of machine learning and tool models of digital twins, are also mentioned, highlighting new opportunities in predictive design, based on simulations, of polyurethane materials.</p>
<p>Keywords:</p> <p>Polyurethane; Finite element; Multiscale coupling; Optimization; Simulation.</p>	

1. Introduction

Polyurethane (PU) is one of the most universal families of polymer which is used in a wide range of applications, including automotive seating and insulation foams, biomedical devices and structural composites. Due to its multi-phase architecture, reaction chemistry and non-linear behavior of mechanical response, computational simulation has served to become an unavoidable supplement to experiment in elucidating, designing and optimization of PU systems. The review is a survey of the major simulation strategies used in polyurethane, based on length

and time scale: molecular dynamics (MD), coarse-grained (CG) and mesoscale methods, finite element modelling (FEM), and process-level computational fluid dynamics (CFD) simulations, and more importantly the strategies of multiscale coupling methods that span between these scales. [1-5]

The connectivity of different modeling strategies at length and time scale is demonstrated by a hierarchical multiscale simulation framework of polyurethane materials. On a microscopic scale, quantum chemical computations and atomistic MD reaction captures the formation of bonds, hydrogen bonding and segmental dynamics. The



results guide CG and dissipative particle dynamics (DPD) models, which are models of the separation of the microphase and the mesoscale morphology. Foaming, mold filling, and processing dynamics at the macroscopic scale is modelled with CFD with phase-field or population balance equation (PBE), whereas the dynamics of global mechanical behaviour of the system is predicted by FEM simulations. The information enters the system and spreads upwards by transfer of the parameters by-parameter fields, constitutive laws and

downwards in terms of boundary conditions and validation and allows an integrated design of materials and processes. Table 1 provides a comparative overview of the main simulation techniques applied to the modeling of polyurethane material, their descriptive length and time scales, strengths and weaknesses. This review is to guide selection of methodology and also to contextualise the multiscale framework addressed in this review.

Table 1. Comparison of simulation approaches for polyurethane materials across length and time scales

Method	Time Scale	Key Strengths	Key Limitations	Typical PU Applications
Atomistic Molecular Dynamics (MD)	ns– μ s	High chemical fidelity; captures hydrogen bonding, chain dynamics, diffusion	High computational cost; limited time/length scales	Tg prediction, HB analysis, diffusion, nanocomposites
Coarse-Grained MD (CG)	μ s–ms	Larger systems; captures phase separation and morphology	Reduced chemical detail; parameterization complexity	Microphase separation, hysteresis, network formation
Dissipative Particle Dynamics (DPD)	μ s–ms	Efficient mesoscale morphology prediction; good for soft matter	Limited molecular specificity; coarse interactions	Domain morphology, shape-memory behavior
Monte Carlo (MC)	Not time-resolved	Efficient equilibrium structure prediction	No real-time dynamics	Phase diagrams, thermodynamic studies
Finite Element Method (FEM)	ms–s	Accurate macroscopic mechanical response; engineering relevance	Requires constitutive models and experimental calibration	Foam mechanics, elastomers, structural behavior
Computational Fluid Dynamics (CFD)	ms–min	Captures flow, heat transfer, and reaction coupling	Highly sensitive to input parameters; complex coupling	Foaming, mold filling, RIM processes
Population Balance Equation (PBE)	ms–min	Predicts bubble size distribution and evolution	Requires coupling with CFD; kernel assumptions	Foam structure prediction
Multiscale Approaches	ns–min	Bridges chemistry to processing; predictive design	Complex implementation; data transfer challenges	Integrated PU design and process optimization

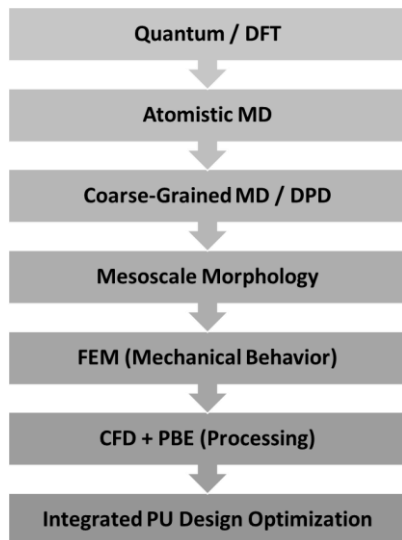


Figure 1. Multiscale simulation framework for polyurethane materials.

2. Atomistic Molecular Dynamics Simulations

Atomistic molecular dynamics (MD) simulation forms the major computational technique that has been used to study the underlying structure-property relationship of polyurethane at the molecular level. In such simulations, explicit models are used to represent individual atoms and their time evolution is modeled by solving Newton equations of movement in the presence of empirical force field terms such as COMPASS, DREIDING or OPLS [6, 7]. One of the main uses of atomistic MD is prediction of thermomechanical properties. E.g. Yeh and Hsieh (2023) used atomistic MD to study HDI-PTMO and MDI-PTMO polyurethane systems and again showed higher glass transition temperatures (T_g) in MDI-PTMO, qualitatively in agreement with experimental results. They explained this trend by the fact that more rigid chain structures are available, and differences in hydrogen-bonding interactions occur. In the MDI-PTMO systems, more hydrogen bonds were identified between the amide-hydrogen atom and ether-oxygen atom of PTMO, in contrast to the HDI-PTMO in which more hydrogen bonds were found to be persistent between the carbamate groups. [6, 8, 9]

Talapatra and Datta studied graphene-reinforced thermoplastic polyurethane (Gr/TPU) nanocomposites using the COMPASS force field in Materials Studio, finding that MD simulations could predict glass transition temperature,

coefficient of thermal expansion, heat capacity, and thermal conductivity with results in reasonable agreement with experimental values [7]. Their work showed that the incorporation of graphene into the TPU matrix increases the T_g due to stronger interlocking between graphene and TPU molecules, and volumetric coefficient of thermal expansion ranged between 2.6×10^{-5} and $2.4 \times 10^{-4} \text{ K}^{-1}$ [7]. MD simulations are also used to study stress-strain behavior: Zhang et al. (2012) simulated a shape memory polyurethane (SMPU60) with 60 wt% hard segments, finding the computed T_g of 328 K in good agreement with the DMA-measured value of 316 K, and revealed that hydrogen bond dissociation with increasing temperature leads to decreased moduli [10]. Wang et al. (2022) further showed through MD simulation that the content and strength of hard segments directly govern the viscoelasticity of the PU elastomer, with phase separation between hard and soft segments being the mechanistic origin of these effects. [11-13]

Molecular dynamics has also been applied to study diffusion phenomena within PU matrices. Wang (2013) investigated the diffusion of nitroglycerin (NG) in elastomeric polyurethane via MD with the COMPASS force field, finding that diffusion coefficients are on the order of $10^{-8} \text{ cm}^2/\text{s}$ in agreement with experiment, and increase with chain flexibility and temperature above 308 K [14]. Pebdani and Miller (2021) used MD to study pull-out of halloysite nanotubes (HNTs) from a PU matrix, employing machine learning particle swarm optimization to parameterize the force field from DFT data and demonstrating that interfacial energy variation can serve as a cohesion strength metric between matrix and nanoparticle [15]. More recently, Pebdani (2022) applied MD to study the Mullins effect in HNT-reinforced PU, showing that residual strain increases with cyclic stretch loading and that increasing hard segment content or HNT volume fraction reduces permanent set. [16-19]

3. Coarse-Grained and Mesoscale Simulations

While atomistic MD captures molecular-level detail, its computational cost limits accessible length and time scales. Coarse-grained (CG) models address this by replacing groups of atoms with single interaction beads, enabling

simulation of larger systems and longer timescales[20]. Uddin and Ju (2017) proposed an enhanced coarse-graining method for thermoplastic polyurethane (TPU) using three beads, incorporating pressure-correction to the force field and demonstrating that the resulting CG model captures bulk properties such as density variation with temperature, phase separation, and mechanical moduli, with bulk modulus substantially exceeding shear modulus as expected for elastomers[20]. In related work, Uddin and Ju (2016) used coarse-grained MD to predict the hysteresis of TPU by varying hard segment weight % from 34.90% to 62.30%, correlating hysteresis losses with bulk moduli and Poisson's ratios across different strain amplitudes and loading frequencies. [21]

The MARTINI force field has been applied to polyurethane step-growth polymerization. Ghermezcheshme et al. (2019) developed a fully automated MARTINI-based CG simulation method for cross-linked PU networks, capable of simulating the cross-linking reactions up to very high conversions and under complex conditions such as non-stoichiometric reactant ratios, solvent evaporation, and multi-step reactant addition [22]. They presented a new network-analysis paradigm akin to size exclusion chromatography carried out via graph theory, which observed that a two step addition strategy gives the greatest integrated network structure and that the dangling chains repress the glass-transition temperature in comparison with networks that exclude such chains. Similarly, Wu et al. (2024) performed a study to describe the three-dimensional cross-linked network of foamed polyurethane by using classical molecular dynamics and coarse-grained modeling and graph-theoretical methods. Their results point to the fact that the improved network connectivity leads to the high rate of shorter simple cycles that restrict the deformation and thus, gives a more homogeneous strain field and higher tensile strength of polyurethane closed cells. [23-26]

Mesoscale simulation methods such as dissipative particle dynamics (DPD) have become a formidable method of explaining phaseseparated morphologies in segmented polyurethane (PU). Hu et al. (2016) used DPD simulations in a recent study to define the nanoscale unit-cell morphological architecture of shape-memory polyurethane in which 30 wt% content of hard

segment was used (HSC). Their analysis showed that there was a linked-spherical netpoint structure that consisted of diphenylmethane diisocyanate (MDI) hard segments, a matrix-switch phase that was dominated by polycaprolactone (PCL), and an interphase that was connected and spider-like in nature and composed of 1,4-butanediol (BDO). [27]. Park et al. (2024) applied DPD to understand the shape-memory mechanism of TPU, finding that as hard segment content increases, the hard-segment domain transitions from isolated to lamellar to interconnected to continuous, providing critical insights into how microstructure governs macroscopic shape-memory behavior [28]. Vakili et al. (2020) used CG-MD to demonstrate microphase separation between polycarbonate and polyethylene glycol soft segments in segmented PUs, showing a core-shell structure where hard segments are squeezed between two incompatible soft segments. [29-32]

Shape-memory PU nanocomposites have also been investigated by CG-MD. Park et al. (2024) studied the thermo-mechanical behavior of semicrystalline SMPU-silica nanocomposites, revealing that elevated silica content triggers nanoparticle clustering that degrades shape recovery, and that HSC determines matrix-nanoparticle compatibility and nanoparticle agglomeration . [33-36]

4. Reaction Kinetics and Polymerization Simulations

Computational simulation of polyurethane reaction kinetics addresses the complex thermoset polymerization that involves dozens of degrees of freedom. Al-Moameri et al. (2015) developed a computer-based simulation framework for rigid PU foam-forming reactions, comparing predictions against experimental data for six blowing agents including methyl formate and C5-C6 hydrocarbons [37]. The evaporation of blowing agents was modeled as an overall mass transfer coefficient time the activity difference between gas foam cells and resin walls, and successful simulation required this coefficient to decrease to near zero as foam approached its gel point. In subsequent work, Al-Moameri et al. (2017) [38] introduced a viscosity-dependent frequency factor in the Arrhenius equation to account for the increase in viscosity during thermoset polymerization, which can span several orders of

magnitude, reducing the number of fitted parameters required and improving the transferability of kinetic models across different polyol systems[38]. The simulation was based on simultaneous solution of over two dozen ordinary differential equations for the many reaction and physical processes occurring during foaming. [39-41]

Al-Moameri et al. [37] explored the effect of maximum foam reaction temperature on decreasing the percentage of shrinkage in rigid polyurethane foams made out of soy based polyols and, as such, demonstrated that simulation is an enabling technology in green chemistry in the polyurethane industry, as it enables the rapid mapping of optimal formulations [42]. A new approach to the simulation of polyurethane foam in the form of a baseline model based on the population balance equation (PBE) was proposed by Karimi and Marchisio (2015), who follows the distribution of bubble sizes (BSD) changes over time as a fundamental determinant of the final thermal and mechanical characteristics. The model predictive results were compared to experimental results based on twelve different chemical formulations, with tolerable concordance found; the next step is to make the PBE a part of a computational fluid dynamics (CFD) program to run the simulations of the mold-filling.[43-45]

5. Finite Element Method (FEM) Simulations

The single most important numerical system used to forecast the macroscopic mechanical behavior of polyurethane (PU) materials is the finite element method (FEM), especially foams and elastomers that possess nonlinear viscoelastic behavior. Petru and Novak (2017) provide a detailed description of FEM-based models of PU foams, but include constitutive relations; rheological models, such as the modified Kelvin model and the Ogden-rubber model; and their implementation into commercial modeling platforms, such as PAM-CRASH, LS-Dyna, Abaqus, and ANSYS. Their model of dynamically compressed PU foam specimens illustrates the high level of correlation with the experimental data, which has a correlation coefficient of 0.961 up to 37.5% deformation, and the FEM method allows visualizing the contact-pressure

distributions and internal stresses that cannot be measured directly. [46-48]

Widdle (2017) combined microstructural and continuum approaches for modeling flexible PU seating foam, representing microscopic structural irregularity with Voronoi tessellations and capturing the nonlinear elastic and linear viscoelastic response through a hereditary-type stress decomposition [46]. Mashhadi (2018) developed a multiscale modeling strategy for rigid PU foams using Laguerre tessellation of representative volume elements (RVEs) to capture cell size distributions, anisotropy, cell wall thickness, and strut shape as determined by SEM and X-ray microtomography, finding that elastic modulus and critical stress at the onset of plastic instability are predominantly controlled by relative density, mass fraction in struts and walls, and cell aspect ratio. [49]

For shape memory PU, Liang et al. (2019) used ABAQUS to simulate the thermo-mechanically coupled deformation of SMPU, finding that the forming of localized plastic flow and temperature rise originate from initial defects and propagate outward, with simulated average temperature rise curves in good agreement with infrared thermometer measurements across different loading rates[50]. Sheikhi et al. (2021) evaluated four hyperelastic material models (Mooney-Rivlin, Ogden, neo-Hookean, and Gent) for FEM analysis of PU elastomers, using the Valanis-Landel method to estimate biaxial and shear data from uniaxial tests, and concluded that the Gent model best described uniaxial stress behavior while neo-Hookean performed optimally for pure shear. [14, 51-53]

6. CFD and Process Simulation of Polyurethane Foaming

Computational fluid dynamics (CFD) simulation of the PU foaming and mold-filling process is critical for reducing manufacturing defects and cutting prototyping costs [54]. Geier and Piesche (2014) developed a macro-scale mold-filling simulation tool for PU foams in complex geometries, coupling it with a micro-scale bubble-growth model through tracer particles that record local density, temperature, and flow history along particle trajectories, providing a foundation for predicting the evolution of local foam microstructure [55]. Samkhaniani et

al. (2013) implemented a numerical model for PU foam reaction injection molding (RIM) in OpenFOAM, treating the foam as a compressible fluid with a volume-of-fluid (VOF) free-surface tracker and incorporating chemical reaction, heat generation, and blowing agent evaporation, establishing a tool for reducing experimental runs with expensive prototypes. [56]

Seo et al. (2003) developed a finite volume method (FVM) for RIM of polymeric foam, predicting mold filling with variable-density fluid, and found that the expanding foam produces a flatter flow front and more complex particle trajectories compared to constant-density fluids [57]. Karimi et al. (2016) further extended the baseline PBE model into a full 3D CFD framework using OpenFOAM, coupling PBE solved by the quadrature method of moments (QMOM) with a VOF solver, and applied the model to predict apparent density and viscosity, bubble size distributions, and polymerization kinetics during mold filling [43]. Abdessalam et al. (2016) employed the Finite Pointset Method (FPM) for 3D mold-filling simulation of PU foam, using an inverse analysis to identify model parameters from FOAMAT system measurements and validating against short-shot foams from both a panel mold and an automotive underlay carpet cavity.

Population balance modeling was advanced by Ortiz et al. (2021), who coupled a pressure-dependent growth kernel with a 3D CFD arbitrary Lagrangian-Eulerian model to track bubble size distributions during foaming, comparing favorably with experimental data including diffusion wave spectroscopy measurements and post-test SEM analysis [58]. Hershey and Jayaraman (2020) demonstrated through simulation that the lag time introduced during batch mold coating is significant: in molds with complex geometries that force flow bifurcation, different filling lag times predict significantly different weld line locations that cannot be captured by instantaneous-filling assumptions in standard CFD codes. [59-62]

7. Reaction Injection Molding (RIM) Simulation

Simulation of the RIM process for PU requires coupling of reaction kinetics, heat transfer, and rheology. Domine and Gogos (1980)

provided one of the earliest comprehensive simulations of non-isothermal, transient reactive flow in RIM molds, investigating the effects of operating, chemical, and rheological variables on process stability and product quality for linear PU systems [63]. Kim and Kim (1987) developed a computer simulation model for RIM of PU-unsaturated polyester blends using reaction kinetics and viscosity models in cylindrical coordinates, demonstrating that feed temperature, wall temperature, and catalyst level significantly affect the maximum exothermic temperature and demolding time [64]. Lee (1980) provided an early and influential review of PU RIM processing, emphasizing that mold filling is governed by the coupled polymerization reactor analysis and melt injection molding dynamics, and that impingement mixing quality is critical to product quality. [63, 65-67]

More recent CFD-based approaches use finite volume methods with more sophisticated constitutive descriptions. Wittemann et al. (2018) proposed a finite volume method for reinforced reactive thermoset injection molding using OpenFOAM, modeling multiphase flow with phase-dependent boundary conditions and incorporating fiber orientation, curing, and viscosity models; the method showed high potential compared to Finite-Element-based approaches and agreed well with experimental pressure data during mold filling [67]. Lee et al. (2002) used a 2D control volume FEM analysis for PU hybrid foam mold-filling, assuming creeping flow and constant viscosity, with theoretical predictions showing good agreement with digital camcorder observations of flow front advancement. [68]

8. Phase Separation and Morphology Studies by Simulation

The unique properties of segmented PU originate from microphase separation between hard segments (HS) and soft segments (SS), forming discrete hard domains dispersed in a soft matrix. Molecular simulation has been used extensively to quantify and understand this phenomenon. Tao et al. (1994) applied a modified Flory-Huggins Monte Carlo method incorporating the orientational contribution of hard segment rigidity to predict phase diagrams of model MDI-PPG polyurethanes, showing that both chain

rigidity and thermodynamic incompatibility determine the degree of phase separation [69]. Sahebi Joubari and Haddadi-Asl (2019) combined MD simulation with spectroscopic, rheological, thermal, and microscopic experiments to study how soft segment molecular weight and molecular architecture influence microphase separation in TPUs, finding that high molecular weight polyether-based TPUs exhibit the highest degree of phase separation and that competition between enthalpic and entropic factors produces different results depending on the analytical method used. [70]

Grujicic et al. (2013) used coarse-grained MD to study shock-wave mitigation in polyurea (PU), attributing its superior ability to attenuate shock waves to shock-induced ordering and crystallization of hard domains and coordinated shuffle-like lateral motion of soft-matrix segments. Zhou et al. (2018) investigated damping property enhancement in TPU/phenolic resin blends through MD simulation, quantifying hydrogen bonds, binding energy, and fractional free volume, finding that at 40% phenolic resin content the system exhibits the largest H-bond number and highest binding energy, which explains the experimentally observed improvement in loss factor and broadening of the effective damping temperature range. [71-74]

9. Nanocomposite Polyurethane Simulations

Simulation of PU-based nanocomposites has become a growing research area as nanofiller reinforcement offers a path to enhanced properties. Pebdani et al. (2023) used MD with DREIDING and Tersoff force fields to study PU-graphene nanocomposites with defective graphene nanosheets, finding that the introduction of defective nanosheets increases Young's modulus to 22.00 MPa and ultimate tensile strength to 71.39 MPa [16]. Talapatra and Datta (2024) performed a comprehensive MD study of Gr/TPU nanocomposites, showing that enhanced mechanical properties depend on graphene concentration, aspect ratio, orientation, and clustering effects, and that interfacial mechanical properties improve with higher aspect ratio due to enlarged surface area [7]. Park et al. (2024) provided a multiscale CG-MD study of semicrystalline SMPU-silica nanocomposites,

demonstrating how nanoparticle clustering at elevated silica content degrades shape recovery, and how HSC governs nanoparticle agglomeration and, consequently, the shape-memory performance. [28, 33]

Drug delivery matrices based on PU have also been explored computationally. Campiñez et al. (2017) used a 3D cellular automaton model to simulate drug release from novel PU sustained-release matrices, revealing that even at only 10% w/w excipient concentration, the polymer creates an almost continuous geometric barrier around the drug particles comparable in efficacy to lipid or waxy excipients, a mechanism undetectable without *in silico* modeling. [66]

10. Multiscale Modeling Approaches

Single-scale simulations are inherently limited—atomistic models cannot reach the length scales of foam cells or the time scales of processing, while continuum models lack molecular detail. Multiscale methods that bridge these scales are therefore highly valued. Mashhadi (2018) developed a multiscale strategy for rigid PU foams that starts from nanoindentation-measured solid PU properties, passes through Laguerre-tessellated RVEs, and delivers macroscopic elastic moduli and critical stresses in compression, capturing the large influence of cell anisotropy on mechanical behavior [49]. Uddin and Ju (2017) proposed a coarse-grained to continuum bridge: by equating potential energy densities of the CG model to strain energy functions at volumetric and isochoric deformation modes, bulk and shear moduli of TPU were directly extracted and used to estimate macroscopic Young's modulus and Poisson's ratio [20]. The coupled macro/micro approach of Geier and Piesche (2014) links CFD mold-filling simulation at the part level with bubble-scale microstructure simulation in representative volumes, providing a path to predict local foam microstructure (and hence local thermal conductivity and impact strength) throughout complex mold geometries. [54, 55]

11. Challenges, Limitations, and Future Directions

Irrespective of the significant progress, there are still enduring issues that are prevalent at all the levels of simulation. At the atomistic level, the

mechanism of the dynamic formation of hard domains during reactive polymerization remains a difficult challenge to solve, since molecular dynamics time scales (nanoseconds to microseconds) are orders of magnitude lower than phase separation kinetics [75]. The question of transferability of force fields remains an issue: force fields calculated with one polyurethane chemistry will not necessarily be a good model of other chemistries, and force fields calculated with very polar urethane bonds will have to compromise between electrostatic interactions and chain flexibility [6, 22]. The coarse-grained models are bounded by the cost of chemical specificity, and the process of inverting the model to atomistic resolution is not yet a simple one when trying to predict fine-sensitive properties [20, 21]. At the macro scale, polyurethane foam constitutive models would have to support the large strains, viscoelastic model, rate dependence, and densification, which would require a large scale of experimental characterization in order to parameterize it correctly [46]. Mould-filling process-level computational fluid dynamics models are highly sensitive to rheological and kinetic model parameters, the computation of which is an expensive undertaking. [29, 54, 55]

Looking forward, several directions appear most promising. Machine learning interatomic potentials parameterized on quantum chemical data offer a path to more transferable and accurate force fields for PU systems [15]. The combination of DPD morphology predictions with atomistic MD for property extraction provides a practical route to structure-property design of segmented PU at the mesoscale [28, 33]. The continued development of PBE-CFD coupling for foam process simulation, together with more refined bubble nucleation and coalescence kernels, will improve the predictive power for cell size distributions that determine final foam performance [58]. Finally, the integration of digital twin frameworks—in which simulation models are continuously updated by experimental sensor data—represents an emerging opportunity to bring polyurethane simulation from the research environment into industrial process control.

12. Conclusions

Polyurethane simulation spans an exceptionally wide range of length and time scales, from quantum chemical force field

parameterization through atomistic MD, coarse-grained and mesoscale modeling, finite element mechanical analysis, to CFD process simulation. Atomistic MD has established quantitative links between PU chemistry (isocyanate type, soft segment molecular weight, hard segment content) and thermomechanical properties, hydrogen bonding, and diffusion. Coarse-grained methods, particularly DPD and MARTINI-based approaches, have illuminated the nanoscale morphology of phase-separated PU and enabled simulation of polymerization up to high conversions. FEM has provided the engineering community with tools to predict nonlinear viscoelastic foam behavior, hyperelastic elastomer response, and shape memory effects under complex loading. CFD-based process simulation, incorporating reaction kinetics, heat transfer, and population balance equations, is increasingly capable of predicting foam expansion, mold filling, bubble size distribution, and density in industrially realistic geometries. Multiscale methods that bridge these domains remain an active frontier, with the ultimate goal of enabling the computational design of PU formulations and processes with predictive confidence across all relevant scales.

Acknowledgements

Authors appreciate the library team of the Materials Engineering Department of University of Duisburg Essen.

Conflict of interest

The authors declare no conflicts of interest concerning this research.

Funding

The authors did not receive support from any organization for the submitted work.

Author Contribution

A.K. Al-Kamal proposed the review, developed the framework, verified the analytical methods.

AI Declaration Statement

The authors confirm that the manuscript has been written without the assistance of generative AI or AI-based writing tools.

Abbreviations

Abbreviation	Definition
PU	Polyurethane
TPU	Thermoplastic Polyurethane
SMPU	Shape Memory Polyurethane
MD	Molecular Dynamics
CG	Coarse-Grained
DPD	Dissipative Particle Dynamics
MC	Monte Carlo
FEM	Finite Element Method
CFD	Computational Fluid Dynamics
RIM	Reaction Injection Molding
PBE	Population Balance Equation
QMOM	Quadrature Method of Moments
VOF	Volume of Fluid
FVM	Finite Volume Method
FPM	Finite Pointset Method
RVE	Representative Volume Element
HB	Hydrogen Bonding
T _g	Glass Transition Temperature
HSC	Hard Segment Content
HS	Hard Segment
SS	Soft Segment
DFT	Density Functional Theory

References

- [1] C. Wilding, S. Knox, R. Bourne, and N. Warren, "Development and Experimental Validation of a Dispersity Model for In Silico RAFT Polymerization," *Macromolecules*, vol. 56, no. 1, pp. 1581-1591, 2023-02-09 2023, doi: <https://doi.org/10.1021/acs.macromol.2c01798>.
- [2] H. Al-Moameri, G. Hassan, and B. Jaber, "Simulation Physical and Chemical Blowing Agents for Polyurethane Foam Production," *IOP Conference Series: Materials Science and Engineering*, vol. 518, no. 1, p. 108, 2019-05-01 2019, doi: <https://doi.org/10.1088/1757-899x/518/6/062001>.
- [3] G. Sun *et al.*, "A constant shear stress strategy for establishing in situ viscosity models of photoinduced polymerization of acrylamide," *Journal of Polymer Science*, vol. 59, no. 1, p. 1686, 2021-06-16 2021, doi: <https://doi.org/10.1002/pol.20210301>.
- [4] S. Rukmani *et al.*, "Source of Processable Vitriimer Viscosities: Swap Frequencies and Steric Factors," *Macromolecules*, vol. 57, no. 23, pp. 11020–11029, 2024-11-28 2024, doi: <https://doi.org/10.1021/acs.macromol.4c01943>.
- [5] Z. Jiang, W. Zhong, Z. Yu, S. Wen, X. Zhang, and Z. Zhang, "Development of polyamide foam by supercritical CO₂: Low density, anti-shrinkage and thermal insulation," *Construction and Building Materials*, vol. 432, no. 6, p. 136674, 2024-06-01 2024, doi: <https://doi.org/10.1016/j.conbuildmat.2024.136674>.
- [6] I.-C. Yeh and A. J. Hsieh, "Molecular dynamics simulation study of thermomechanical properties and hydrogen bonding structures of two-component polyurethanes," *Journal of Polymer Science*, vol. 61, no. 23, pp. 3095-3104, 2023/12/01 2023, doi: <https://doi.org/10.1002/pol.20230347>.
- [7] A. Talapatra and D. Datta, "Molecular dynamics-based simulations to study structures and properties of graphene/polyurethane nanocomposites," in *Functional Nanocomposites and Their Applications*, 1st ed. New York: Apple Academic Press, 2024, ch. 4, pp. 75-135.
- [8] H. Wang, Y. Liu, and L. Lin, "Behavior Characteristics and Thermal Energy Absorption Mechanism of Physical Blowing Agents in Polyurethane Foaming Process," *Polymers*, vol. 15, no. 10, p. 2285, 2023-05-01 2023, doi: <https://doi.org/10.3390/polym15102285>.
- [9] Y. Shi, M. Yu, J. Liu, F. Yan, Z. H. Luo, and Y. N. Zhou, "Quantitative Structure–Property Relationship Model for Predicting the Propagation Rate Coefficient in Free-Radical Polymerization," *Macromolecules*, vol. 55, no. 21, pp. 9397–9410, 2022-09-26 2022, doi: <https://doi.org/10.1021/acs.macromol.2c01449>.
- [10] C. Zhang, J. Hu, F. Ji, Y. Fan, and Y. Liu, "A combined experimental and computational study on the material

- properties of shape memory polyurethane," *Journal of Molecular Modeling*, vol. 18, no. 4, pp. 1263-1271, 2012/04/01 2012, doi: <https://doi.org/10.1007/s00894-011-1098-0>.
- [11] Y. Wang *et al.*, "Effect of the content and strength of hard segment on the viscoelasticity of the polyurethane elastomer: insights from molecular dynamics simulation," *Soft Matter*, 10.1039/D2SM00463A vol. 18, no. 21, pp. 4090-4101, 2022, doi: <https://doi.org/10.1039/D2SM00463A>.
- [12] Y. Song, R. Damiani, and D. Lange, "Continuous monitoring of the moisture, shrinkage, and carbonation effects on foam concrete performance," *Construction and Building Materials*, vol. 411, no. 12, p. 134185, 2024-01-01 2024, doi: <https://doi.org/10.1016/j.conbuildmat.2023.134185>.
- [13] E. Malewska, A. Prociak, N. Świdzińska-Grela, and M. Kurańska, "The Polyurethane-Polystyrene Composite—Influence of the Blowing Agent Type on the Foaming Process, the Structure and the Properties," *Journal of Composites Science*, vol. 8, no. 4, p. 135, 2024-04-05 2024, doi: <https://doi.org/10.3390/jcs8040135>.
- [14] Y. Wang *et al.*, "Combustion behaviour and dominant shrinkage mechanism of flexible polyurethane foam in the cone calorimeter test," *Journal of hazardous materials*, vol. 365, no. 3, pp. 395-404, 2019-03-05 2019, doi: <https://doi.org/10.1016/j.jhazmat.2018.11.027>.
- [15] M. H. Pebdani and R. E. Miller, "Molecular dynamics simulation of pull-out Halloysite nanotube from polyurethane matrix," *Advances in Mechanical Engineering*, vol. 13, no. 9, pp. 1-10, 2021, doi: 10.1177/16878140211044663.
- [16] M. Heidari Pebdani, "Study Mullins effect of polyurethane reinforcement with halloysite nanotube by molecular dynamics simulation," *Journal of Elastomers & Plastics*, vol. 54, no. 5, pp. 659-675, 2022, doi: <https://doi.org/10.1177/00952443211060407>.
- [17] M. Tewes and U. Peuker, "Viscosity function of a fast reactive polymerization—Aqueous solution of acrylic acid in a rheometer," *Polymer Engineering and Science*, vol. 56, no. 8, pp. 874-888, 2016-08-01 2016, doi: <https://doi.org/10.1002/pen.24316>.
- [18] S. Xiao *et al.*, "High temperature and mesostructure effect on aluminum foam compression responses," *International Journal of Mechanical Sciences*, vol. 275, no. 8, p. 109344, 2024-05-01 2024, doi: <https://doi.org/10.1016/j.ijmecsci.2024.109344>.
- [19] S. E. Khezraji, B. Youcef, L. Belachemi, M. L. Manchado, R. Verdejo, and M. Lahcini, "Recent Progress of Non-Isocyanate Polyurethane Foam and Their Challenges," *Polymers*, vol. 15, no. 2, p. 254, 2023-01-01 2023, doi: <https://doi.org/10.3390/polym15020254>.
- [20] M. S. Uddin and J. Ju, "Enhanced Coarse-Graining of Thermoplastic Polyurethane Elastomer for Multiscale Modeling," *Journal of Engineering Materials and Technology*, vol. 139, no. 1, p. 011001, 2016, doi: <https://doi.org/10.1115/1.4034328>.
- [21] M. S. Uddin and J. Ju, "Prediction of Hysteresis of a Thermoplastic Polyurethane Using Coarse-Grained Molecular Dynamics," in *ASME 2016 International Mechanical Engineering Congress and Exposition*, Arizona, USA, 2016, vol. Volume 9: Mechanics of Solids, Structures and Fluids; NDE, Diagnosis, and Prognosis, V009T12A080: ASME, p. V009T12A080, doi: 10.1115/imece2016-65903. [Online]. Available: <https://doi.org/10.1115/IMECE2016-65903>
- [22] H. Ghermezcheshme, H. Makki, M. Mohseni, M. Ebrahimi, and G. de With, "MARTINI-based simulation method for step-growth polymerization and its analysis by size exclusion characterization: a case study of cross-linked polyurethane," *Physical Chemistry Chemical Physics*,

- <https://doi.org/10.1039/C9CP03407B> vol. 21, no. 38, pp. 21603-21614, 2019, doi: 10.1039/C9CP03407B.
- [23] Y. Wu, S. Lu, C. Zhang, C. Wang, and H. Fang, "Unveiling the three-dimensional network and deformation mechanism of foamed polyurethane by coarse-grained and graph theory," *Journal of Materials Research and Technology*, vol. 29, no. 3, pp. 4650-4661, 2024/03/01/ 2024, doi: <https://doi.org/10.1016/j.jmrt.2024.02.156>.
- [24] R. Kol, P. Nachtergaele, T. De Somer, D. D'hooge, D. Achilias, and S. De Meester, "Toward More Universal Prediction of Polymer Solution Viscosity for Solvent-Based Recycling," *Industrial & Engineering Chemistry Research*, vol. 61, no. 30, pp. 10999-11011, 2022-07-14 2022, doi: <https://doi.org/10.1021/acs.iecr.2c01487>.
- [25] S. K. Yeh, R. Rangappa, T.-H. Hsu, and S. Utomo, "Effect of extrusion on the foaming behavior of thermoplastic polyurethane with different hard segments," *Journal of Polymer Research*, vol. 28, no. 1, p. 244, 2021-06-09 2021, doi: <https://doi.org/10.1007/s10965-021-02604-z>.
- [26] L. Miele, E. Di Lorenzo, C. Guissart, and E. Di Maio, "Liquid foaming of TPU with Methylal," *Heliyon*, vol. 10, no. 12, p. e32420, 2024-06-01 2024, doi: <https://doi.org/10.1016/j.heliyon.2024.e32420>.
- [27] J. Hu, C. Zhang, F. Ji, X. Li, J. Han, and Y. Wu, "Revealing the morphological architecture of a shape memory polyurethane by simulation," *Scientific Reports*, vol. 6, no. 1, p. 29180, 2016/07/04 2016, doi: <https://doi.org/10.1038/srep29180>.
- [28] S. Park, J.-h. Lee, M. Cho, Y. S. Lee, H. Chung, and S. Yang, "Understanding the shape-memory mechanism of thermoplastic polyurethane by investigating the phase-separated morphology: A dissipative particle dynamics study," *Polymer Testing*, vol. 137, no. 8, p. 108531, 2024/08/01/ 2024, doi: <https://doi.org/10.1016/j.polymer.2024.108531>.
- [29] H. Vakili *et al.*, "Self-assembly of a patterned hydrophobic-hydrophilic surface by soft segment microphase separation in a segmented polyurethane: Combined experimental study and molecular dynamics simulation," *Polymer*, vol. 195, no. 5, p. 122424, 2020/05/08/ 2020, doi: <https://doi.org/10.1016/j.polymer.2020.122424>.
- [30] J. Heidarian, N. Ghasem, and W. Daud, "Study on kinetics of polymerization of dimer fatty acids with ethylenediamine in the presence of catalyst," *Chemical Engineering Journal*, vol. 100, no. 6, pp. 85-93, 2004-07-15 2004, doi: <https://doi.org/10.1016/j.ccej.2004.01.010>.
- [31] Y. Ryu, J. S. Sohn, C.-S. Yun, and S. Cha, "Shrinkage and Warpage Minimization of Glass-Fiber-Reinforced Polyamide 6 Parts by Microcellular Foam Injection Molding," *Polymers*, vol. 12, no. 4, p. 889, 2020-04-01 2020, doi: <https://doi.org/10.3390/polym12040889>.
- [32] P. Sarika, P. Nancarrow, and T. Ibrahim, "Phenolic Foam Preparation Using Hydrofluoroolefin Blowing Agents and the Toughening Effect of Polyethylene Glycol," *Polymers*, vol. 16, no. 18, p. 2558, 2024-09-01 2024, doi: <https://doi.org/10.3390/polym16182558>.
- [33] S. Park, J. Moon, M. Cho, Y. S. Lee, H. Chung, and S. Yang, "Multiscale Study of Shape-Memory Behavior of Semicrystalline Polyurethane Nanocomposites Doped with Silica Nanoparticles Based on Coarse-Grained Molecular Dynamics Simulation," *ACS Applied Polymer Materials*, vol. 6, no. 6, pp. 3192-3206, 2024/03/22 2024, doi: <https://doi.org/10.1021/acsapm.3c02968>.
- [34] P. Daripa and R. Mishra, "Modeling shear thinning polymer flooding using a dynamic viscosity model," *Physics of Fluids*, vol. 35, no. 1, p. 046606 2023-01-11 2023, doi: <https://doi.org/10.1063/5.0145061>.
- [35] Z. Gu, B.-Y. Zhao, L. Zhang, and J. b. Bao, "Supercritical carbon dioxide foamed

- thermoplastic polyester elastomer with poly(lactic acid) blending: shrinkage reduction and expansion ratio improvement," *Colloid and Polymer Science*, vol. 303, no. 1, pp. 67-80, 2024-10-18 2024, doi: <https://doi.org/10.1007/s00396-024-05329-9>.
- [36] J. Ruiz, M. Vincent, J. Agassant, T. Sadik, C. Pillon, and C. Carrot, "Polymer foaming with chemical blowing agents: Experiment and modeling," *Polymer Engineering and Science*, vol. 55, no. 9, pp. 2018-2029, 2015-09-01 2015, doi: <https://doi.org/10.1002/pen.24044>.
- [37] H. Al-Moameri, R. Ghoreishi, Y. Zhao, and G. Suppes, "Impact of the maximum foam reaction temperature on reducing foam shrinkage," *RSC Advances*, vol. 5, no. 22, pp. 17171-17178, 2015-02-05 2015, doi: <https://doi.org/10.1039/c4ra12540a>.
- [38] H. Al-Moameri, L. Jaf, and G. Suppes, "Viscosity-dependent frequency factor for modeling polymerization kinetics," *RSC Advances*, vol. 7, no. 43, pp. 26583-26592, 2017-05-17 2017, doi: <https://doi.org/10.1039/c7ra01242j>.
- [39] Y. Zhao *et al.*, "Study on Chain Extension Blending Modification and Foaming Behavior of Thermoplastic Polyamide Elastomer," *ACS Omega*, vol. 8, no. 11, pp. 9832-9842, 2023-03-06 2023, doi: <https://doi.org/10.1021/acsomega.2c06285>.
- [40] H. Al-Moameri, Y. Zhao, R. Ghoreishi, and G. Suppes, "Simulation Blowing Agent Performance, Cell Morphology, and Cell Pressure in Rigid Polyurethane Foams," *Industrial & Engineering Chemistry Research*, vol. 55, no. 8, pp. 2336-2344, 2016-02-17 2016, doi: <https://doi.org/10.1021/acs.iecr.5b04711>.
- [41] E. Pashayev and P. Georgopoulos, "Optimizing the Synthesis of CO₂-Responsive Polymers: A Kinetic Model Approach for Scaling Up," *Polymers*, vol. 17, no. 8, p. 1115, 2025-04-01 2025, doi: <https://doi.org/10.3390/polym17081115>.
- [42] H. Al-Moameri, Y. Zhao, R. Ghoreishi, and G. Suppes, "Simulation of liquid physical blowing agents for forming rigid urethane foams," *Journal of Applied Polymer Science*, vol. 132, no. 34, p. 42454, 2015-09-10 2015, doi: <https://doi.org/10.1002/app.42454>.
- [43] M. Karimi, H. Droghetti, and D. L. Marchisio, "Multiscale Modeling of Expanding Polyurethane Foams via Computational Fluid Dynamics and Population Balance Equation," *Macromolecular Symposia*, vol. 360, no. 1, pp. 108-122, 2016/02/01 2016, doi: <https://doi.org/10.1002/masy.201500108>.
- [44] M. Karimi and D. L. Marchisio, "A Baseline Model for the Simulation of Polyurethane Foams via the Population Balance Equation," *Macromolecular Theory and Simulations*, vol. 24, no. 4, pp. 291-300, 2015/07/01 2015, doi: <https://doi.org/10.1002/mats.201500014>.
- [45] F. Bueche, "Viscosity, Self-Diffusion, and Allied Effects in Solid Polymers," *Journal of Chemical Physics*, vol. 20, no. 12, pp. 1959-1964, 1952-12-01 1952, doi: <https://doi.org/10.1063/1.1700349>.
- [46] M. Petrú and O. Novák, "Measurement and Numerical Modeling of Mechanical Properties of Polyurethane Foams," in *Aspects of Polyurethanes*, F. S. Yılmaz Ed. London: IntechOpen, 2017.
- [47] H. Tian *et al.*, "Preparation of shrink-resistant environmentally friendly foam," *Journal of CO₂ Utilization*, vol. 82, no. 4, p. 102769, 2024-04-01 2024, doi: <https://doi.org/10.1016/j.jcou.2024.102769>.
- [48] L. Jaf, H. Al-Moameri, A. Ayash, A. Lubguban, R. Malaluan, and T. Ghosh, "Limits of Performance of Polyurethane Blowing Agents," *Sustainability*, vol. 15, no. 8, p. 6737, 2023-04-17 2023, doi: <https://doi.org/10.3390/su15086737>.
- [49] M. Marvi Mashhadi, "Multiscale Characterization and Modelling of Polyurethane Foams," Ph.D. Ph.D., Ciencia de los Materiales, Universidad Politécnica de Madrid, Madrid, Spain, 2018.

- [50] Z.-h. LIANG and L. Jian, "Experiment and finite element simulation on thermo-mechanically coupled deformation behavior of shape memory polyurethane," *Journal of Materials Engineering*, vol. 47, no. 10, pp. 133-140, 2019, doi: <https://doi.org/10.11868/j.issn.1001-4381.2018.001334>.
- [51] M. R. Sheikhi, B. Shamsadinlo, Ö. Ünver, and S. Gürgen, "Finite element analysis of different material models for polyurethane elastomer using estimation data sets," *Journal of the Brazilian Society of Mechanical Sciences and Engineering*, vol. 43, no. 12, p. 554, 2021/11/23 2021, doi: <https://doi.org/10.1007/s40430-021-03279-9>.
- [52] M. P. Kransnovskikh and I. G. Mokrushin, "Physical Foaming Agent Influence on Rigid Polyurethane Foams Properties," *ChemChemTech*, vol. 65, no. 11, pp. 90-97, 2022-01-01 2022, doi: <https://doi.org/10.6060/ivkkt.20226511.6657>.
- [53] A. Jimada, R. Olayiwola, M. Shehu, A. Cole, and A. Mohammed, "Modeling and analytical simulation of anterior polymerization in the presence of an inert material," *Journal of Applied Sciences and Environmental Management*, vol. 21, no. 1, pp. 101-109, 2017-03-10 2017, doi: <https://doi.org/10.4314/jasem.v21i1.11>.
- [54] S. Geier, C. Winkler, and M. Piesche, "Numerical Simulation of Mold Filling Processes with Polyurethane Foams," *Chemical Engineering & Technology*, vol. 32, no. 9, pp. 1438-1447, 2009/09/01 2009, doi: <https://doi.org/10.1002/ceat.200900202>.
- [55] S. Geier and M. Piesche, "Coupled Macro and Micro-Scale Modeling of Polyurethane Foaming Processes," *The Journal of Computational Multiphase Flows*, vol. 6, no. 3, pp. 207-220, 2014, doi: <https://doi.org/10.1260/1757-482X.6.3.207>.
- [56] N. Samkhaniani, A. Gharehbaghi, and Z. Ahmadi, "Numerical simulation of reaction injection molding with polyurethane foam," *Journal of Cellular Plastics*, vol. 49, no. 5, pp. 405-421, 2013, doi: <https://doi.org/10.1177/0021955X13485594>.
- [57] D. Seo, J. Ryouon Youn, and C. L. Tucker Iii, "Numerical simulation of mold filling in foam reaction injection molding," *International Journal for Numerical Methods in Fluids*, vol. 42, no. 10, pp. 1105-1134, 2003/08/10 2003, doi: <https://doi.org/10.1002/flid.582>.
- [58] W. Ortiz, L. Mondy, C. Roberts, and R. Rao, "Population balance modeling of polyurethane foam formation with pressure-dependent growth kernel," *AIChE Journal*, vol. 68, no. 3, p. e17529, 2022/03/01 2022, doi: <https://doi.org/10.1002/aic.17529>.
- [59] C. J. Hershey and K. Jayaraman, "Numerical simulation of mold filling water blown polyurethane foams: Effects of sequential pour," *Journal of Cellular Plastics*, vol. 57, no. 2, pp. 193-209, 2021, doi: <https://doi.org/10.1177/0021955X20932920>.
- [60] M. Vonka, M. Šooš, and G. Storti, "Viscosity and drop size evolution during suspension polymerization," *AIChE Journal*, vol. 62, no. 1, pp. 4229-4239, 2016-12-01 2016, doi: <https://doi.org/10.1002/aic.15320>.
- [61] Y. Xiong, B. Pang, Z. Liu, C. Liu, Z. Hu, and Ligu, "Effect of foam temperature on foam stability of foamed concrete and stabilization mechanisms," *Journal of Building Engineering*, vol. 77, no. 10, p. 107492, 2023-10-01 2023, doi: <https://doi.org/10.1016/j.jobbe.2023.107492>.
- [62] M. Modesti, V. Adriani, and F. Simioni, "Chemical and physical blowing agents in structural polyurethane foams: Simulation and characterization," *Polymer Engineering and Science*, vol. 40, no. 1, pp. 2046-2057, 2000-09-01 2000, doi: <https://doi.org/10.1002/pen.11337>.
- [63] J. D. Domine and C. G. Gogos, "Simulation of reactive injection molding," *Polymer Engineering & Science*, vol. 20, no. 13, pp.

- 847-858, 1980/09/01 1980, doi: <https://doi.org/10.1002/pen.760201304>.
- [64] J. Kim and S. C. Kim, "Analysis of reaction injection molding process of polyurethane-unsaturated polyester blends. Part I: Computer simulation," *Polymer Engineering & Science*, vol. 27, no. 16, pp. 1243-1251, 1987, doi: <https://doi.org/10.1002/pen.760271607>.
- [65] L. Lee, "Polyurethane reaction injection molding: process, materials, and properties," *Rubber chemistry and Technology*, vol. 53, no. 3, pp. 542-599, 1980, doi: <https://doi.org/10.5254/1.3535053>.
- [66] M. D. Campiñez, I. Caraballo, M. Puchkov, and M. Kuentz, "Novel Polyurethane Matrix Systems Reveal a Particular Sustained Release Behavior Studied by Imaging and Computational Modeling," *AAPS PharmSciTech*, vol. 18, no. 5, pp. 1544-1553, 2017/07/01 2017, doi: <https://doi.org/10.1208/s12249-016-0613-0>.
- [67] F. Wittemann, R. Maertens, A. Bernath, M. Hohberg, L. Kärger, and F. Henning, "Simulation of Reinforced Reactive Injection Molding with the Finite Volume Method," *Journal of Composites Science*, vol. 2, no. 1, p. 5, 2018. [Online]. Available: <https://www.mdpi.com/2504-477X/2/1/5>.
- [68] W. H. Lee, S. W. Lee, T. J. Kang, K. Chung, and J. R. Youn, "Processing of polyurethane/polystyrene hybrid foam and numerical simulation," *Fibers and Polymers*, vol. 3, no. 4, pp. 159-168, 2002/12/01 2002, doi: 10.1007/BF02912661.
- [69] H.-J. Tao, W. J. MacKnight, S. L. Hsu, and C. F. Fan, "Application of a Molecular Simulation Technique for Prediction of Phase-Separated Structures of Semirigid Model Polyurethanes," *Macromolecules*, vol. 27, no. 7, pp. 1720-1728, 1994/03/01 1994, doi: <https://doi.org/10.1021/ma00085a009>.
- [70] I. Sahebi Jouibari, V. Haddadi-Asl, and M. M. Mirhosseini, "A novel investigation on micro-phase separation of thermoplastic polyurethanes: simulation, theoretical, and experimental approaches," *Iranian Polymer Journal*, vol. 28, no. 3, pp. 237-250, 2019/03/01 2019, doi: <https://doi.org/10.1007/s13726-019-00695-6>.
- [71] R. Zhou, W. Gao, L. Xia, H. Wu, and S. Guo, "The study of damping property and mechanism of thermoplastic polyurethane/phenolic resin through a combined experiment and molecular dynamics simulation," *Journal of Materials Science*, vol. 53, no. 12, pp. 9350-9362, 2018/06/01 2018, doi: <https://doi.org/10.1007/s10853-018-2218-3>.
- [72] Y. Wang, Y. Fang, H. Zhou, and H. Gao, "A Machine Learning Model for Predicting the Propagation Rate Coefficient in Free-Radical Polymerization," *Molecules*, vol. 29, no. 19, p. 4694, 2024-10-01 2024, doi: <https://doi.org/10.3390/molecules29194694>.
- [73] J. Wang, C. Zhang, Y. Deng, and P. Zhang, "A Review of Research on the Effect of Temperature on the Properties of Polyurethane Foams," *Polymers*, vol. 14, no. 21, p. 4586, 2022-10-28 2022, doi: <https://doi.org/10.3390/polym14214586>.
- [74] H. Wang, X. Yang, Y. Liu, and L. Lin, "Changes and Trends—Efficiency of Physical Blowing Agents in Polyurethane Foam Materials," *Materials*, vol. 16, no. 8, p. 3186, 2023-04-01 2023, doi: <https://doi.org/10.3390/ma16083186>.
- [75] D. J. Yontz, "An analysis of molecular parameters governing phase separation in a reacting polyurethane system," Ph.D. Ph.D., Polymer Science and Engineering, University of Massachusetts Amherst, Massachusetts, USA, 1999. [Online]. Available: https://scholarworks.umass.edu/dissertations_1/1000

Blank Page



Deposit number at the National Library in Baghdad 2922 for 2025